Fall 12-14-2018

Modulating Hallmarks of Cholangiocarcinoma

Cody Wehrkamp
University of Nebraska Medical Center

MODULATING HALLMARKS OF CHOLANGIOCARCINOMA

by

Cody J. Wehrkamp

A DISSERTATION

Presented to the Faculty of
the University of Nebraska Graduate College
in Partial Fulfillment of the Requirements
for the Degree of Doctor of Philosophy

Biochemistry and Molecular Biology
Graduate Program

Under the Supervision of Professor Justin L. Mott

University of Nebraska Medical Center
Omaha, Nebraska

November 2018

Supervisory Committee:

Kaustubh Datta, Ph.D.

Melissa Teoh-Fitzgerald, Ph.D.

Richard G. MacDonald, Ph.D.

Acknowledgements

This endeavor has led to scientific as well as personal growth for me. I am indebted to many for their knowledge, influence, and support along the way.

To my mentor, Dr. Justin L. Mott, you have been an incomparable teacher and invaluable guide. You upheld for me the concept that science is intrepid, even when the experience is trying. Through my training, and now here at the end, I can say that it has been an honor to be your protégé. When you have shaped your future graduates to be and do great, I will be privileged to say that I was your first one. For your unwavering confidence in me and my abilities, even if mine faltered. I will always be grateful the time I was able to do science with you, and for the impact it has made on me, personally and professionally. For all you have done for me, I cannot adequately express my thanks; I only hope to deserve it. Thank you Justin.

I thank the members of my supervisory committee, Dr. Richard MacDonald, Dr. Kaustubh Datta, and Dr. Melissa Teoh-Fitzgerald, for their insight and guidance during our meetings, and for helping me to ask the right questions to properly test my hypotheses. I am additionally grateful to the entire BMB faculty for their varied expertise but moreover for their enthusiastic desire to impart it on us students. All of the BMB staff and especially Karen their sincere care and efforts to make my graduate career successful. My fellow students, who never ceased to impress me with the breadth of talents and intelligence they possess, I thank them for the comradery and standards they set.

Thanks to the model organisms from which we learn about and improve our own malignancies. I love animals, and a career path in cancer research makes interaction specific and minimal, but more than none, so I am thankful for that.

Thanks to the Mott Lab members for making true my oft-repeated phrase, “teamwork makes the dream work.”

To Sathish, your infectious work ethic, unyielding kindness, and lasting excitement for what we do is a motivation.

To Ashley, thank you for listening to all and, having answers to most, of my questions, on the entire spectrum of quality, without judgement. Also for showing me what a Ph.D. that can do anything looks like.

To Andrew and Matt, for challenging me to know the answer, or to at least be able to get there together. For allowing me to see the value and reward that comes with being in a

mentor role, and making me want to be better at it. Thank you both for your help, and for letting me help.

To Mary Anne, you add the laughter to the lab, and put a smile in the science. You remind us why we study these things, and for whom, and your continued creation of outreach is an inspiration. For making me a better person by knowing you. For being there. For everything. I am glad you forced me out of my shell those years ago. You made it all special.

Thanks to my friends and family

To Trevor, thanks for your true friendship, you are an always friend, family.

Mom, thanks for being a good mom, and for always being there for Adam and I. Of the many things that are your strengths, perseverance is one I am thankful you ingrained in me.

To Adam, you make me proud to be your brother. I value our bond, and our conversations about all things. I am inspired by your skill of living fully and by your effort to make change for the betterment of your fellow man.

And to my father. While not a man of science by trade, my father always had a scientific curiosity and an interest in the natural world that I think was instilled in me. Since I was a boy I wanted to be a scientist, and here I am. I thank him for this, and for the example of what makes a good man. Thanks dad, I hope you would be proud.

MODULATING HALLMARKS OF CHOLANGIOCARCINOMA

Cody J. Wehrkamp, Ph.D.

University of Nebraska Medical Center, 2018

Supervisor: Justin L. Mott, M.D., Ph.D.

Abstract

How are cholangiocarcinoma cells different from non-malignant cholangiocytes?

All of the hallmarks of cancer apply- those reported in this dissertation include cell proliferation, migration, apoptosis, and evasion of growth suppression. My studies began with testing how apoptosis might be regulated through embelin, a small molecule reported to sensitize cells to apoptosis by blocking XIAP. My data however revealed that embelin reduced the proliferative capacity in cholangiocarcinoma cells, but did not increase cell death. Malignant cells exhibit dysregulation of microRNA processing and expression. Hence, my studies seeking ways that cholangiocarcinoma eludes apoptosis transitioned to the oncomiR miR-106b, which is overexpressed in cholangiocarcinoma. I observed that miR-106b protected cholangiocarcinoma cells from apoptosis. Genome-wide screening identified the landscape of miR-106b-targeted genes in a cholangiocarcinoma cell line, some with roles in tumor biology. MiR-106b targets included members of the Krüppel-like factor (KLF) family of transcription factors.

The function of KLF2 in biliary epithelia or cholangiocarcinoma is unknown. I describe in part how the cholangiocyte senses the environment through the primary cilium and translates this to regulation of KLF2, a flow-responsive regulatory protein and tumor

suppressor in several cancers. I observed lower expression of KLF2 in malignant cholangiocarcinoma cells and tumors compared to normal, and its enforced expression inhibited proliferation and migration while reducing sensitivity to apoptosis. In the normal bile duct epithelium, environmental cues are detected by the cholangiocyte primary cilium, a sensory organelle that functions as a signaling nexus for the cell. Cholangiocarcinoma cells are highly proliferative despite extracellular signals to remain quiescent. Cholangiocarcinoma cells often lose their cilia, resulting in altered communication and unchecked cell growth. I identified a cholangiocyte signaling axis in which the primary cilium maintains quiescence through enhanced KLF2 expression. I present the first finding of a ciliary-dependent KLF2 flow response in cholangiocytes. Overall, this dissertation sought deeper understanding of biochemical and molecular features of cholangiocarcinoma and added to our understanding of microRNAs and mechanosensory pathways.

Table of Contents

List of Figures

List of Tables

List of Abbreviations

α-SMA	alpha smooth muscle actin
ABC	ATP-binding cassette
Abs	absorbance
AD	activation domain
AC6	adenylyl cyclase type 6
ADP	adenosine 5′-diphosphate
AKT	protein kinase B
ANOVA	analysis of variance
Arl13b	ADP-ribosylation factor-like protein 13B
ARPKD	autosomal recessive polycystic kidney disease
ATP	adenosine 5′-triphosphate
ATPγS	adenosine 5′-O-(3-thio)triphosphate
BAPTA-AM	1,2-bis(2-aminophenoxy)ethane-N,N,N′,N′-tetraacetic acid tetrakis(acetoxymethyl ester)
Bcl-2	B-cell lymphoma 2
BH3	Bcl-2 homology 3
BIR3	baculoviral IAP repeat 3
bp	base pair
C2H2	cysteine2 histidine2
cAMP	cyclic adenosine 5′-monophosphate
CCA	cholangiocarcinoma
cFLIP	cellular FLICE-inhibitory protein

CFTR	cystic fibrosis transmembrane conductance regulator
ChIP	chromatin immunoprecipitation
CICR	calcium-induced calcium release
CLASH	crosslinking ligation and sequencing of hybrids
CPD	CDC4 phosphodegron
CpG	cytosine phosphate guanine
CT	cycle threshold
CXCR4	C-X-C chemokine receptor 4
DAPI	4′6-diamidino-2-phenylindole
DIABLO	direct IAP-binding protein with low pI
DMEM	Dulbecco's modified Eagle medium
DMSO	dimethyl sulfoxide
DNA	deoxyribonucleic acid
DR5	death receptor 5
dsRNA	double-stranded RNA
DTT	dithiothreitol
ECGS	endothelial cell growth supplement
EDTA	ethylenediaminetetraacetic acid
EGTA	ethylene glycol-bis(β-aminoethyl ether)-N,N,N′,N′-tetraacetic acid
EKLF	erythroid Krüppel-like factor
EMT	epithelial to mesenchymal transition
ErbB2	erythroblastic oncogene B2
EREG	epiregulin
ERK5	extracellular signal-regulated kinase 5

ERO1L	endoplasmic oxidoreductin-1-like protein
ES	embryonic stem cell
EZH2	enhancer of zeste homolog 2
FADD	Fas-associated protein with death domain
FAM91A1	family with sequence similarity 91 member A1
FBS	fetal bovine serum
FBW7	F-box and WD repeat domain-containing 7
FDR	false discovery rate
FLICE	FADD-like IL-1β-converting enzyme
FOS homolog	Finkel-Biskis-Jinkins murine osteosarcoma viral oncogene
G2/M	gap 2 phase/mitosis
GAPDH	glyceraldehyde 3-phosphate dehydrogenase
GLO1	glyoxalase 1
GSK3	glycogen synthase kinase-3
GTPase	guanosine triphosphate hydrolase
GW182	glycine-tryptophan protein of 182 kDa
H3K27	histone 3 lysine 27
HDAC5	histone deacetylase 5
HMG-CoA	3-hydroxy-3-methylglutaryl coenzyme A
HOXA11-AS	homeobox A11-antisense
HRAS	Harvey rat sarcoma viral oncogene homolog
HRP	horseradish peroxidase
HUVEC	human umbilical vein endothelial cell

IAP	inhibitor of apoptosis protein
IBDU	intrahepatic bile duct unit
IFT	intraflagellar transport
IL-1	interleukin 1
IP3	inositol triphosphate
ITGA2	integrin, alpha 2
kb	kilobase
kDa	kilodalton
KLF	Krüppel-like factor
Ldlr	low-density lipoprotein receptor
LKB1	liver kinase B1
LKLF	lung Krüppel-like factor
LNA	locked-nucleic acid
lncRNA	long non-coding RNA
Luc	luciferase
M6PR	mannose 6-phosphate receptor
MAP	mitogen-activated protein
MATE1	multidrug and toxin extrusion protein 1
MCM7	minichromosome maintenance complex component 7
MEF2	myocyte enhancer factor 2
MEK5	MAP kinase/ERK kinase 5
MEME	multiple expectation maximization for motif elicitation
mESC	mouse embryonic stem cell
miRNA	microRNA

mRNA	messenger RNA
mTOR	mammalian target of rapamycin
MTT	3-(4,5-dimethylthiazol-2-yl)-2,5-diphenyltetrazolium bromide
NC	negative control
NCEH	neutral cholesterol ester hydrolase 1
NF-κB	nuclear factor kappa-light-chain-enhancer of activated B cells
ns	not significant
OCT1	organic cation transporter-1
OE	overexpression
oncomiR	oncogenic microRNA
p21	cyclin-dependent kinase inhibitor 1
PARP	poly-ADP-ribose polymerase
PBS	phosphate-buffered saline
PC1	polycystin-1
PFKFB3	6-phosphofructo-2-kinase/fructose 2,6-bisphosphatase isoform 3
pI	isoelectric point
PI(4)P	phosphatidylinositol 4-phosphate
PI(4,5)P2	phosphatidylinositol 4,5-bisphosphate
PI3K	phosphoinositide 3-kinase
PIPES	piperazine-1,4-bis-2-ethanesulfonic acid
PKD	polycystic kidney disease
PPARγ	peroxisome proliferator-activated receptor gamma
PRC2	Polycomb Repressive Complex 2
pre-microRNA	precursor microRNA

pri-microRNA	primary microRNA
PSC	primary sclerosing cholangitis
PSD3	Pleckstrin and Sec7 domain containing 3
PTEN	phosphatase and tensin homolog
qRT-PCR	quantitative real-time polymerase chain reaction
RB1	retinoblastoma 1
RD	repression domain
RISC	RNA-induced silencing complex
RNA	ribonucleic acid
RNase	ribonuclease
RPM	revolutions per minute
RPMI	Roswell Park Memorial Institute medium
RRM2	ribonucleotide reductase M2
rRNA	ribosomal RNA
SA	streptavidin
SCID	severe combined immunodeficiency disease
SDS-PAGE	sodium dodecyl sulfate-polyacrylamide gel electrophoresis
SEM	standard error of the mean
shRNA	short hairpin RNA
siRNA	small interfering RNA
SKP1	S-phase kinase associated protein 1
SMAC	second mitochondria-derived activator of caspases
SMAD	mothers against decapentaplegic homolog
Smurf1	SMAD-specific E3 ubiquitin protein ligase 1

Sp1	specificity protein 1
S phase	synthesis phase
SV	splice variant
SV-40	simian vacuolating virus 40
T3-T	triiodothyronine-transferrin
TGFβ	transforming growth factor beta
TGR5	Takeda G-protein-coupled receptor 5
TNF	tumor necrosis factor
Tris	tris(hydroxymethyl)aminomethane
TRAIL	TNF-related apoptosis-inducing ligand
tRNA	transfer RNA
TRPV4	transient receptor potential cation channel subfamily V member 4
U	enzyme unit
UTR	untranslated region
Veh	vehicle
WWP1	WW domain-containing E3 ubiquitin protein ligase 1
XIAP	X-linked inhibitor of apoptosis
XIST	X-inactive specific transcript
XRN1	5′-3′ exoribonuclease 1
Z-VAD-fmk	Z-Val-Ala-Asp-fluoromethylketone

Chapter 1 - Introduction

Cholangiocyte biology

The biliary system is composed of an extensive branching network of bile ducts throughout and exiting the liver and the gall bladder. At the base or trunk of the biliary tree, all of the intrahepatic ducts funnel to the common hepatic duct, which then meets the cystic duct of the gall bladder to form the common bile duct. This joins the pancreatic duct and finally drains to the duodenum. This biliary apparatus functions in the production, modification, storage, and drainage of bile to aid in the digestion of dietary fats. The biliary epithelium is formed by cholangiocytes, which themselves are heterogeneous. Two cell types exist, small and large. Small cholangiocytes line small intrahepatic bile ducts and have cuboidal shape, while large cholangiocytes are more columnar and form the epithelium of larger bile ducts (lumen diameter >15 mm) [1]. In normal physiologic conditions, cholangiocytes remain mitotically dormant. Injury causes a proliferative response in order to maintain homeostasis and there is differential responsiveness to injury between the two cell types. Large cholangiocytes proliferate in response to cholestatic liver injury via cAMP signaling. Small cholangiocytes do not proliferate during cholestasis but can differentiate to large cholangiocytes in an IP_3/Ca^{2+}-dependent manner [2]. One of the major roles of cholangiocytes is a structural one, to form the epithelial channel for the delivery of hepatic bile, but it is now recognized that they are also involved in diverse and important cellular processes for normal liver function [3]. Cholangiocytes are a liver minority, constituting just 3%-5% of the total cells [4], compared to hepatocytes, which make up about 65% of the cell number and a

larger percentage of the liver mass due to their large size. Hepatocytes are responsible for the initial generation of primary bile [5], but about 30% of the bile volume is made by cholangiocytes, which modify its composition through secretory and reabsorptive processes [6]. Secretion from hepatocytes is continuous and not well controlled, while a highly regulated system of secretion by cholangiocytes is well documented [7, 8]. Bile is a compendium of suspended or dissolved organic and inorganic substances. It consists of ~95% water with electrolytes, bile salts, bilirubin, cholesterol, amino acids, steroids, enzymes, porphyrins, vitamins, and heavy metals. Biliary excretion also provides a route for the elimination of exogenous drugs, xenobiotics, and environmental toxins [9]. The mean basal flow rate of bile in a normal human liver is approximately 620 mL/day [6] and its regulation is complicated. In general, through the actions of aquaporins, ion channels and exchangers, and ABC (ATP-binding cassette) transporters, bile acids and ions are secreted or resorbed to modulate the flux of water and adjust the local osmotic luminal gradient [10-12]. As an example, the cystic fibrosis transmembrane conductance regulator, CFTR, is an apical chloride channel in cholangiocytes that helps regulate bile volume–hepatocytes do not express CFTR. Opening of CFTR allows chloride to enter the bile duct lumen, where it can be used by a chloride-bicarbonate exchanger for reuptake of chloride and net excretion of bicarbonate. This bicarbonate can then osmotically draw water into the bile duct lumen, resulting in increased volume, flow, and pH. Loss of CFTR function results in poorly hydrated, acidic bile that can promote biliary fibrosis and cirrhosis [13].The importance of cholangiocyte function is highlighted by the recognition of the many pathologies arising from cholangiocyte dysfunction, collectively

called cholangiopathies. The initial causes and progression mediators of cholangiopathies are wide-ranging, from genetic to neoplastic, infectious, immune-mediated, idiopathic, and toxin- or drug-induced [14]. The most devastating of the cholangiocyte-targeting diseases is cholangiocarcinoma, which will be discussed in the next section.

Cholangiocarcinoma

Cholangiocarcinoma is a bile duct epithelial cell neoplasm and is the second most common primary malignant liver cancer. This cancer is particularly aggressive with a 5-year survival rate below 15% [15]. Incidence is on the rise. Treatment options are few. Surgical resection represents the most favorable option, as it is the only potentially curative one; however, due to the location of the tumor and late onset of symptoms and diagnosis, most patients are ineligible for resection. Patients who do undergo surgery have an overall survival of about 36 months, and 5-year survival of less than 30% [16]. For non-resectable tumors, treatment options are palliative only, and most patients receive the current standard-of-care regimen of combination chemotherapy (gemcitabine and cisplatin) [17]. However, overall survival in this case is less than one year [18]. More investigation is essential to address the specific characteristics of this cancer and to tailor and improve treatment strategies. Cholangiocarcinoma is classified into three types, intrahepatic, perihilar, and distal, based on the primary anatomical location relative to the liver. Intrahepatic tumors are

those that arise in the smallest bile ducts within the liver itself, while perihilar are those that occur within the area including the second-order bile ducts, the largest branches connecting to the main hepatic duct, up to the junction of the cystic duct; and distal tumors are extrahepatic, including the region after the cystic duct to the ampulla of Vater, where the common bile duct joins the pancreatic duct [19]. (**Figure 1.1**) Relative incidence of each type is 50% perihilar, 40% distal, and less than 10% for intrahepatic [20], although the incidence of intrahepatic cholangiocarcinoma is on the rise [21]. Each subtype has unique cancer biology, epidemiology, and prognosis, and consequently different, limited, therapeutic options [22]. Cholangiocarcinoma is characterized by its association with inflammation, a desmoplastic stroma, resistance to apoptosis, and induction of cell survival mechanisms. Liver injury, chronic inflammation and obstruction of the bile ducts are common features of the disease. Bile duct obstruction can arise from conditions that predispose to cancer, such as primary sclerosing cholangitis (PSC) or intrahepatic cholelithiasis, or it can be caused by tumor-induced ductal blockage. Most cholangiocarcinomas are of *de novo* origin, with no identifiable associated risk factors. However, some diseases and conditions exist that predispose patients to development of cholangiocarcinoma. Risk factors that contribute to U.S. incidence are PSC, intrahepatic cholestasis, hepatitis viruses, and cirrhosis. Chronic inflammation of the bile ducts as seen in PSC leads to increased incidence of cholangiocarcinoma, with PSC patients having a lifetime risk of approximately 10-15% of developing cholangiocarcinoma, a vastly higher rate than in the general population [23, 24].

Figure 1.1 Cholangiocarcinoma anatomy

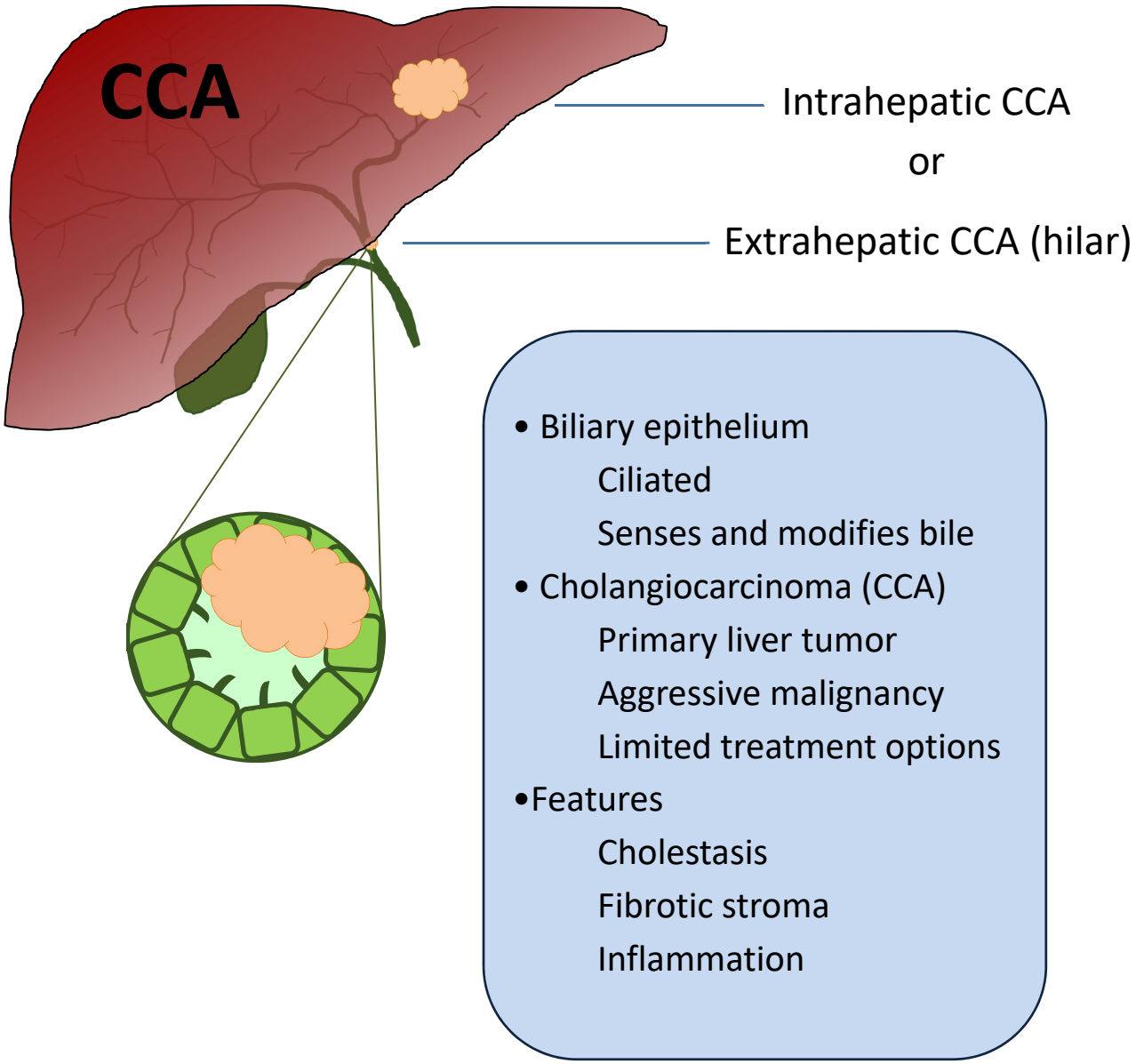

Figure 1.1. Cholangiocarcinoma anatomy. Cholangiocarcinoma tumors are heterogenous and can differ in anatomical location. This can lead to some variability in presentation of malignant features. For instance, the severity of ductal obstruction may depend in part on the location and size of the tumor. Feasibility for resection may also be contigent on tumor accessibility.

The highest incidence rates of cholangiocarcinoma in the world are in Southeast Asia, where the main risk factor is liver fluke infection [22]. These hepatobiliary parasites cause chronic inflammation and cell turnover and have been classified as carcinogens [25].

Solid tumors are commonly under exposure to hypoxic conditions. Rapid, unchecked cell growth comes at the cost of nutrient deprivation in the tumor microenvironment when neovascularization lags behind. The normal biliary epithelium is distinctly sensitive to hypoxia and undergoes apoptosis under low oxygenation [26]. Cholangiocarcinoma tumors are typically hypovascular and highly fibrotic. These harsh conditions puzzlingly accelerate a malignant phenotype by promoting pro-survival mechanism and increased metastatic potential [27, 28]. Therefore, an important characteristic of cholangiocarcinoma cells is their ability to evade cell death either by activation of cell survival pathways or through alteration of pro-apoptotic molecules. One example is the increased activity of X-linked inhibitor of apoptosis protein (XIAP). High expression of XIAP in cholangiocarcinoma patients is correlated with poor survival, and increased levels of inflammatory cytokine IL-6 have been shown to increase translation of XIAP in cholangiocarcinoma cells, which results in greater resistance to chemotherapeutic drug-induced cell death [29, 30]. We investigated the effect of an XIAP inhibitor in cholangiocarcinoma cells, and the results of that project form the bulk of Chapter 3 [31]. Cancer cells are often characterized by their sensitivity to TNF-related apoptosis-inducing ligand (TRAIL). TRAIL is a significant cytokine that induces apoptosis in transformed (but not healthy) cells via the extrinsic cell death

pathway. It is expressed in normal tissues, particularly NK and NK-T cells, and acts as a tumor surveillance mechanism to induce apoptosis in cancer cells. Paradoxically, some cancer cells including cholangiocarcinoma cells express TRAIL, which would be expected to result in paracrine apoptosis of neighboring malignant cells. Cholangiocytes therefore must employ pro-survival signaling and methods of resistance [32]. These features make TRAIL a useful tool for investigating cell death resistance mechanisms in cholangiocarcinoma cells [33]. The dismal prognosis, difficulty and delay in detection, and dearth of treatment options for cholangiocarcinoma warrant continued and increased effort toward the understanding of survival pathways and targeted therapies for this disease.

MicroRNAs

MicroRNAs are short, non-coding RNAs of approximately 22 nucleotides in length. Mammalian microRNAs function as post-transcriptional gene regulators to fine-tune expression of their gene targets by repression. The human genome may encode over 1000 microRNAs; however, a recent annotation study indicated that the number may be closer to 600 [34]. MicroRNAs collectively play a role in the regulation of approximately 60% of all human protein-coding genes [35]. They act by recognition of target mRNAs through complementary binding to specific transcript sequences. The most important point of interaction is binding of the seed region of the microRNA, a 7 to 8-nucleotide stretch at the 5′ end. This seed region recognizes a seed-binding site on the

cognate mRNA transcript through Watson-Crick base pairing. The seed-binding site is conserved among target mRNAs, which allows for regulation of several to hundreds of transcripts by a single microRNA [36].

Biogenesis of a microRNA is a multistep process involving many interacting protein partners and consequently many points of regulation. Approximately 40% of microRNAs are produced from introns or sometimes exons of other genes, while most others are generated from their own dedicated genes [37]. MicroRNAs can be transcribed individually or in pairs or clusters from the same primary RNA molecule [38]. They are generally transcribed by RNA polymerase II into large primary microRNA (pri-microRNA) molecules of a few hundred to over a thousand bases in length. Additional processing by the Microprocessor complex, cleaves the pri-microRNA to a hairpin loop structure that is termed pre-microRNA. This 50 to 80-nucleotide RNA is then exported from the nucleus to the cytoplasm via the transport protein Exportin 5. Cleavage of the hairpin pre-microRNA by RNase III enzyme Dicer generates a double-stranded RNA molecule. One strand of the dsRNA, termed the mature or guide strand, is loaded onto the RNA-induced silencing complex (RISC). This forms a ribonucleoprotein complex in which the bound microRNA acts as a sequence-specific guide for mRNA target recognition. RISC can then directly cleave the bound mRNA through action of a central protein complex member Argonaute. In order for direct cleavage, or "slicing," of a transcript to occur, there must be perfect or near-perfect complementarity between microRNA and messenger RNA as well as an active slicer protein [39]. More commonly, mammalian microRNAs dampen expression of their

targets through mRNA destabilization and decay and translation inhibition, with both playing a role in gene silencing [40]. However, expansive studies investigating the genome-wide effect of microRNAs on mRNA and protein levels, coupled with ribosome profiling experiments, have shown mRNA degradation to be the dominant effector of repression [41, 42].

Evidence suggests that microRNA target degradation occurs through mRNA disassembly. mRNAs are first deadenylated and then decapped, allowing for enzymatic degradation by the cytoplasmic nuclease 5′-3′ exoribonuclease 1 (XRN1) [43, 44]. Argonaute-bound microRNAs direct mRNA degradation by guiding the necessary degradation machinery composed of several components. GW182 family proteins interact directly with Argonaute and act as a scaffold, recruiting deadenylase and decapping complexes. The bridging of these effector complexes with RISC allows the components to interact directly and couple the deadenylation, decapping, and degradation processes, making microRNA-mediated mRNA decay both rapid and efficient [45, 46]. Nevertheless, because the magnitude of degradation is small compared to the total amount of target mRNA, the net result is a fine-tuning of expression, not silencing. Global analysis of microRNA-mediated gene dampening indicates that while most of the repressive effect can be attributed to mRNA degradation, some is accounted for directly by translational repression and not secondary to mRNA degradation [42]. Exactly how microRNAs repress translation has been an ongoing question, but the general consensus is that they inhibit cap-dependent translation at initiation. This mechanism suggests the displacement of the ternary eukaryotic translation initiation

factor 4F (eIF4F) complex, which is responsible for unwinding of secondary structures in the 5′ UTR of mRNAs by RNA helicase and recruitment of the 43S pre-initiation complex [45, 47, 48].

MicroRNAs in cancer

The significance of microRNAs as biologic mediators, therapeutic targets, and diagnostic markers has been demonstrated in a myriad of disorders including nearly all cancers, cholangiocarcinoma among them. And, microRNA dysregulation has been implicated in every aspect of cancer biology, either through increased or decreased expression of important regulatory members. Different microRNA species can thus act as tumor suppressors or oncogenes with roles in cancer cell apoptosis, proliferation, differentiation, and metastasis [49-51]. The expression and functions of microRNAs in cancer are often cell type- and disease-specific [52, 53]. Consequently, not only can microRNAs serve as potential targets for therapies, there has also been a large effort to characterize the expression signatures in cancer, so they may be used as diagnostic biomarkers [54]. Additionally, since the expression pattern can also change with disease progression, the specific microRNA fingerprint could be useful as a prognostic tool, helping to identify patients that would benefit from a more aggressive therapy [55, 56]. The dysregulation of many microRNAs has been studied in cholangiocarcinoma, and many of their target genes and functional effects have been revealed.

Figure 1.2 MicroRNA regulation in cancer

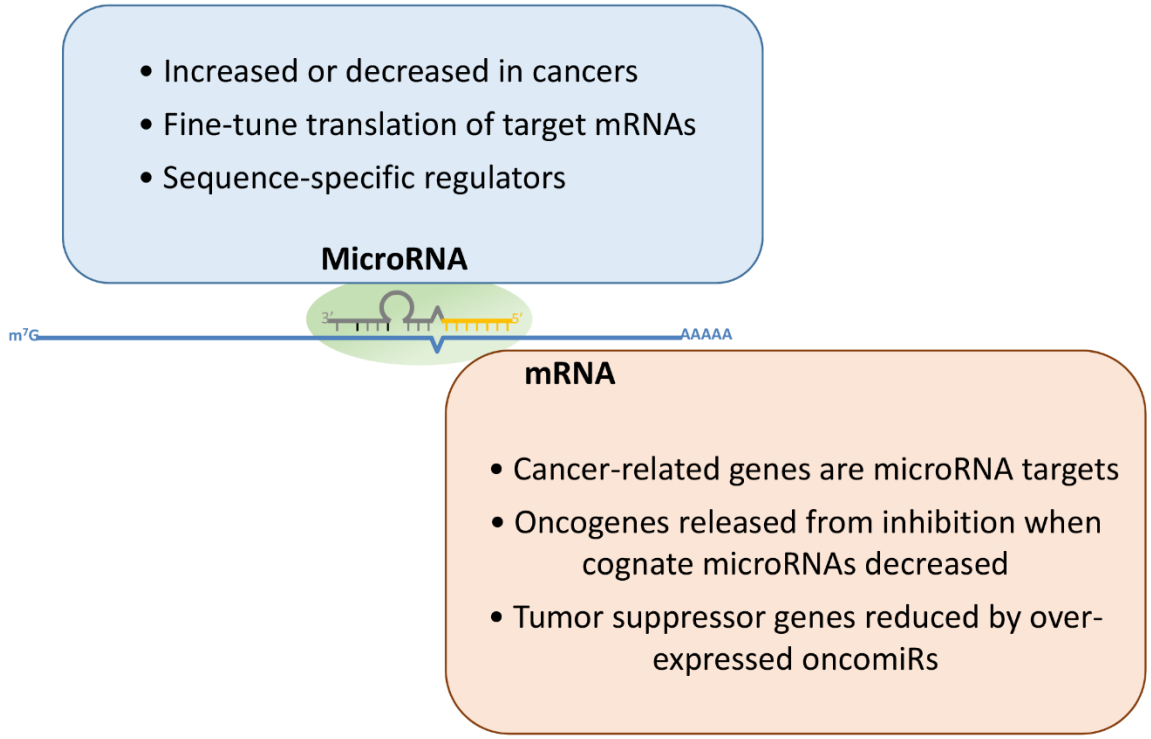

Figure 1.2. MicroRNA regulation in cancer. MicroRNAs associate with nucleoproteins in the cytoplasm to form RISC, depicted as a green oval. They then direct RISC to the target mRNA through sequence complementarity. Recognition occurs with a 6-8 nucleotide "seed" sequence (shown in yellow) with complementarity to specific seed binding sites (SBS). The degree of microRNA:mRNA hybridization varies outside of the seed region and can contribute to the degree of transcript regulation.

miR-106b

MicroRNAs are grouped into families based on sequence homology. The miR 17~92 family contains three clusters with 15 total members and is one of the most studied microRNA families in cancer biology [57], including miR-17~92, miR-106a~363, and miR-106b~25. The 106b~25 cluster is located in the 13th intron of the minichromosome maintenance complex component 7 (MCM7) gene. MCM7 is a licensing factor for DNA replication, which, with MCM protein complex members 2-6, acts as a DNA helicase for replication initiation. Intronic microRNAs are often predicted to reflect the expression status of their host gene, and studies do show MCM7 and 106b~25 to be co-transcribed [58]. However, novel transcriptional and post-transcriptional mechanisms have been revealed that can stratify expression patterns of MCM7 and its hosted microRNAs [59]. Moreover, the expression of the individual microRNAs can be uncoupled, through independent transcription of pri-microRNAs from an alternate promoter and via alternative splicing [59-61]. Through these and other mechanisms, cancer cells are able to utilize processes that sometimes favor varied and selective expression of microRNA cluster members. Multiple studies have characterized miR-106b as an oncomiR. Its expression is increased in many cancers including prostate [62], breast [63], gastric [64], hepatocellular carcinoma [65], renal cell carcinoma [66], colorectal [67], and cholangiocarcinoma [68-72]. Several miR-106b target genes are significant to cancer physiology for their roles as tumor suppressors, transcription regulators, or apoptosis signaling proteins. Some of the known targets of miR-106b that are relevant to cancer biology include retinoblastoma 1 (RB1) [73], phosphatase and

tensin homolog (PTEN) [74], caspase 8 [75], and twist1 [76]. Through repression of these and other gene targets, miR-106b is often a promoter of tumor progression, contributing to the cancer phenotype via abnormal cell proliferation, apoptosis, migration, and invasion [59]. MiR-106b had a predominantly inhibitory effect on the expression level of over one hundred mRNAs in cholangiocarcinoma cells, described in detail in Chapter 4 of this dissertation [77]. Typically, oncomiRs are upregulated and tumor suppressor microRNAs are downregulated. **Tables 1.1** and **1.2** are a derived from our published review [78], and have been updated here to be a comprehensive catalog to date, of those microRNAs that have expression changes in cholangiocarcinoma and their described targets and functional effects when available.

Table 1.1 MicroRNAs upregulated in cholangiocarcinoma

Upregulated microRNAs			
MicroRNA	**Target(s)**	**Function(s)**	**References**
10a			[79]
15a			[80]
15b			[80]
17			[70, 71, 80]
19a	PTEN	cell growth, invasion	[71, 80, 81]
20a			[79, 80]
20b			[79]
21	PTEN, PDCD4, TIMP3, 15-PGDH, PTPN14, DNAJB5	invasion, metastasis, tumor growth, apoptosis, cell growth, tumor development, fibrosis, chemoresistance	[70, 80, 82-91]
22			[79]
24	Menin	proliferation, tumor growth	[79, 92]
25	DR4	apoptosis	[71]
26a	GSK-3β, 15-PGDH	proliferation, cell growth	[93, 94]
26b	15-PGDH	cell growth	[93]
27a			[79]
29a			[79, 95]
29b			[79]
30b			[79]
30e			[79]
31	RASA1	proliferation, apoptosis	[96]
34a	Per1	proliferation, invasion	[97]
92	PTEN	cell growth, invasion	[81]
93			[70, 71, 79]
96			[79]
103a			[79, 80]
106a			[70, 80]
106b		apoptosis	[70, 71, 77, 79]
107			[79]
122			[79]
130b			[80]
130	PPARγ	chemoresistance	[98]
135b			[79]
141			[68, 99]
142			[80]

150			[100]
151a			[79]
181a	P27	cell cycle	[79, 101]
181c	NDRG2		[102]
191	sFRP1, TET1	proliferation, migration, invasion, apoptosis, metastasis, cell viability	[103, 104]
192			[69, 105]
193a	TGFBR3	proliferation, migration, invasion	[80, 106]
200a			[99]
200b		apoptosis	[68, 99]
200c			[69, 90, 99]
203a			[79]
210	HIF-3α	cell growth, cell viability, chemoresistance	[107, 108]
221	P27, PTEN	cell cycle, EMT	[79, 90, 101, 109]
223			[80, 86]
224	p21	cell cycle	[80, 110]
324			[80]
331			[80]
340			[79]
374a			[80]
376c			[79]
383	IRF1	proliferation, migration, invasion	[111]
424			[79]
429	CDH6		[79, 99, 112]
663b			[79]
675			[113]

Table 1.1. MicroRNAs upregulated in cholangiocarcinoma. A list of the microRNAs that are upregulated in cholangiocarcinoma. If one or more *bona fide* targets were discovered they are listed in the second column, followed by functional effects if they were observed.

Table 1.2 MicroRNAs downregulated in cholangiocarcinoma

Downregulated microRNAs			
MicroRNA	**Target(s)**	**Function(s)**	**References**
1			[79]
let-7a	NF2	apoptosis	[80, 114]
let-7b	cyclin D1	cell cycle	[80, 101]
let-7c	IL-6, IL-6R, EZH2	migration, invasion, tumor growth, metastasis	[79, 90, 115]
15a	PAI-2	proliferation, migration	[116]
16	YAP1	proliferation, invasion, metastasis	[117]
22	HDAC6	proliferation, migration	[69, 118]
26a	KRT19	proliferation, tumor growth	[119]
26b	S100A7	cell viability, invasion	[120]
27b	CDK2, cyclin D1	cell cycle	[101]
29a	HDAC4	cell growth, migration, invasion	[121]
29b	Mcl-1	apoptosis	[122]
30e	Snail	proliferation, migration, invasion	[123]
31			[86]
32			[90]
34a	SMAD4, Notch1	cell growth, EMT	[124, 125]
98			[80]
99a	IGF1R	migration, invasion, tumor growth	[79, 90]
100			[79]
106b	Zbtb7a	chemoresistance	[126]
101	VEGF-C	migration, invasion	[127]
122	ALDOA	proliferation, apoptosis, migration, invasion	[86, 90, 128, 129]
124	SMYD3, CDK2, CDK4, cyclin D1, cyclin E1, GATA6, EZH2, STAT3	proliferation, apoptosis, cell cycle, migration, invasion, autophagy	[101, 130-132]
125a			[69]
125b	IL-6R, SIRT7	cell growth, migration, invasion, tumor growth	[79, 90, 133]
126			[79]
127			[69, 79]
138	RhoC	migration, cell viability	[134]
139			[79]
140	SEPT2	proliferation, migration, invasion	[135]
144	LIS1	proliferation, invasion	[79, 136]

145	NUAK1	proliferation, invasion	[79, 80, 86, 137]
146a			[86]
148a	DNMT1	proliferation	[138]
150	ELK1	proliferation, migration	[139]
152	DNMT1	proliferation	[138, 140]
182	CDK2, cyclin D1	cell cycle	[101]
184			[80]
185			[80]
188			[70]
191			[70]
195		cell growth, migration, invasion	[141]
198			[70, 80]
199a	mTOR	chemoresistance	[69, 141]
200b	SUZ12, ROCK2	tumor growth, metastasis	[142]
200c	NCAM1, SUZ12, ROCK2, ZEB1	migration, EMT, tumor growth, metastasis	[80, 142-144]
204		cell growth	[80, 145]
214	Twist	EMT	[69, 80, 83]
221			[80]
222			[80, 86]
302b			[80]
302d			[80]
320	Mcl-1	apoptosis	[80]
328			[80]
337			[79, 80]
338			[80, 113]
370	MAP3K8	proliferation	[70, 146]
371a			[80]
373			[80]
376a			[69]
376c	GRB2	migration	[147]
424			[69]
433	HDAC6	proliferation, migration	[118]
451a			[79]
494	PTTG1, TOP2A, WDHD1	cell viability, migration, invasion, metastasis, cell cycle	[70, 84, 148]
512			[70]
513a			[70]
517c			[79]
519a			[79]
520e			[70, 79]

605	PSMD10	proliferation, migration, apoptosis	[149]
630			[79]
652			[113]
662			[70]
5095	MYCN	cell viability, migration, invasion	[150]

Table 1.2. Downregulated microRNAs in cholangiocarcinoma. A list of the microRNAs that are downregulated in cholangiocarcinoma. If one or more *bona fide* targets were discovered they are listed in the second column, followed by functional effects if they were observed.

KLF2 review: "KLF2 regulation and function"

Krüppel-like factors (KLFs) comprise a broad family of transcription factors that contain conserved zinc finger DNA-binding domains and are critical regulators in a span of biological processes including proliferation, cell death, differentiation, development, inflammation and metabolism. As such, their dysregulation is associated with the pathobiology of many diseases including cancer. Originally discovered and described as a lung-specific transcription factor (LKLF), KLF2 has crucial roles in embryogenesis and cell differentiation, the development and maintenance of blood vessels, activation of T-cells, and inhibition of adipocyte differentiation. Some studies, especially more recently, implicate KLF2 as a player in cancer biology as well. Much evidence has established roles for KLF2 in T-cell biology, including the regulation of survival, migration, and trafficking, and promotion of cell quiescence. These immune functions are outside of the scope of this review, but are well-described [151-153] and reviewed [154-156] elsewhere. This review aims to cover the regulators of KLF2 and its functions as they pertain to normal cell expression versus disease.

Development and cell differentiation

Human KLFs share homology with the *Drosophila melanogaster* protein Krüppel. Krüppel is a member of the "gap" class of segmentation genes that are responsible for programming correct body segmentation in the thorax and abdomen of the *Drosophila* embryo [157], and deficiencies cause lethality and a dysmorphic embryo appearance [158]. KLF2, along with KLF4 and KLF5, is known to be involved in mammalian cell programming. They are coordinately upregulated in embryonic stem (ES) cells and

promote self-renewal [159]. Simultaneous deletion of these three factors results in differentiation of embryonic stem cells [160]. Moreover, single or double knockout of any of the three members does not induce differentiation, and any single member was sufficient to maintain pluripotency in mouse embryonic stem cells (mESCs) [161]. These data indicate that these three KLFs have functional redundancy in ES self-renewal. However, although they display compensatory targeting of reprogramming factors, their other regulatory functions make each member indispensable, as all knockout mice are lethal either pre- or postnatally [162-164]. KLF2 is also a key molecular regulator of adipogenesis and suppressor of adipocyte differentiation. Multiple KLFs (KLF4, -5, -9, and -15) induce adipocyte differentiation by activating peroxisome proliferator-activated receptor γ (PPARγ), a master transcription regulator of adipogenesis [165]. However, KLF2 is the only KLF member that represses PPARγ and inhibits adipocyte differentiation through this interaction [166]. Thus, while KLF2 can functionally complement the absence of KLF4 in ES cells, these two proteins also have distinct and non-overlapping functions.

Structure

KLF2 was first isolated, sequenced, and characterized in the mouse [167, 168]. This gene was initially identified based on its homology to EKLF or KLF1, with a high degree of similarity in the DNA-binding zinc finger domain. KLF1 is able to bind to a CACCC sequence in the promoter region of the β-globin gene and regulate its expression. KLF2 was able to bind this same sequence and promote β-globin expression

as well [167]. This finding led to the first classification of KLFs as members of a distinct family of transcription factors. Generally, KLFs are classified by their ability to bind DNA in CACCC boxes and other GC-rich motifs at control regions of target genes such as promoters and enhancers. This DNA binding is accomplished with a highly conserved KLF family structural domain containing three tandem C-terminal zinc finger motifs. Each finger coordinates a zinc ion with two cysteine and two histidine residues (C_2H_2). In addition, KLF transcription factors contain nuclear localization sequences, which can occur within or adjacent to the zinc finger motifs [169]. The N-terminal regions of KLFs are much less conserved among members and can vary widely, which allows for a myriad of distinct roles in cellular processes either through activation or repression of target genes by promoter binding or interaction with coregulators [170].

KLF2 is highly expressed in the lung and in adipose tissue, as well as erythroid, lymphoid, and other select tissues [171]. The human and mouse KLF2 homologs share 85% nucleotide identity and a corresponding amino acid similarity of 90%. The human KLF2 gene is made up of three exons, which are separated by two introns. Remarkably, no splice variants are reported for KLF2, and family-wide investigation of Krüppel splicing did not reveal alternative isoforms [172]. The entire gene is approximately 3 kb located on the short arm of chromosome 19, at 19p13.1. [173]. The 5'-flanking region of KLF2 is GC-rich and this promoter region contains several Sp1 binding sites, another C2H2 zinc finger transcription factor related to the KLFs. A portion spanning from the

promoter region to the end of the second exon contains a large CpG island in which 76% of the nucleotides are C or G [174].

Expression of KLF2 in the mouse embryo begins as early as embryonic day 9.5 (E9.5) in the vasculature. By E14.5, expression in blood vessels increases and is present in lung buds, becoming abundant by E18.5. KLF2 knockout mouse embryos die between E12.5 and E14.5. This is due to abnormal formation of the tunica media, the middle layer of the artery or vein composed of smooth muscle cells and elastic tissue, leading loss of vessel wall stability and severe hemorrhaging [162].

Degradation

KLF2 contains an autoinhibitory domain that can bind to the E3 ubiquitin ligase WWP1 and subsequently cause suppression of target gene transactivation [175]. A later study showed poly-ubiquitination by WWP1 leads to rapid proteasomal degradation of KLF2. Additionally, the specific residue predominantly responsible for ubiquitin conjugation is lysine 121. Mutation of this lysine to arginine abrogates proteolytic destruction of KLF2 [176]. It is not known, however, what regulates KLF2 proteolytic degradation and what the biologic function of this KLF2 degradation in any cell type may be. The presence of a transcriptional inhibitory domain upstream of the DNA-binding zinc finger motifs is a characteristic of KLF2, KLF1, and KLF4. This is a unique feature of these members of the KLF family and they are accordingly grouped in a subfamily. KLFs 1 and 4 have both activation domains located near the N-terminus in addition to inhibitory domains adjacent to the zinc fingers, allowing them to function

both as transcriptional activators and repressors [177]. KLF2 also contains both an activation domain and a repression domain; however, most evidence indicates that its repressor function dominates. Further phylogenetic analysis and sequence alignment expanded the grouping of this subfamily to include KLFs 5, 6, and 7 based on the common structural and functional domains of these six KLFs and their ability to bind acetylases [155]. Within this subfamily of KLFs, KLF5, -6, and -7 possess only an activator domain and not an inhibitory domain [178-180].

Regulation by flow

In mammals, blood must be transported throughout a branching network of vessels by pumping of the heart in order to continuously circulate oxygen to all cells in the body. This constant pulsatile flow creates shear stress at the vascular interface. Endothelial cells lining the blood vessels are adapted to regulate vascular homeostasis through anti-coagulation and anti-inflammation functions and response to shear stress [181]. Alterations in shear stress lead to endothelial response through activation of mechanosensors and intracellular signaling to induce transcription factors for the expression of specific genes [182, 183]. Dekker et al. were the first to demonstrate that KLF2 responds to fluid shear stress [184]. HUVECs exposed to flow versus static conditions saw a sharp induction in KLF2 mRNA. Interestingly, the type of flow was also important. Pulsatile flow over 7 days led to a 20-fold induction, while steady flow caused about a 5-fold induction that quickly peaked at 4 hours. Adding to this, Wang et al. showed that different flow patterns elicited different KLF2 responses in endothelial

cells. Pulsatile flow with significant forward direction caused sustained KLF2 expression in endothelial cells. However, oscillatory flow with little forward direction induced KLF2 expression transiently but then caused prolonged suppression [185]. Using a rat aortic stenosis model to artificially constrict the abdominal aorta and increase local shear, the authors observed differential KLF2 expression. KLF2 imaging by immunohistochemistry showed high expression in regions of laminar flow upstream of the lesion while little to none was expressed in the regions of disturbed flow at the poststenotic site. Specific inhibition of shear stress-responsive Src, a non-receptor protein tyrosine kinase, had no effect on KLF2 induction during pulsatile flow but did prevent suppression under oscillatory flow, suggesting a role in mediating inhibition of KLF2 expression under disturbed flow conditions.

The varied and complex architecture of the vasculature system results in distinct local environments with differing levels of shear stress that must be sensed by endothelial cells. They can respond to biomechanical stimuli by releasing vasoactive metabolites and/or altering transcriptional programs to adjust functional phenotype in both normal and disease state [186]. To evaluate the global transcriptional profile of KLF2 in flow-mediated gene expression, genome-wide transcriptional profiling was reported. Under flow conditions in the presence of KLF2 siRNA or control, microarray analysis revealed that approximately 15% of genes regulated by flow were dependent on KLF2. Analysis of their raw data shows that approximately two-thirds of the regulated genes were increased by adenoviral KLF2-enforced expression, while the other one-third

were decreased ([187]; Supplemental). Moreover, they show by categorizing flow-activated genes by fold-change of induction, that 46% of the most highly flow-activated genes were dependent on KLF2 upregulation [187]. Importantly, KLF2-upregulated genes were largely vasodilatory while KLF2-downregulated genes were vasoconstrictive and pro-inflammatory. These results point to KLF2 as an important master regulator of transcriptional response to atheroprotective flow—both activating and repressing transcription—and in maintenance of functional integrity in the normal endothelium.

The promoter region responsible for KLF2 shear stress response has been mapped to a defined region -157 to -95 base pairs from the transcription start site [188]. Additionally, endothelial KLF2 is upregulated via the MEK5/ERK5/MEF2 signaling pathway. Previous studies showed that ERK5 is activated by shear stress and that it can subsequently directly phosphorylate and activate myocyte enhancer factor-2 (MEF2) in endothelial cells [189, 190]. KLF2 sequence analysis discovered a MEF consensus binding sequence in the KLF2 promoter region. Further, MEF2 binding to the KLF2 promoter was confirmed by chromatin immunoprecipitation assays. To test if MEF2 is required for KLF2 upregulation in the presence of flow, a dominant negative MEF2 adenoviral construct was infected in HUVECs. Basal KLF2 expression was unchanged, but upregulation of KLF2 after exposure to flow was prevented by the dominant-negative MEF2. Inhibition with a dominant-negative construct of upstream pathway member MAPK kinase 5 (MEK5) under flow conditions also failed to upregulate KLF2, and the downstream target ERK5 was also not activated. This reveals a molecular mechanism for

the flow response of KLF2 in which MEK5 is both sufficient and necessary for KLF2 upregulation [187]. Control of KLF2 expression by the MEK5/ERK5/MEF2 axis was separately demonstrated in mouse embryonic fibroblast cells as well as in T-cells. [191].

An additional factor that has been found to bind the KLF2 promoter and regulate shear stress response is nucleolin, a ubiquitous protein with many, varied functions as a transcriptional regulator [192]. Nucleolin acts on KLF2 via the PI3K signal transduction pathway and is required for induction of KLF2 by laminar shear stress in endothelial cells [193]. Histone deacetylase 5 (HDAC5) was also shown to play a role in flow-mediated KLF2 expression [194]. Fluid shear stress induced phosphorylation of HDAC5, which led to its nuclear export. HDAC5 is normally bound to the MEF2 gene and represses MEF2 transcription. Flow-dependent phosphorylation of HDAC5 allowed for derepression of MEF2 transcriptional activity and subsequent increase in KLF2 expression. Cells expressing a phosphorylation-null mutant of HDAC5 exhibited less HDAC5 nuclear export under flow and less MEF2 activity. KLF2 expression was suppressed. It was further shown that the HDAC5 N-terminal region directly interacts with the C-terminal domain of KLF2 protein to inhibit its transcriptional activity [195], suggesting both transcriptional and post-translational roles for HDAC5 in control of KLF2 function.

The direct relationship between fluid shear stress levels and KLF2 expression in the cardiovascular system has demonstrated implications in endothelial homeostasis and disease, namely atherosclerosis [196, 197]. Atherosclerosis is the build-up of plaque

in arteries and is associated with chronic inflammation of endothelial cells. Localization of plaque lesions is non-random and generally, they are distributed in areas of branching where there is disturbed or decreased flow. Disturbed flow induces a local, chronic, low-level inflammatory environment that is more atherosusceptible [198]. Regions with high shear stress arising from constant laminar flow are protected from atherosclerosis [199].

The critical role of KLF2 in shear stress response is well-documented in endothelial cells. Whether it plays a part in flow sensing and physiologic response in other tissues in which fluid flow is present remains an unanswered question. Pancreatic ductal cells, bile ducts in the liver, and lymphatic vessels are all sites of fluid flow, albeit at lower rates than in blood vessels. Lymphatic cells exposed to shear stress at much lower levels than employed in endothelial studies showed a significant increase in KLF2 expression, though more modest than seen in those vascular endothelial cells [200]. It would be expected that the coexistence of mechanical stress and KLF2 expression in these tissues would be linked, through causal signaling. However, data to this point demonstrate that low or disturbed flow causes a modest or even negative KLF2 profile. Nevertheless, it should be noted that in the vasculature, the default condition, or control, is high laminar flow. Therefore, the relative shear stress differential, i.e., static or very low flow, versus low or moderate flow, may result in relatively similar, though reduced, KLF2-derived signaling response mechanisms. The potential induction of KLF2 by shear stress in pancreatobiliary cell types is not yet reported.

Statins

Inhibitors of 3-hydroxy-3-methylglutaryl coenzyme A (HMG-CoA) reductase, or statins, are lipid-lowering compounds that are used in the treatment and prevention of cardiovascular disease. They have also been shown to have non-lipid-lowering, pleiotropic effects including anti-inflammation, reduction of reactive oxygen species, and improvement of endothelial function [201]. Studies have shown that statins induce KLF2 expression in vascular endothelial cells and that KLF2 is, at least in part, responsible for the non-lipid lowering atheroprotective effects in endothelial cells [202, 203]. An important branch point in the HMG-CoA pathway is the production of geranylgeranyl pyrophosphate or farnesyl pyrophosphate by their respective synthases. These are used to make isoprenoids, a large class of biomolecules that includes vitamins, heme, coenzyme Q, and importantly, cholesterol [204]. They are also important post-translational modifiers of Rho and Ras GTPases. Statin-induced increase in KLF2 expression was reversed in the presence of either HMG-CoA downstream metabolite mevalonate or geranylgeranyl pyrophosphate, but not farnesyl pyrophosphate. These data indicated that Rho proteins, which are mainly geranylgeranylated, negatively regulate KLF2 expression [202]. In support of these results, inhibition of Rho caused an increase in KLF2 expression, and conversely, overexpression of Rho led to reduced KLF2 expression [203]. Statins also have immunomodulatory effects, able to act on both the innate and adaptive immune response systems to reduce inflammation [205]. These properties were demonstrated as KLF2-dependent at least in part. Pro-inflammatory T-cell proliferation and function was reduced with a concurrent increase in KLF2

expression with statin treatment in human and mouse T-cells. Knockdown of KLF2 with shRNA prevented these statin-induced effects [206]. Unchecked immune activation is problematic in the liver as well, where chronic inflammation and fibrosis can lead to the end-stage condition cirrhosis. The anti-fibrotic and anti-inflammatory properties of KLF2 were mitigating in *in vitro* and *in vivo* liver cirrhosis models when KLF2 was overexpressed. Induced increase in KLF2 expression with statin treatment caused a reduction in the fibrotic markers α-SMA and procollagen I in activated human and rat hepatic stellate cells. Furthermore, increased KLF2, either by statin treatment or administration of a KLF2 adenoviral construct, ameliorated hepatic endothelium dysfunction and liver fibrosis in a cirrhotic rat model [207]. Taken together, the protective effects of statins extend beyond modulation of lipid levels, and it is clear that at least some pleiotropic effects can be attributed to the amplification of KLF2.

Regulation by microRNAs: 92a, 93, 106b, 150

One mechanism of control of KLF2 expression is through post-transcriptional regulation via the action of microRNAs. MicroRNAs regulate gene expression through sequence-specific binding to target mRNA transcripts. With over 1000 known human microRNAs, which often have from several to hundreds of transcript binding partners, an estimated 60% of human protein-coding genes are regulated by microRNAs [35]. Some microRNAs have been discovered to bind and functionally affect *KLF2* mRNA. Nearly all studies pertaining to microRNA regulation of KLF2 to date focus on endothelial cell biology, but there are emerging roles in cancer biology more recently,

including my research on miR-106b in cholangiocarcinoma, which can be found in Chapter 4.

miR-92a

Studies in human umbilical vein endothelial cells (HUVECs) showed that shear stress due to laminar flow could regulate miR-92a and in turn affect KLF2 levels. The KLF2 3' UTR contains a miR-92a binding site, and direct targeting was confirmed using luciferase reporter constructs. Overexpression of miR-92a led to reduced KLF2 levels while miR-92a inhibition caused an increase in KLF2 expression. In response to atheroprotective, or pulsatile flow, there was a decrease in miR-92a, which resulted in derepression of KLF2 [208]. In an atherosclerotic mouse model, *in vivo* blocking of miR-92a led to protection of endothelial function. Treatment of hypercholesterolemic *Ldlr*-/- mice with a miR-92a antagonist resulted in increased KLF2 expression in the aorta, resulting in reduced inflammation and decreased plaque size [209]. These studies are similar to the work described with use of statins, in that increased KLF2, either due to statin treatment or decreased microRNA-mediated inhibition, resulted in atheroprotection. MiR-92a was also shown to co-regulate both KLF2 and KLF4 expression in endothelial cells. Interestingly, miR-92a showed site-specific differential expression based on arterial region. It was highly expressed in athero-prone aortic arch compared to the athero-resistant descending thoracic aorta, and KLFs 2 and 4 displayed reciprocal expression [210]. These studies indicate an athero-promoting role for miR-92a

in atherosclerosis via KLF2 repression and reinforces KLF2 as an endothelial protector in cardiovascular function.

miR-93

Screening for potential regulators of endothelial activation including glycolysis and proliferation revealed miR-93 targeting of KLF2. Modulation of miR-93 levels followed by transcriptome screening by RNA-Seq revealed KLF2 to be significantly decreased by miR-93 in HUVECs. These studies also revealed miR-93 control of endothelial proliferation and glycolysis. Previously, repression of endothelial glycolytic metabolism was shown to be mediated by flow-induced KLF2 expression. Further, these effects were mediated by KLF2-directed suppression of 6-phosphofructo-2-kinase/fructose-2,6-biphosphatase 3 (PFKFB3), a potent stimulator of glycolysis [211]. MiR-93 suppression of KLF2, a glycolysis inhibitor, was therefore hypothesized to be responsible for the overall observed increased glycolysis in endothelial cells [212]. Interestingly, however, it was also found that miR-93 could target and repress PFKFB3. Biotin pull-down assays confirmed direct binding of PFKFB3 and KLF2 transcripts by miR-93. Thus, miR-93 appears to regulate endothelial activation by targeting either KLF2 (the inhibitor), or PFKFB3 (the activator), depending on their relative expression levels. A role for KLF2 in quiescence of these cells was also described [212]. It is of note that miR-93 shares the same seed binding sequence as miR-106b, the next microRNA on our list.

miR-106b

MiR-106b is clustered together with miR-93 and miR-25. We have investigated the target landscape of miR-106b in cholangiocarcinoma. Genome-wide transcriptome analysis of a cholangiocarcinoma cell line revealed miR-106b targeting of several members of the KLF family including KLF2. Binding and repression of KLF2 by miR-106b was verified through multiple methods at mRNA and protein levels. Increased expression of miR-106b led to protection from apoptosis. The individual role of KLF2 among miR-106b targets in apoptotic regulation was not tested, but we postulate that KLF2 may play a role in the tumor biology of cholangiocarcinoma [77].

miR-150

An osteoarthritis study investigating the effect of the pro-inflammatory cytokine IL-1 on chondrocytes found that miR-150 expression was increased in response to IL-1, and that miR-150 was responsible for some IL-1's damaging effects. Cell death and expression of pro-inflammatory cytokines in response to IL-1 treatment could be aggravated or ameliorated either by increasing or suppressing miR-150, respectively. KLF2 expression was then shown to be reduced by miR-150 and demonstrated as a miR-150 target by luciferase assay in chondrocyte cells. Further, careful experiments described an inverse expression status and function between miR-150 and KLF2. Overall, KLF2 was a protective factor in chondrocytes and suppressed IL-1-mediated miR-150 cell injury [213]. Curiously, KLF2 was shown to promote miR-150 expression in

macrophages [214]. This suggests different molecular roles for KLF2 depending on cell type or a potential regulatory loop.

KLF2 in cancer

Krüppel-like factors regulate varied cell processes including proliferation, apoptosis, differentiation, and migration. In addition to contribution to normal cell functions, many KLF members have important roles as tumor suppressors or oncogenes [215]. KLF2 has emerging roles in several cancer types as well. While KLF2 mutations are seen in splenic marginal zone lymphoma [216], there are no evidence of mutations in human solid tumors; instead, KLF2 often has significantly reduced expression in many cancer types. KLF2 is significantly downregulated in ovarian tumors compared to normal tissue. Re-expression in ovarian cancer cell lines reduced proliferation and increased sensitivity to DNA damage-induced apoptosis. WEE1, a nuclear kinase involved in cell cycle progression, was shown to be repressed by KLF2, and WEE1 was at least part of the mechanism through which KLF2 regulated proliferation and apoptosis in ovarian cancer cells [217]. Another transcriptional target of KLF2 is the cancer metastasis-associated chemokine CXCR4. In oral squamous carcinoma cells, treatment with vesnarinone, a quinolone derivative with chemotherapeutic properties [218], inhibited migration and lymph node metastasis, and caused an increase in KLF2 expression. Vesnarinone significantly inhibited CXCR4 expression in these cells. ChIP experiments then showed that KLF2 could bind to the CXCR4 promoter and decrease its expression, contributing to reduced cell migration and lymph node metastasis in an oral

squamous cell carcinoma model [219]. KLF2 was suppressive of cancer cell growth in leukemia cells as well. Inducible expression of KLF2 contributed to cell cycle arrest, and this effect was demonstrated to be through the activation of p21. Additionally, both the activation and inhibitory domains of KLF2 were required for the cell growth inhibition [220]. Other cancers that have downregulated KLF2 expression include pancreatic ductal adenocarcinoma [221] and breast cancer [222]. These studies examined the tumor suppressive features of KLF2 by way of some of its transcriptional targets. Post-translational modification and epigenetic silencing are other mechanisms through which cancer cells stifle the anti-tumorigenic activities of KLF2.

KLF2 is known to be regulated via ubiquitination and proteasomal degradation [176]. This mechanism has been shown to be employed in lung cancer cells to reduce KLF2 expression. Specifically, the ubiquitin ligase Smurf1 directly targeted KLF2 for ubiquitination and degradation, and depletion of Smurf1 resulted in upregulation of KLF2 protein [223]. Similarly, a regulatory pathway involving post-translational modification of KLF2 was initially identified in endothelial cells and then in a tumor model. Endothelial function was impaired through negative regulation of KLF2 by F-box and WD repeat domain-containing 7 (FBW7), the substrate recognition member of the SKP1-cullin-1-FBW7 E3 ubiquitin ligase complex. FBW7 was verified as an E3 ubiquitin ligase for KLF2, and sequence analysis revealed two conserved CDC4 phosphodegrons (CPDs), the recognition sites contained in most FBW7 substrates. Next, the kinase responsible for phosphorylation of KLF2 was determined to be glycogen synthase

kinase-3 (GSK3) and further, that phosphorylation of KLF2 by GSK3 at the CPDs was necessary for interaction with FBW7, which polyubiquitinated KLF2 thereby directing its degradation via the proteasome. FBW7 promoted endothelial cell migration and angiogenesis through the degradation of KLF2. Lastly, using an inducible knockdown system in a mouse teratoma model, FBW7-mediated degradation of KLF2 was shown to be required for tumor growth [224, 225].

An additional mechanism by which KLF2 is regulated in cancer is through epigenetic silencing. In *Drosophila*, the protein Zeste was identified as a sequence-specific DNA binding protein that contributes to the repressive function of the polycomb complex [226]. Mammals lack Zeste and instead utilize lncRNAs that bind in a sequence-specific manner to DNA and recruit the polycomb repressive complex 2 (PRC2) to sites for epigenetic silencing. Enhancer of zeste homolog 2 (EZH2) is the major functional enzyme in the PRC2 complex. EZH2 is a histone methyltransferase enzyme and a transcriptional repressor that is often overexpressed or mutated in cancer [227]. Epigenetic silencing of KLF2 was mediated by EZH2-driven trimethylation of the KLF2 promoter region. The EZH2 inhibitory effect on KLF2 was seen in osteosarcoma, breast and prostate cancer cell lines. Moving forward with osteosarcoma cells, it was revealed that KLF2 enforced expression caused increased apoptosis and reduced cell viability both *in vitro* and *in vivo*. Lastly, breast and prostate cancer patient expression data revealed that low KLF2 and high EZH2 were correlated with shorter overall survival [228]. Another group investigating a different component of PRC2, suppressor of zeste

12 (SUZ12), found that it was overexpressed in gastric cancer cells. SUZ12 reduced apoptosis and promoted cancer cell proliferation, invasion, and metastasis. They then investigated potential silenced targets responsible for the observed effects. When SUZ12 was knocked down, there was an increase in KLF2. However, no data directly linked KLF2 expression or activity with the observed features of gastric cancer cells in this case [229]. In addition to silencing by EZH2-mediated H3K27 trimethylation, it was observed that KLF2 transcription was suppressed by H3K4 demethylation resulting in reduced proliferation and invasion in gastric cancer cells [230]. Finally, region-specific hypermethylation of histones located on the KLF2 promoter was responsible for reduced KLF2 expression in non-small cell lung cancer cell lines and tissues, promoting malignant features [231].

After the pioneering work of the Taniguchi group, the relationship between EZH2 and KLF2 in cancer has since been examined in several cancer types. Importantly, many of these reports describe a role for long non-coding RNAs (lncRNAs) in the promotion of tumorigenesis. In fact, more than a dozen different lncRNAs have been specifically characterized as tumor promoters via interaction with EZH2 subsequent suppression of KLF2 [232-244]. This oncogenic lncRNA-EZH2-KLF2 axis has been observed in gastric, non-small cell lung, pancreatic, and colorectal cancer cell types thus far. One example is the lncRNA HOXA11-AS, which promoted gastric cancer tumorigenesis by recruiting EZH2 as well as the histone DNA methyltransferase DMNT1 and functioning as a scaffold to repress KLF2 transcription [237]. These studies

together suggest that KLF2 is often epigenetically silenced via EZH2-PRC2, a promiscuous DNA/RNA binding protein complex, and many lncRNAs can recruit and guide this regulatory complex to its targets, and act as a scaffold to mediate transcriptional repression.

While the vast majority of research into the role of KLF2 in cancer suggests an anti-tumorigenic profile, there is a conflicting report in a hematologic malignancy that depicts KLF2 not as a tumor suppressor but rather as a tumor promoter. Ohguchi et al. established KLF2 as important for the survival of multiple myeloma cells. Knockdown of KLF2 increased cleaved forms of initiator caspases and inhibited cell growth while increased KLF2 expression promoted cell growth. Stably transduced shKLF2 multiple myeloma cells injected subcutaneously in SCID mice developed significantly smaller tumors than control cells over 8 weeks [245]. While the majority of studies to date indicate a tumor suppressive role for KLF2, there are some data that suggest it can promote a more malignant phenotype. This differing biologic character could be a result of cell type specificity, broadly including solid tumors versus hematopoietic malignancies, or differences in tumor environment.

Primary cilia

Cilia are microtubule-based organelles that are classified into two types, motile, and immotile or sensory. The sensory cilia are also called primary cilia and they are present on almost every mammalian cell. These non-motile structures were discovered

over a century ago but were long considered vestigial. Investigation into biological function and relevance has only gained prominence in the last few decades. The primary cilium is now known to be an essential organelle responsible for sensing extracellular mechanical and chemical stimuli and transducing that information to the cell's interior. The functional importance of cilia in normal cell biology is reinforced by the existence of several human disorders that manifest through the disruption of cilia activity. Collectively, these disorders are called ciliopathies. Through a complex interplay of various channels and receptors, effector and transport proteins and their downstream targets and intracellular pathways, primary cilia exist as signaling antennae that connect and facilitate interaction between the cell and its environment.

Structure

Primary cilia are elongated, solitary, specialized structures that protrude into the extracellular space and have a high surface-to-volume ratio, which is thought to allow for efficient signal amplification [246]. As an extension of the cell membrane with a microtubule-based cytoskeletal core, they are architecturally robust but also flexible and dynamic. The structural core of a cilium consists of nine microtubule doublets organized radially in a symmetrical column at the cilium periphery termed the axoneme. Motile cilia have an extra, central microtubule pair and the arrangement is referred to as 9 + 2, while the primary cilium axoneme is 9 + 0 and forms an empty interior lumen. Motile cilia have additional machinery to allow for movement, including radial spokes interconnecting the microtubules as well as dynein arms to generate force [247]. The

axoneme extends directly from a basal body, which is derived from the mother centriole and serves as a microtubule organizing center [248]. Surrounding the axoneme is the ciliary membrane, which although it is extended from and continuous with the plasma membrane, has a distinct compositional makeup, with an enrichment in transmembrane signaling receptors to allow for response to external stimuli [249]. The phospholipid profile for the ciliary membrane is distinct from the contiguous plasma membrane. Specifically, phosphoinositides define subcellular membranes based on ratios of specific species [250]. The plasma membrane is rich in phosphatidylinositol 4,5-bisphosphate, PI(4,5)P2 and phosphatidylinositol 4-phosphate, PI(4)P, while the ciliary membrane contains mostly PI(4) [251]. The species of phosphoinositide helps determine the complement of cilia-interacting proteins.

Ciliary signaling

Many signaling molecules are implicated in association with the primary cilium. There are estimated to be over 1000 proteins involved in the structure or function of cilia [252]. The pathways through which cilia participate in signal transduction are diverse and still under investigation, including Hedgehog, Hippo, G-protein coupled receptors, Wnt, Notch, mTOR, platelet-derived growth factor receptor (and other receptor tyrosine kinases including fibroblast growth factor receptors), and TGFβ [249, 253]. The ciliary membrane is specialized and an array of receptors and ion channels locate to it. The specific localization of proteins and enrichment of receptors and channels to the primary

cilium create a nexus of signal transduction pathways for the cell with the cilium at its center [254, 255].

Ciliogenesis

Cilium formation is a dynamic, highly regulated, and complex process. Ciliogenesis is tightly linked to cell cycle progression. Cilia are disassembled before the cell divides and the centrioles are passed to the daughter cells, where they act as templates for new cilia formation. Cilia are usually formed in G0 or G1 and disassembled at mitosis [256]. Assembly occurs in a stepwise manner. First, the centriole forms the basal body, which then docks onto the actin cortex at the inner face of the plasma membrane. Growth of the axoneme is dependent on recruitment of proteins from the cytoplasm. The basal body nucleates microtubule extension while the membrane extends [256]. A specialized transport system called intraflagellar transport (IFT) based on molecular motors allows for selective trafficking of proteins required for cilium elongation. IFT is a dynamic process for bidirectional movement of axonemal components, ciliary membrane proteins, and proteins for signal transduction, using anterograde kinesin motor proteins and retrograde dynein motor proteins [257]. After elongation is complete, the cilium is actively maintained by a steady-state assembly/disassembly of tubulin filaments at its tip. This ongoing and active turnover determines cilium length and also allows for regulated ciliary resorption [258].

The cholangiocyte primary cilium

The existence of primary cilia on cholangiocytes has been long recognized, but their role in bile duct biology has been unclear until recently. The first description of the cholangiocyte cilium occurred over half a century ago, and the sparse information produced for the subsequent few decades was largely descriptive only [259-261]. Not until 15 years ago was a functional role for primary cilia in cholangiocytes reported [262]. The pioneering investigations into cilia functions were in kidney cells, through studies of polycystic kidney disease (PKD), a genetic disorder that causes abnormal renal tubule structure and the formation of cysts [263]. In addition to kidney pathology, extrarenal manifestations of PKD commonly include hepatic cysts [264] and liver fibrosis in addition to biliary dilatation characteristic of Caroli's disease [265]. Currently, evidence suggests that the primary abnormality leading to dysfunction in PKD results from defects in primary cilia [266]. Two types of murine models have been important for the study of PKD, spontaneous hereditary models that display similar features of PKD, and engineered models that modify human orthologs of genes coding for cilia-localizing proteins such as *cpk*, *orpk*, *inv* in mice and *pck* in rat [267, 268]. The *pck* rat contains a mutation in *Pkhd1*, the gene responsible for autosomal recessive polycystic kidney disease (ARPKD) in humans. Rats with this mutation develop liver injury in the form of fibrosis and cysts, similar to the clinical presentation of ARPKD in humans [269, 270]. Additionally, PKD rat livers displayed a striking increase in cholangiocyte proliferation and remodeling of the biliary tree. Cilia from mutant cholangiocytes were structurally

abnormal, significantly shorter than in normal cholangiocytes, and had bulbous extensions of the ciliary membrane [271].

Signaling and function of primary cilia in cholangiocytes.

Cilia extend from the apical membrane of cholangiocytes into the ductal lumen. Studies in renal cells gave the first clues that primary cilia possess sensory function. The first investigation of primary cilia in cholangiocytes as sensory organelles used a model to induce luminal flow and test their capacity as mechanosensors. Isolated intrahepatic bile duct units (IBDUs) from Fisher 344 rats allowed for manipulation of artificial luminal flow via microperfusion, followed by measurement of intracellular signaling [272]. Principal findings from these experiments demonstrated that luminal flow induced increased intracellular levels of Ca^{2+} and decreased cAMP signaling, and that these changes were a result of bending of the cilia. The mechanosensory ciliary proteins polycystin-1 (PC1), a cell-surface receptor, and polycystin-2 (PC2), a calcium ion channel, were shown to localize to cilia and to be responsible for the flow-induced increase in intracellular Ca^{2+} and cAMP decrease was secondary to calcium influx. Lastly, adenylyl cyclase isoform 6 (AC6), which was present on cilia, was the Ca^{2+}-inhibited protein responsible for cAMP suppression. While the downstream functional response was not yet determined in this study, it was later shown that expression of cilium-localized PC-1 and PC-2 was inversely correlated with increased rat cholangiocyte proliferation (induced in this study by 17β-estradiol). This indicated that primary cilia might act as modulators of cholangiocyte proliferation by responding to

cell injury [273]. Specifically, reduced cilium-dependent signaling permitted increased proliferation.

In addition to mechanosensation, cholangiocyte primary cilia can act as osmosensors. It was reasoned that transient receptor protein member TRPV4, a cation channel that is activated by changes in fluid tonality, might be important in ciliary signaling, as it has been shown to be a player in signal transduction of osmotic stimuli [274]. It is expressed on cholangiocyte cilia and was shown to respond to hypotonicity and channel an influx of extracellular Ca^{2+}. This induced secretion of bicarbonate, the primary factor for formation of bile, (by increasing water efflux following bicarbonate), through a mechanism involving ATP release [275]. Research into the chemosensory properties of cholangiocyte cilia first focused on purinergic receptors both because ATP and ADP function as extracellular signaling molecules in bile [276], and based on the previous study, which revealed the cAMP signaling pathway member AC6 to be present and functional in ciliary signaling [272]. Employing rat cholangiocytes, it was demonstrated that purinergic receptor $P2Y_{12}$ is expressed on cholangiocyte cilia. $P2Y_{12}$ is a G_i-protein coupled receptor that is activated in cholangiocytes most potently by ADP and to a lesser degree by ATPγS, a non-hydrolyzable analog of ATP. Forskolin, an activator of adenylyl cyclase enzymes, was used to increase intracellular cAMP levels. Treatment with ADP or ATPγS attenuated the increase in forskolin-stimulated cAMP levels in normal rat cholangiocytes. Suppression of $P2Y_{12}$ with siRNA or inhibitor prevented the effects of ADP to reduce cAMP. Lastly, removal of cilia by pretreatment

with chloral hydrate abolished the purinergic effect on cAMP levels. Together, these data showed ADP-induced cAMP signaling occurred specifically via $P2Y_{12}$ receptors in cholangiocytes and that this signaling was dependent on primary cilia [277].

Further investigation into cholangiocyte ciliary signaling examined exosomes as signaling vesicles. The LaRusso group, again using a rat model, showed that exosomes attached to cilia in intrahepatic bile ducts *in vivo*. They then isolated exosomes and added them to cholangiocytes *in vitro*, to show that these exosomes increased miR-15a expression and caused a decrease in cholangiocyte cell proliferation. Antisense miR-15a or chloral hydrate were used to inhibit this cilium-initiated signaling and the proliferative response was altered. Finally, ERK signaling was examined based on its involvement in cholangiocyte function [278]. Exosome treatment decreased phospho-ERK to total-ERK ratios by more than 60% and this result was dependent on the presence of cilia. It was not addressed if the observed miR-15a and ERK signaling effects were related or dependent on one another. These data revealed exosomes to be another important signaling component in bile for intracellular communication dependent on cholangiocyte primary cilia [279].

Additional examination of cAMP and ERK signaling in cholangiocytes focused on TGR5, a G protein-coupled bile acid receptor known to be involved in cholangiocyte signaling, including bile acid proliferative response and cAMP activation [280]. Subcellular location of TGR5 can vary from the apical membrane, the nuclear membrane, and the ciliary membrane. Specific localization of TGR5 to subcellular

compartments seemed to be important to its functional response. When activated in ciliated cells, TGR5 decreased cAMP levels, activated ERK and inhibited proliferation. However, the opposite changes were observed in non-ciliated cholangiocytes. These opposed results were then shown to be associated with differential coupling of TGR5 to specific G proteins, $G\alpha_i$ in ciliated cells and $G\alpha_5$ in non-ciliated cells [281]. These data provide further evidence of the complexity and context dependence of cilia signaling in cholangiocytes. Taken together, the primary cilium in the bile duct acts as a mechano-, osmo-, chemo-, and exosomal-sensory organelle with diverse and physiologically important signaling functions.

Primary cilia and cholangiocarcinoma

The regulatory role of the primary cilium in the cholangiocyte depends on its ability to detect signaling molecules in bile and changes in luminal flow, which can be transduced into functional cellular responses, including secretion of bile, proliferation, and apoptosis. Some of the molecular pathways dysregulated in cholangiocarcinoma are associated with loss of cilia [282]. Primary cilia have been shown to be reduced or absent in cholangiocarcinoma cells [283, 284]. However, the mechanisms responsible for deciliation, and whether the lack of cilia is a contributing factor in cholangiocarcinoma or a consequence, requires further investigation. One such mechanism that was identified involved histone deacetylase 6 (HDAC6). When HDAC6 expression was enforced in normal cholangiocytes, the cells had decreased cilia expression and displayed a more malignant profile, with increased proliferation and anchorage-

independent growth. Conversely, when HDAC6 was targeted for inhibition in malignant cells, cilia expression was restored and this correlated with a decrease in proliferation and invasion. Lastly, treatment with the selective HDAC6 inhibitor tubastatin-A in a rat orthotopic model of cholangiocarcinoma led to decreased tumor growth and an increase in frequency of ciliated malignant cholangiocarcinoma cells [283]. These data are the first to describe a potential role for primary cilia in cholangiocarcinoma pathogenesis and were interpreted as an implication of the cilium as a tumor-suppressive organelle.

The disparate expression of cilia (lost in malignant cells) was confirmed in a subsequent study that examined Hedgehog signaling in cholangiocarcinoma cells [284]. Aberrant Hedgehog signaling is characteristic of many cancers including cholangiocarcinoma [285, 286]. However, canonical Hedgehog signaling requires translocation of a transmembrane receptor protein to the cilium where it can then activate transcription factors, and as demonstrated, the cilia in these cells are lost [287]. This paradox was unraveled in part through demonstration of a non-canonical, cilia-independent Hedgehog signaling pathway that was employed by cholangiocarcinoma cells [284].

Additional efforts from the Gradilone laboratory recently have further defined the mechanisms of regulation of primary cilia in cholangiocarcinoma and in addition, illuminated ciliary signaling pathways involved in the control of disease progression. As a follow-up to their previous study [283], they examined post-transcriptional

mechanisms of HDAC6 regulation by microRNAs. Two HDAC6-targeting microRNAs, miR-433 and miR-22, were shown to be downregulated in cholangiocarcinoma cells and tumors. Restoration of these microRNAs in cholangiocarcinoma cells resulted in reduced proliferation, colony formation, and migration, in addition to decreased HDAC6 expression and increased ciliogenesis. Deeper interrogation revealed the microRNA processing nuclear transport protein Exportin-5 to be reduced in cholangiocarcinoma cells. Experimental manipulation of Exportin-5 levels to increase expression showed that it could increase the export of microRNAs, allowing cytoplasmic processing of HDAC6-targeting microRNAs -433 and -22 to their mature form, thereby suppressing HDAC6 and reducing malignant features in a cholangiocarcinoma cell line. Alternatively, knock down of Exportin-5 in normal cholangiocytes reduced ciliary length and increased proliferation [118]. In the next study, they outlined a role for the chemosensory function of cholangiocyte cilia in the regulation of cell migration and invasion. As a component of bile, nucleotides are important autocrine and paracrine signaling molecules in cholangiocytes that are sensed by purinergic receptors localized in the primary cilium [277]. ATP signaling in ciliated cells reduced migration and invasion. In contrast, ATP stimulated migration and invasion in experimentally deciliated cells and cholangiocarcinoma cells without cilia. The Gradilone lab went on to investigate LKB1, a serine/threonine kinase that is responsible for maintenance of cell polarity and a negative regulator of migration. The ciliary-dependent regulation of cholangiocarcinoma cell migration and invasion was driven by LKB1 activation via phosphorylation. LKB1 activation regulated the PTEN-PI3K-AKT signaling axis to inhibit F-actin and filopodia

formation. Finally, activation of LKB1 mimicked the chemosensory function of cilia and reduced cholangiocarcinoma malignant features *in vitro* and *in vivo* [288]. Together, these results describe a signaling axis in cholangiocytes in which ciliary-dependent nucleotide induction of LKB1 regulates cell migration and invasion through PTEN-PI3K-AKT control of cytoskeleton rearrangement.

Summary

This introduction serves as an abbreviated and selective review of the relevant literature to date concerning cholangiocyte biology, and in particular the malignant manifestation thereof, cholangiocarcinoma. Chapter 3 reports on some of the aberrant growth and evasion of cell death characteristics of cholangiocarcinoma with investigation of a small-molecule inhibitor of X-linked inhibitor of apoptosis, XIAP. Next, the function of microRNAs as posttranscriptional regulators of their mRNA targets, and specifically their dysregulation in cancer was addressed. Chapter 4 contains a focused examination of microRNA 106b specifically, and its target landscape (including members of the KLF family) in cholangiocarcinoma. A focused review of the available literature on the function and regulation of KLF2 showed features of this transcription factor as a flow responder and tumor suppressor that is often dysregulated in cancer. Finally, the primary cilium is a multi-sensory organelle with important functions in the maintenance of biliary homeostasis that are relevant to its malignant state. Chapter 5 attempts to synthesize the biological functions of cilia and KLF2 as potentially coordinated members within a signaling axis, and to link their altered expression between the normal and malignant biliary cell.

Chapter 2 - Materials and methods

Cell lines

Human cholangiocarcinoma cell lines were previously derived from a female patient with metastatic gallbladder cancer, Mz-ChA-1 [289], a male patient with combined histologic features of hepatocellular carcinoma and cholangiocarcinoma, KMCH [290], and from the malignant cells of ascites from a male patient with intrahepatic cholangiocarcinoma, HuCCT-1 [291], a bile duct carcinoma of a male patient, OZ [292], and an extrahepatic cholangiocarcinoma tumor, EGI-1 [293]. Recently-derived patient cholangiocarcinoma cell lines ICC2, ICC3, ICC8, and ICC11 were from resected intrahepatic cholangiocarcinoma tumors [294]. BDEneu rat cholangiocarcinoma cells were derived from primary Fisher 344 rat cholangiocytes [295]. H69 cells are an SV-40 transformed non-malignant immortalized cholangiocyte cell line [296]. NHC cells are normal human cholangiocytes isolated from normal tissue during surgical dissection of a local hepatic adenoma in a female patient [297]. HEK293T cells are human embryonic kidney cells transformed with adenovirus type 5 [298]. Human umbilical vein endothelial cells (HUVECs) were purchased from American Type Culture Collection (ATCC CRL-1730). Cholangiocarcinoma cells and HEK293T cells were grown in Dulbecco's modified Eagle medium (DMEM) supplemented with 10% fetal bovine serum (FBS), insulin (0.5 μg/mL) and G418 (50 μg/mL). Recently-derived patient cell lines were grown in Roswell Park Memorial Institute (RPMI) medium supplemented with 20% FBS, 1% L-glutamine, 1% MEM non-essential amino acids solution, 1% sodium pyruvate, 50 μg/mL G418, and 5 μg/mL insulin on collagen-coated culture dishes. H69

and NHC cells were grown in DMEM supplemented with 10% FBS, insulin (5 μg/mL), adenine (24.3 μg/mL), epinephrine (1 μg/mL), T3-T (triiodothyronine (T3)-transferrin (T), [T3- 2.23 ng/ml, T-8.19 μg/mL]), epidermal growth factor (9.9 ng/mL) and hydrocortisone (5.34 μg/mL). HUVECs were grown in F-12K medium with 10% FBS, 0.1 mg/mL heparin, and 5 mL endothelial cell growth supplement (ECGS, BD Biosciences). Cholangiocarcinoma is a rare cancer and there is no central source of cholangiocarcinoma cell lines to be used as standards for validation by genetic testing. We employ immunostaining for keratin-19, an intermediate filament protein and marker of cholangiocyte differentiation to indicate that a cell is cholangiocyte derived. Additionally, all members of the lab are trained to identify the unique cell morphologies of the cholangiocyte cells when grown in standard culture conditions and to monitor cell appearance with each experiment.

Tissue isolation

Frozen samples were obtained from patient-resected normal liver or cholangiocarcinoma tumor tissues aquired from the UNMC Tissue Bank. Samples were kept frozen until isolation and all materials for isolation were sterile or bleached and rinsed, and then chilled with liquid nitrogen or dry ice before contact with tissues. Tissues were transferred from dry ice to a mortar containing a small volume of liquid nitrogen and ground to a fine powder with a chilled pestel. Samples were lysed in RNA lysis buffer (mirVana, see RNA transfection methods), or protein lysis buffer (see Immunoblotting methods), and immediately frozen in a dry ice/isopropanol bath or used for isolation by the traditional protocols described.

RNA transfection

Cells were transfected either with mature miR-106b mimic (Life Technologies), locked-nucleic acid (LNA) antagonist to miR-106b, LNA-106b (Exiqon), or LNA Negative Control A (Exiqon) for 24-48 hours using Lipofectamine RNAiMAX (Thermo Fisher) to a final oligonucleotide concentration of 20 nM. MiR-106b levels were quantified by TaqMan Small RNA assay (Life Technologies). siRNA against KLF2 (ID: 116130, Ambion), IFT88 (ID: 149319, Ambion), or Negative Control siRNA (Cat# 1027310, Qiagen) were reverse-transfected using Lipofectamine RNAiMAX to a final oligonucleotide concentration of 20 nM by seeding cells directly onto the transfection reaction.

RNA-Seq

High-quality total RNA was extracted from Mz-ChA-1 cells transfected with either miR-106b (n=3) or LNA-106b (n=3) for RNA-Seq using RNeasy Mini Kit (Qiagen). The quality of the RNA was established by RNA Integrity Analysis using an Agilent Bioanalyzer. RNA sequencing libraries were prepared by the UNMC Next Generation Sequencing Core Facility beginning with 1 μg of total RNA and a TruSeq RNA Prep V2 (Illumina Inc., San Diego, CA). Samples were sequenced using the Illumina HiSeq 2000 system with 100 bp paired-end reads. An average of 76.99 million reads per sample were collected (range 58.99-87.00 million).

Sequences were analyzed by the Bioinformatics and Systems Biology Core at the University of Nebraska Medical Center (UNMC) using the Tuxedo protocol [299]. Reads

were mapped to the human genome using Top Hat. Transcripts were assigned by Cuff links and the transcriptome defined using Cuffmerge. Finally, differential expression between miR-106b and LNA-106b was calculated with Cuffdiff. Sequencing data have been deposited to the NCBI as BioProject PRJNA355109.

Using a false discovery rate (FDR)-corrected p value, genome-wide transcripts were ranked from most significant to least. This ranked list of genes was submitted to the SylArray online server to detect enrichment of microRNA seed-binding sites [300].

MiR-106b binding site analysis

RefSeq sequences for the 129 significant genes (112 decreased and 17 increased) were collected in Fasta format and analyzed by direct search for the known miR-106b binding site as well as subjected to k-mer analysis to generate a k table of all possible 7-mer and 8-mer sequences and their frequency in this gene set. Several genes had more than one RefSeq sequence, so the final size of this Fasta file was 191 transcripts. For comparison, 1,000 random sets of 191 transcripts each from the RefSeq database were generated.

RNAhybrid [301] was used to identify the single best miR-106b predicted binding site for each decreased transcript based on minimum free energy hybridization. The resulting miR-106b-binding sites were manually curated for discovery of ungapped motifs using MEME Suite [302].

Quantitative reverse-transcription PCR

Total RNA for mRNA qRT-PCR was isolated using TRIzol Reagent (Life Technologies). Two micrograms of RNA were reverse-transcribed using Moloney leukemia virus reverse transcriptase and random hexamers. Quantitative real-time PCR was performed using SYBR Green DNA binding (Roche). RNA for microRNA measurement was extracted using lysis in chaotropic salt and acid phenol:chloroform (miRVana, Life Technologies). Fifteen nanograms of RNA was converted to cDNA using specific primers for miR-106b or Z30 (Applied Biosystems). qRT-PCR was performed using RedTaq master mix (Applied Biosystems) and specific TaqMan primers (Applied Biosystems) on an iCycler (BioRad) thermocycler. Relative RNA expression was calculated using the delta CT method. Primer pairs are listed in **Table 2.2**.

Table 2.1 Primers used for qRT-PCR

Gene	Forward Primer (5' -> 3')	Reverse Primer (5' -> 3')
RB1	GTCGTTCACTTTTACTGAGC	TCCAATTTGCTGAAGAGTGC
ITGA2	GAGTGGCTTTCCTGAGAACC	CTGGTGAGGATCAAGCCGAG
M6PR	GATTCTGAGCTTTGGCTACT	GTCTGCCAGGATTCTCTCAC
PSD3	CTGGCGATGGAAGATGGAAG	CATATTTGGCCTTGGCAACAC
GLO1	GATACTGCAGCGCAGCCATG	CCAGTGACTTCTTAGGATCC
EREG	GTCCTCAGTACAACTGTGAT	GACACTTGAGCCACACGTGG
RRM2	TCTGCTTCGCTGCGCCTCCA	TGGAAGATCCTCCTCGCGGT
HRAS	CCATCCAGCTGATCCAGAAC	TGTCCAACAGGCACGTCTC
ITGA3	TGCGTCGTCTCCGCCTTCAA	CATCCGCTCACAGTCATCCT
NCEH1	GAAGCTGATGCTGCTGGACG	AACACTCTGACTTCCACACC
FOS	GCCTAACCGCCACGATGATG	GGACTGGTCGAGATGGCAGT
IL8	CAAGAGCCAGGAAGAAACCA	ATTTGGGGTGGAAAGGTTTG
KLF2	ACTCACACCTGCAGCTACGC	GCACAGATGGCACTGGAAT
KLF4	CAGAGGAGCCCAAGCCAAAG	CCAGTCACAGTGGTAAGGTT
KLF6	CTGCCGTCTCTGGAGGAGT	TCCACAGATCTTCCTGGCTGTC
KLF10	ACCAAACGAGTCTGGACAGT	TCAGATACTGGTGTAACAGG
KLF11	ACTGTGCATATGGATGCAGC	TACGGCAGAGGACTGGAGAA
KLF13	CTCAAGGCGCACCTGAGAAC	GTCAGGTGGTCGCTGCGCAT
18S	CGTTCTTAGTTGGTGGAGCG	CGCTGAGCCAGTCAGTGTAG

Table 2.1. Primers used for qRT-PCR

MicroRNA biotinylation

Mature microRNA for *C. elegans* microRNA 67 (control) and *H. sapiens* microRNA 106b (both leading and passenger strand) were obtained from Integrated DNA Tech, Coralville, IA. Biotinylation of Cel-miR-67 and miR-106b was performed as described [303]. The leading strands of Cel-miR-67 and human miR-106b were biotinylated at the 3′ ends using T4 RNA ligase enzyme. Briefly, biotin-conjugated cytidine (bis) phosphate was incubated with the microRNAs overnight at 16 °C with T4 RNA ligase reaction mixture, followed by a 30 minute incubation at 37 °C. Chloroform:isoamyl alcohol was used to separate the RNA ligase from the aqueous phase containing RNA. The biotinylated RNA in the aqueous phase was ethanol-precipitated using Pierce RNA 3′ End Biotinylation Kit (Thermo Scientific, Cat #20160). Labeled biotinylated RNA was quantified by dot blot (hybond N+, a positively charged nylon membrane) using a known concentration of biotinylated control RNA, and detected using streptavidin-HRP-conjugated antibody. An equal amount of biotinylated mature microRNA (leading strand) was mixed with its respective passenger strand RNA.

Pull-down of biotinylated RNA

Mz-ChA-1 cells were transfected in triplicate with 50 nM of biotinylated Cel-miR-67 or biotinylated miR-106b using Lipofectamine RNAiMAX. After 24 hours of transfection, cells were lysed in lysis buffer (20 mM Tris, pH 7.5, 100 mM KCl, 5 mM $MgCl_2$, 0.3% NP40, 50 U of RNase OUT (Life Technologies) and complete protease inhibitor) and incubated on ice for 10 minutes. Prior to the addition of cell lysate, beads

were blocked with 1 mg/mL of yeast tRNA and 1 mg/mL BSA in lysis buffer and then washed 6 times with lysis buffer only. Ninety percent of cell lysate was incubated with streptavidin magnetic beads (New England Biolabs) for 6 hours at 4 °C and 10% of cell lysate was used for input RNA extraction using TRIzol reagent. Streptavidin magnetic bead-bound biotinylated RNAs were washed five times with wash buffer containing 20 mM Tris, pH 7.5, 0.5 M NaCl and 1 mM ethylenediaminetetraacetic acid (EDTA). Biotin-bound RNA was isolated from the miR-106b- and Cel-miR-67-transfected Mz-ChA-1 cells using mirVana kit. Relative expression values of miR-106b targets (IL8, KLF2 and αTubulin1A) were analyzed by qRT-PCR. 18S was used as a control RNA.

Immunoblotting

Cells were lysed in lysis buffer containing 50 mM Tris-HCl (pH 7.4), 150 mM sodium chloride, 1 mM EDTA, 1 mM DTT (dithiothreitol), 1 mM sodium orthovanadate, 100 mM sodium fluoride, and 1% Triton X-100 (w/v) supplemented with complete protease inhibitors (Roche). Lysates were incubated on ice for 15 minutes and vortexed at 5-minute intervals. After lysis, insoluble proteins were removed by centrifugation at 15,700 *g* for 10 minutes. Soluble protein was resolved by sodium dodecyl sulfate-polyacrylamide gel electrophoresis (SDS-PAGE), transferred to nitrocellulose. The membrane was blocked with 5% dry milk (w/v) in TBST for 45-60 minutes and incubated with the indicated primary antibody (**Table 2.2**) overnight at 4°C. Incubation with HRP-conjugated secondary in blocking buffer was performed at room temperature for 1 hour. Protein bands were detected using enhanced chemiluminescence (ECL) and radiographic film.

Table 2.2 List of primary antibodies used

Protein	Source	Manufacturer	Product number
KLF2	rabbit polyclonal	Aviva Systems Biology	ARP32760
KLF4	rabbit monoclonal	Cell Signaling	D1F2
KLF6	rabbit polyclonal	Santa Cruz Biotechnology	sc-7158
KLF10	rabbit polyclonal	abcam	ab73537
DR5	rabbit monoclonal	Cell Signaling	D4E9
RB1	mouse monoclonal	Cell Signaling	4H1
E2F1	rabbit polyclonal	Cell Signaling	3742S
XIAP	mouse monoclonal	BD Biosciences	D2Z8W
PARP	rabbit polyclonal	Cell Signaling	9542S
Arl13b	rabbit polyclonal	proteintech	17711-1-A
IFT88	rabbit polyclonal	proteintech	13967-1-AP
Actin	mouse monoclonal	Sigma	A2228
GAPDH	mouse monoclonal	ProSci	2D4A7

Table 2.2. List of primary antibodies used

Immunofluorescence

Cells were seeded onto glass coverslips that were pre-coated with collagen by application of collagen solution (Sigma, Cat # C8919) with a cotton swab and allowing it to dry. After drying, coverslips were added to culture dishes containing growth medium and cells plated as usual. The coverslips were transferred to a new 6-well plate and rinsed with PBS at room temperature. They were fixed for 20 minutes at 37 °C in PBS with 3% paraformaldehyde, 100 mM piperazine-1,4-bis-2-ethanesulfonic acid (PIPES), 3 mM $MgSO_4$, and 1 mM EGTA. After washing 3 times with PBS, the cells were permeabilized for 5 minutes with 0.1% Tween-20 in PBS. Cells were washed again 3 times in PBS then blocked for 60 minutes at 37 °C in blocking solution containing PBS with 5% glycerol, 5% donkey serum, and 0.0 % sodium azide. Primary antibodies were diluted 1:200-1:500 in blocking solution and 150 μL was pipetted on top of each coverslip. Antibodies were incubated overnight at 4 °C in a 6-well plate that was sealed with parafilm to prevent evaporation. The coverslips were transferred to a new 6-well plate and washed 3 times with PBS. They were then incubated with 1:2000 secondary Alexa Fluor antibodies (Alexa488, Alexa594, Thermo Fisher) in blocking buffer for 45-60 minutes at 37 °C. After washing 3 times in PBS and with a final water rinse to remove salts, coverslips were mounted onto glass slides in a drop of Vectashield with DAPI (Vector Laboratories) mounting medium. Immunofluorescence images were captured using a Zeiss 710 confocal laser scanning microscope in the UNMC Advanced Microscopy Core Facility.

Embelin treatment

Embelin was purchased from Sigma-Aldrich (Cat # E1406) and resuspended in dimethyl sulfoxide (DMSO). Staurosporine (Fisher Scientific, Cat # BP2541) was used at 1 μg/mL final concentration. Cells were treated with 0-50 μM embelin for 2-48 hours, as indicated in the figure legends, and compared to DMSO-treated cells (vehicle). Recombinant human TRAIL was obtained from R&D Systems (Cat # 375-TL-010) and used at a final concentration of 4-8 ng/mL.

Cellular thermal shift assay

Mz-ChA-1 cells were grown to 80% confluence and lysed in PBS containing Complete protease inhibitors (Roche) by three cycles of freeze-thaw (liquid nitrogen), as described [304]. Cell debris were pelleted by centrifugation (15,700 *g* for 20 minutes). Lysates were divided into identical aliquots, which were incubated with either embelin (50 μM) or an equal volume of DMSO for 30 minutes and were then heated for 3 minutes on a gradient thermal cycler. The lowest temperature was set to 46 °C and the highest temperature was set to 70 °C. Heated samples were then cooled at room temperature for 3 minutes and centrifuged at 15,700 *g* for 20 minutes to pellet denatured protein aggregates. Supernatants were analyzed by SDS-PAGE and immunoblotted for XIAP.

Nuclear morphology apoptosis assay

Treated living cells were stained with the nuclear dye 4'6-diamidino-2-phenylindole (DAPI; Sigma, Cat # D9542) at a final concentration of 5 μg/mL for 20

minutes at 37 °C prior to live cell imaging by epifluorescence (Leica DMI6000B). Cells were counted as DAPI-positive if the nucleus showed bright staining and as apoptotic if there was characteristic nuclear fragmentation, blebbing, or pyknosis. Total cell number was determined in the same field by phase contrast microscopy, and data are expressed as the percent of DAPI-positive nuclei out of the total.

DNA fragmentation assay

Mz-ChA-1 cells were treated with vehicle (DMSO), embelin (15 μM), or staurosporine (1 μg/mL) for 4-24 hours. Fragmented DNA was then isolated essentially following the protocol of Shiraishi et al. [305] except that DNA was extracted by phenol:chloroform:isoamyl alcohol prior to RNase A treatment. DNA was run on a 2% agarose gel and visualized by ethidium bromide staining. The image was then digitally inverted and brightness-optimized without altering other aspects of the image.

Caspase 3/7 activity assay

Cells were seeded in a 96-well plate in 200 μL medium. The following day, they were treated or transfected for 24-48 hours. Cell death was induced with treatment of 4-50 ng/mL TRAIL or 5 μg/mL staurosporine for 6 hours. Then, 170 μL medium was removed and 30 μL caspase 3/7 reaction (1:100 Z-DEVD-R110 fluorogenic substrate:Homogenous buffer; ApoONE, Promega) was added to each well. The plate was covered with aluminum foil and mixed by gentle shaking for at least 30 seconds, then allowed to incubate for 1-16 hours. Fluorescence was measured at 535 nm on a Tecan Infinite 200 Pro plate reader. The pan-caspase inhibitor Z-VAD-fmk (Santa Cruz,

Cat # sc-3067) was resuspended in DMSO and used at a final working concentration of 50 μM.

MTT proliferation assay

Cell proliferation was assayed by reduction of 3-(4,5-dimethylthiazol-2-yl)-2,5-diphenyltetrazolium bromide (MTT; Invitrogen, M6494). MTT was freshly dissolved into PBS at a stock concentration of 12 mM and diluted into phenol red-free DMEM with 10% FBS for a final MTT concentration of 2 mM. Reactions were carried out at 37 °C for four hours and stopped by removing the medium. Reduced MTT was dissolved in 100 μL isopropanol and absorbance measured at 540 nm on a plate reader. All data are corrected to the initial signal, set at 100%. Assays were repeated four times for each condition.

Cell cycle analysis

Cells were stained with propidium iodide using the Telford method [306]. Approximately 2 million cells per treatment condition were fixed by adding 70% ethanol and incubating at 4 °C for 15 minutes to 1 hour. The cells were pelleted and ethanol was removed, followed by washing with PBS and again pelleted. Cell DNA was stained using 1 mL of Telford reagent (16.81 mg EDTA, 13.4 mg RNase A (93 U/mg), 25 mg propidium iodide, 500 μL Triton X-100 in 500 mL PBS) added to cells and allowed to incubate for at least 30 minutes at 4 °C. DNA content was analyzed by flow cytometry. Cells were quantified as a percentage of those with 2N or 4N nuclear DNA content, and cells with intermediate DNA content between 2N and 4N (S phase).

Scratch assay

Cells were grown to confluence in a 6-well plate and a linear wound was created in the cell monolayer with a 200 μL pipet tip. Wells were rinsed once with medium before replacing the medium. Phase contrast pictures at 5X magnification were taken for a zero hour time point. Repeat pictures were taken 12 to 48 hours later. Picture location was identified and kept constant either through demarcation with a fine-tip marker or capturing images at reproducible locations near the ends of the scratches. Fraction of wound closure was calculated using ImageJ software and measuring the total two demensional area unoccupied by cells at the same magnification.

Transwell assay

Twenty-five thousand cells in 100 μL serum-free medium were seeded into the upper inserts of a Corning Costar 24-well 8-μm membrane pore size plate containing 600 μL regular medium with 10% FBS in the bottom of the wells. Cells were allowed to migrate for 24 to 72 hours. To mount the membranes for quantification of migrated cells, inserts were rinsed with PBS, then the upper side of the membrane was thoroughly wiped with two cotton swabs to remove adhering cells that had not migrated. Cells were fixed by dipping the insert 20 times in isopropanol followed by a water rinse. The membrane was removed from the insert with a scalpel and mounted cells-down on a glass slide with a drop of ProLong Gold antifade reagent with DAPI (Thermo Fisher) and covered with a cover slip. Cells were imaged by epifluorescence on a Leica DMI6000B microscope.

Stable transfection

Cells were transfected with a KLF2 expression plasmid containing a puromycin resistance marker and a DsRed expression cassette (pBRPyCAG-hKlf2-DsRed-Ip; addgene, Cat # 26277) using Lipofectamine 3000 (Thermo Scientific). Clones were selected by treatment with 2 μg/mL puromycin in normal medium that was replaced every few days. Puromycin-resistant cells were reseeded thinly in selection medium to allow for isolated growth of colonies from individual cells. Colonies were screened for positive DsRed fluorescence and transferred to new dishes. Positive clones were then further screened for KLF2 expression by qRT-PCR and immunoblot.

Orbital shear stress model

To induce shear stress over a cell monolayer, cells were seeded in barrier-separated peripheries (as below, in blue) of 10-cm culture dishes and rotated on an orbital shaker. To create each of these "racetracks," a 6-cm dish was fixed in the center of a 10-cm dish with a small volume of chloroform to fuse the plastic together (**Figure 2.1**). The fused dishes were set aside to allow any remaining chloroform to dissipate before cells were seeded.

Figure 2.1 Schematic of orbital shear stress model

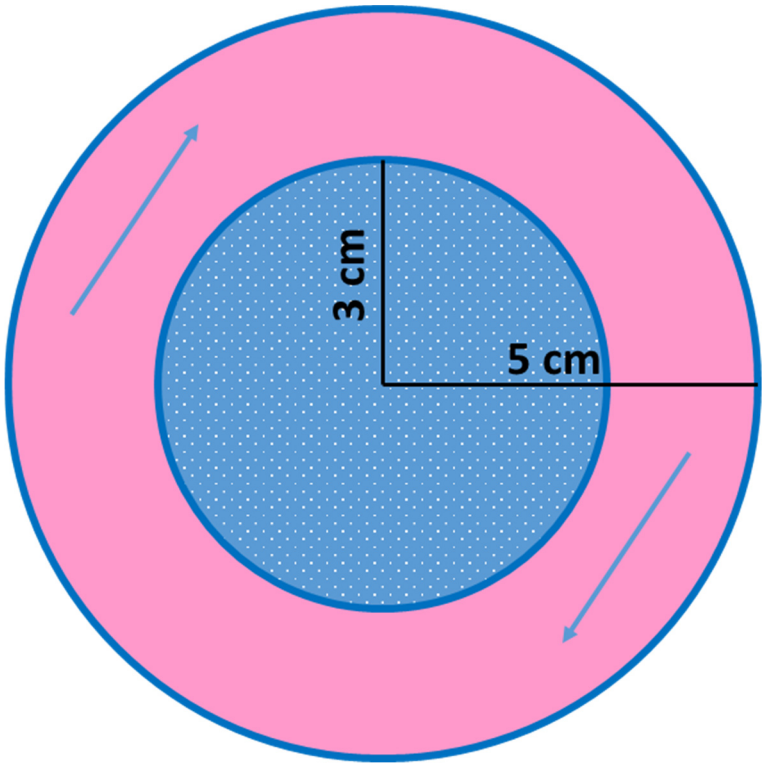

Figure 2.1. Schematic of orbital shear stress model. Depicted is a scale image of the experimental setup for orbital flow over cells in culture. Cells were seeded in the annulus (pink) and arrows indicate the direction of flow induced by oscillation on an orbital shaker.

Cells were seeded in 8 mL of medium in the peripheral annulus, and shear stress was generated with rotation between 60-120 rpm for 24 to 96 hours on a remote CO_2-resistant orbital shaker (Thermo Scientific, Cat # 88881101) inside a cell incubator under normal culture conditions. Shear stress was calculated using the formula $\tau_{max} = a\sqrt{\eta\rho(2\pi f)^3}$ where a is the radius (4 cm, using the radius to the midpoint of the peripheral cell track), η is the viscosity of the medium (0.0101 poise), ρ is the density of the medium (1.007 g/mL), and f is the frequency of rotation (rotations/second) [307-309]. By this equation, 60 rpm was equivalent to 6.4 dyne/cm^2, 80 rpm was equivalent to 9.8 dyne/cm^2, and 120 rpm was equivalent to 18 dyne/cm^2, where 10 dyne/cm^2 is equal to 1 pascal of force.

Statistical analysis

Data were analyzed by ANOVA with *post hoc* Bonferroni correction when multiple comparisons were possible. When only two conditions were measured, 2-tailed, equal variance Student's *t*-test was employed. Comparisons between groups were considered significantly different when the p-value was less than or equal to 0.05. Where applicable: * = $p < 0.05$, ** = $p < 0.01$, *** = $p < 0.001$.

Chapter 3 - XIAP antagonist embelin inhibited proliferation of cholangiocarcinoma cells[1]

Cody J. Wehrkamp
Ashley R. Gutwein
Sathish Kumar Natarajan
Mary Anne Phillippi
Justin L. Mott

[1]Adapted from: Wehrkamp CJ, Gutwein AR, Natarajan SK, Phillippi MA, Mott JL. (2014) XIAP antagonist embelin inhibited proliferation of cholangiocarcinoma cells. *PLoS One* 9(3):e90238. With minor modifications for continuity and clarity.

Abstract

Cholangiocarcinoma cells are dependent on anti-apoptotic signaling for survival and resistance to death stimuli. Recent mechanistic studies have revealed that increased cellular expression of the E3 ubiquitin-protein ligase X-linked inhibitor of apoptosis (XIAP) impairs TRAIL- and chemotherapy-induced cytotoxicity, promoting survival of cholangiocarcinoma cells. This study was undertaken to determine if pharmacologic antagonism of XIAP protein was sufficient to sensitize cholangiocarcinoma cells to cell death. We employed malignant cholangiocarcinoma cell lines and used embelin to antagonize XIAP protein. Embelin treatment resulted in decreased XIAP protein levels by 8 hours of treatment with maximal effect at 16 hours in KMCH and Mz-ChA-1 cells. Assessment of nuclear morphology demonstrated a concentration-dependent increase in nuclear staining. Interestingly, embelin induced nuclear morphology changes as a single agent, independent of the addition of TNF-related apoptosis inducing ligand (TRAIL). However, caspase activity assays revealed that increasing embelin concentrations resulted in slight inhibition of caspase activity, not activation. In addition, the use of a pan-caspase inhibitor did not prevent nuclear morphology changes. Finally, embelin treatment of cholangiocarcinoma cells did not induce DNA fragmentation or PARP cleavage. Apoptosis does not appear to contribute to the effects of embelin on cholangiocarcinoma cells. Instead, embelin caused inhibition of cell proliferation, and cell cycle analysis indicated that embelin increased the number of cells in S and G2/M phases. Our results demonstrate that embelin decreased proliferation in cholangiocarcinoma cell lines. Embelin treatment resulted in decreased XIAP protein

expression, but did not induce or enhance apoptosis. Thus, in cholangiocarcinoma cells the mechanism of action of embelin may not be dependent on apoptosis.

Introduction

Cholangiocarcinoma is a liver tumor with cellular features of bile duct epithelial cells and is the second most common primary liver cancer. Biliary tract inflammation predisposes to cholangiocarcinoma, although most patients do not have recognized underlying liver disease at the time of diagnosis. Chemotherapy has been shown to prolong survival, but only modestly [18], and five-year survival remains less than 10%. This may be due to decreased tumor cell death in response to chemotherapy. A number of mechanisms contribute to apoptosis resistance, including overexpression of the caspase-inhibitory protein X-linked inhibitor of apoptosis protein (XIAP).

XIAP is an E3 ubiquitin-protein ligase that binds and inhibits caspases 3, 7, and 9 [310, 311]. XIAP is ubiquitously expressed at the mRNA level [312] and is induced in cholangiocarcinoma cells by the inflammatory mediator IL-6 [30]. XIAP protects cholangiocarcinoma cells from apoptosis induced by chemotherapeutic drugs [30] and by the death receptor ligand TNF-related apoptosis-inducing ligand (TRAIL) [313]. Treatment of cholangiocarcinoma cells with the small molecule triptolide resulted in decreased XIAP protein levels and increased sensitivity to TRAIL [314]. Together, these data suggest that targeting XIAP in cholangiocarcinoma cells increases sensitivity to apoptosis. XIAP's anti-apoptotic effects are overcome upon mitochondrial membrane permeabilization and release of SMAC/DIABLO [315], a protein that binds the BIR3 domain of XIAP [316, 317].

The small molecule embelin has been found to inhibit XIAP, and computer modeling as well as fluorescence polarization competition assays suggest it binds the SMAC-binding pocket of XIAP [318]. Treatment with embelin has been shown to sensitize cells to apoptosis through TRAIL, chemotherapy, and targeted therapy plus cFLIP knockdown. Further, embelin treatments decreased XIAP protein levels in leukemia cells [319]. Based on these findings, embelin has been described as an XIAP antagonist. However, alternate/additional mechanisms of embelin action have been described, including inhibition of NF-kB [320] and inhibition of Akt/mTOR/S6K1 [321].

In this study, we sought to assess the effects of embelin on XIAP protein levels, apoptosis, and proliferation in cholangiocarcinoma cells. While embelin decreased cellular XIAP protein levels, caspase activity was not increased. Proliferation was inhibited by embelin and cells were arrested in S and G2/M phases. These observations indicate that embelin reduced tumor cell survival and proliferation, but did not increase apoptosis.

Results

To assess the potential for antagonism of XIAP in cholangiocarcinoma cells, we first determined XIAP expression at the protein level in several cell lines. XIAP protein was expressed in all three cell lines with highest expression in Mz-ChA-1 cells and HuCCT cells, and somewhat lower XIAP protein levels in KMCH cells (**Figure 3.1A**). Upon treatment with embelin, cellular XIAP protein levels decreased with time in Mz-ChA-1 and KMCH cells, while XIAP was essentially unchanged in HuCCT cells treated with embelin for up to 32 hours (**Figure 3.1B**).

We sought evidence that embelin binds directly to XIAP protein in our cells by employing the cellular thermal shift assay [304]. This assay is based on the observation that ligand binding often stabilizes the cognate target protein [322-325]. The cellular thermal shift assay measures heat-induced protein denaturation in the absence and presence of the small molecule ligand. In this case, lysed Mz-ChA-1 cells were incubated with vehicle or embelin and XIAP denaturation was measured by loss of solubility upon heat treatment. We observed that XIAP protein in cell lysates became insoluble at about 60°C. The denaturation temperature was not different in the presence or absence of embelin (61.0 +/- 1.4 °C versus 59.9 +/- 0.7 °C, respectively; $p = 0.49$ by *t*-test; **Figure 3.1C**).

Figure 3.1. Embelin caused XIAP degradation in cholangiocarcinoma cell lines.
(**A**) Immunoblot of XIAP in untreated cholangiocarcinoma cell lines. Actin was included as a loading control. Apparent molecular mass for each band is indicated to the right. (**B**) Cells were treated with 15 μM embelin in DMSO or DMSO alone (Veh) for the indicated times. Whole-cell lysates were blotted for XIAP and actin. (**C**) For the cellular thermal shift assay, Mz-ChA-1 cells were lysed by freeze-thaw and then incubated with embelin (50 μM) or DMSO (Vehicle) for 30 minutes and separated into 20 μL aliquots. Aliquots were heated to the indicated temperatures and cooled to room temperature and soluble XIAP measured by immunoblot. Band intensity was determined by densitometry of scanned films and data are plotted compared to the signal intensity observed at 45°C (100%). Data are fitted using the Boltzman function; the dashed line indicates the fit for vehicle-treated samples, the solid line for embelin-treated samples. Blot is representative of four replicates used in the graph.

Figure 3.1 Embelin caused XIAP degradation in cholangiocarcinoma cell lines

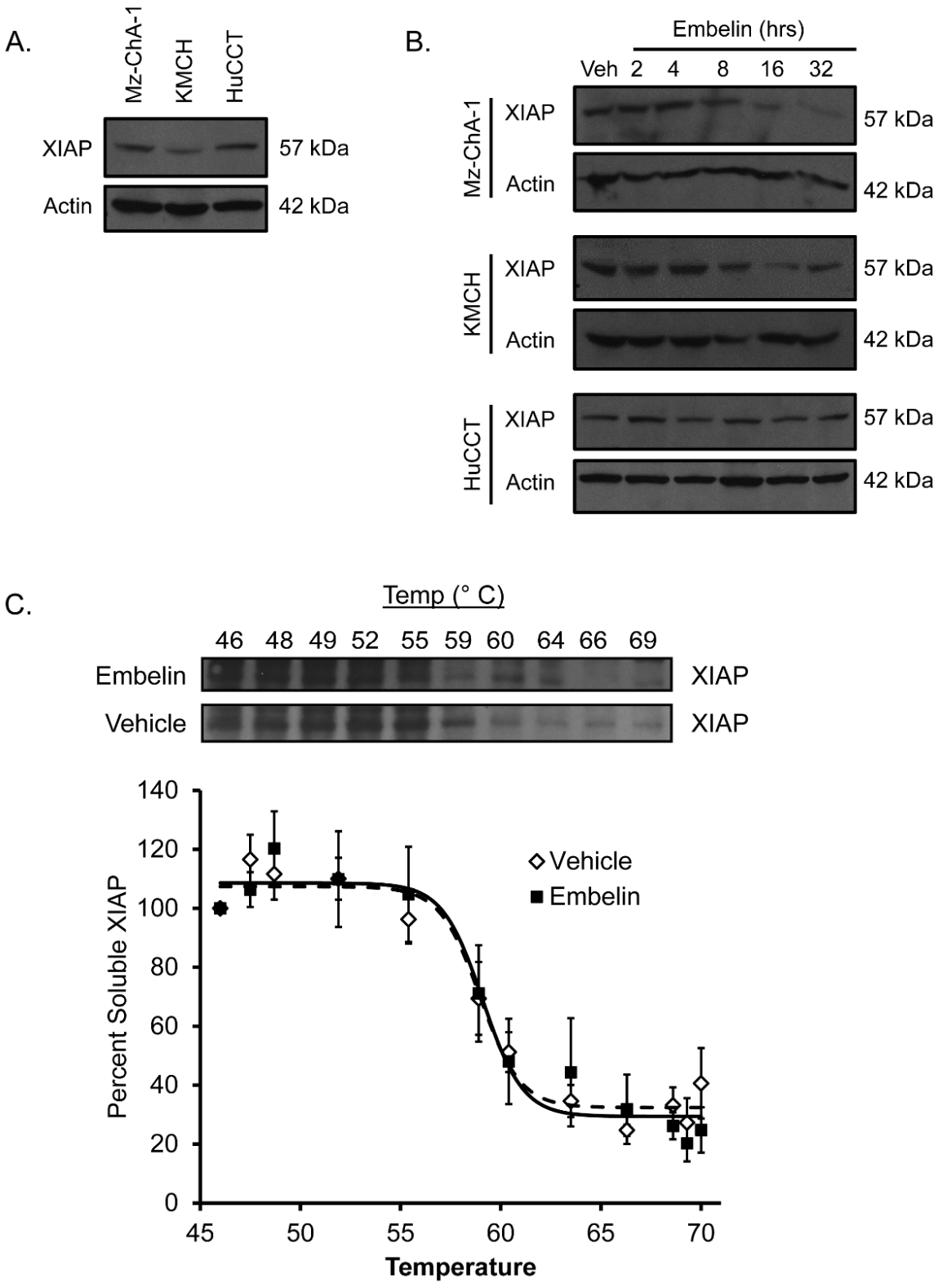

Previous studies have found that siRNA-mediated depletion of XIAP was sufficient to sensitize cholangiocarcinoma cells to apoptosis. We tested cell treatment with embelin or embelin plus TRAIL in KMCH (**Figure 3.2A**) and Mz-ChA-1 cells (**Figure 3.2B**) by quantifying altered nuclear morphology after staining with the DNA-binding dye, 4'-6-diamidino-2-phenylindole (DAPI). The addition of embelin (1-10 μM) increased TRAIL-induced DAPI-positive nuclei in both cell types. Interestingly though, in Mz-ChA-1 cells, embelin alone appeared to have as much effect as embelin plus TRAIL (**Figure 3.2B**). Additional testing of the highly tumorigenic rat-derived BDEneu cell line also showed increased numbers of DAPI-positive nuclei after embelin treatment (**Figure 3.2C**). This suggested embelin may have single-agent activity in cholangiocarcinoma cells. Single-agent activity was somewhat unexpected and (in conjunction with the caspase data, see below) prompted us to closely examine the nuclear staining. Untreated live Mz-ChA-1 cells stained with DAPI showed very low nuclear fluorescence (unstained nuclei outlined), while a sporadic apoptotic nucleus showed bright staining and obvious fragmentation (**Figure 3.2D**). Close examination of nuclei in embelin-treated cells revealed DAPI-positive staining with local regions of bright signal; however, nuclei did not appear fragmented or condensed, and were not consistent with apoptotic nuclei (**Figure 3.2E**).

Because apoptosis is a process, assessment at a single time point may not accurately capture the apoptotic signal. We have performed a time course of DNA laddering upon embelin treatment (4, 8, 16, and 24 hours) compared to the positive control staurosporine over the same time. The results demonstrate minimal DNA

laddering in vehicle (DMSO)-treated cells at 24 hours (Veh) that was similar to the laddering seen in embelin-treated cells at 24 hours. In contrast, the kinase inhibitor staurosporine was included as a positive control and showed rapid formation of a DNA ladder with ~180 bp spacing, consistent with apoptotic internucleosomal fragmentation (**Figure 3.2F**). The results of this experiment support the previous conclusions based on DAPI staining and add additional evidence that the nuclear morphology changes we initially observed were unlikely to reflect apoptosis.

Figure 3.2. Embelin induced an altered nuclear morphology in cholangiocarcinoma cell lines. (**A**) KMCH cells were treated for 24 hours with TRAIL at the indicated concentrations with or without embelin (1 and 10 μM). Cells were then stained with DAPI and bright nuclei were counted as a percentage of total nuclei. Data from one experiment are plotted as percent DAPI-positive nuclei on the vertical axis. (**B**) Mz-ChA-1 cells were treated with TRAIL (4 ng/mL) or medium for 24 hours with 5 or 10 μM embelin, and DAPI-positive nuclei counted as a percent of total cells. Data are mean of 3 experiments +/− standard error of the mean. n.s.=not significantly different. * $p<0.05$, ** $p<0.01$ by ANOVA with Bonferroni compared to medium alone. (**C**) Rat BDEneu cholangiocarcinoma cells were treated with DMSO (Vehicle; open bar) or embelin (50 μM, filled bar) for 48 hours, followed by DAPI staining. Data are mean of 3 experiments +/− SEM. *** $p<0.001$ compared to vehicle, Student's *t*-test. (**D**) Vehicle-treated Mz-ChA-1 cells were stained with DAPI and imaged by epifluorescence without fixation. Healthy nuclei (indicated by outlines) did not stain with DAPI, while a sporadic apoptotic nucleus (arrow) was brightly stained. Bar=10 μm. (**E**) DAPI-positive nuclei of Mz-ChA-1 cells treated with embelin (15 μM for 24 hours) did not show characteristic apoptotic fragmentation or pyknosis. (**F**) Mz-ChA-1 cells were treated with DMSO (Veh), embelin (15 μM), or staurosporine followed by analysis of DNA fragmentation on a 2% gel. Vehicle treatment was for 24 hours. Embelin and staurosporine treatments were for 4, 8, 16, and 24 hours. M=100 bp DNA marker. The gel was stained with ethidium and photographed and the image was inverted to show DNA as a dark signal on a light background. Images in Panel D, E, and F were adjusted for brightness and contrast to ensure that features were visible and the entire image was treated equally.

Figure 3.2 Embelin induced an altered nuclear morphology in cholangiocarcinoma cell lines

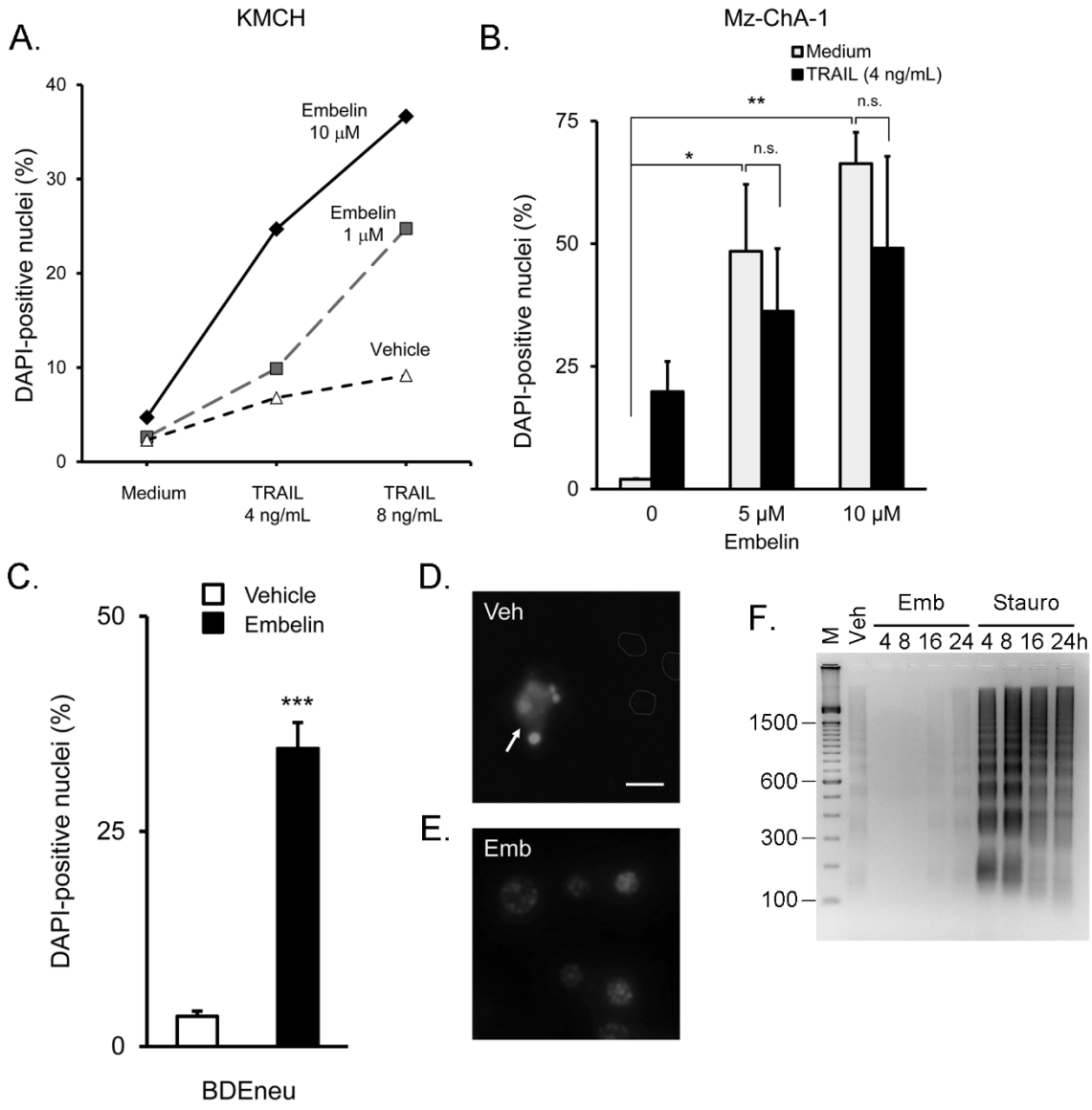

Based on the known function of XIAP in inhibiting caspase activity, it was anticipated that embelin treatment would increase caspase activation and can increase the levels of cleaved poly (ADP-ribose) polymerase (PARP), a marker of caspase-induced apoptosis. Surprisingly, treatment of Mz-ChA-1 cells with embelin did not result in increased caspase 3/7-like hydrolase activity, but instead caused decreased caspase activation at 30 μM (**Figure 3.3A**). This observation was repeated in BDEneu cells, which also showed inhibition rather than activation of caspase 3/7 (**Figure 3.3B**). Caspase activity was then assessed at an earlier time point, 4 hours, in case caspase activation was an early rather than late event. Embelin treatment did not increase caspase activity at 4 hours, while the positive control staurosporine caused robust caspase activity in Mz-ChA-1 and KMCH cells (**Figure 3.3C**). Staurosporine did not increase caspase activity to a significant degree in HuCCT cells, possibly indicating resistance or slower apoptosis kinetics in HuCCT cells. To determine if embelin-induced nuclear DAPI staining was caspase-dependent, we treated BDEneu cells with vehicle, embelin, or embelin plus the pan-caspase inhibitor Z-VAD-fmk and quantified DAPI-positive nuclei. Embelin treatment resulted in nuclear changes in the presence or absence of Z-VAD-fmk (**Figure 3.3D**), consistent with morphology changes that were not caspase-dependent. Control experiments using the same Z-VAD-fmk concentration confirmed that the inhibitor blocked caspase activity (data not shown). Next, we tested whether embelin treatment affected total PARP protein levels or PARP cleavage in Mz-ChA-1 cells. Clearly, there was no change in the levels of PARP or cleaved PARP with

embelin treatment (**Figure 3.3E**). Together, these results suggest that embelin treatment did not alter caspase activity.

Figure 3.3 Embelin partially inhibited caspase activation and did not induce caspase-dependent cell death in cholangiocarcinoma cells

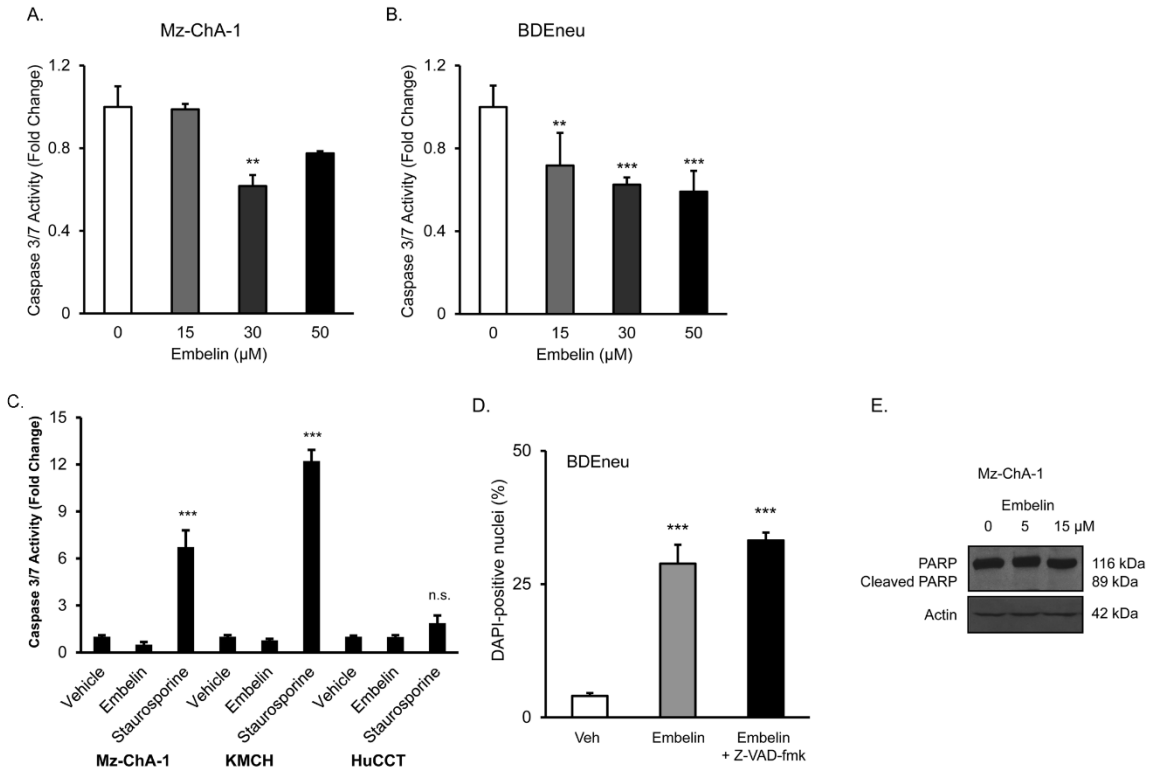

Figure 3.3. Embelin partially inhibited caspase activation and did not induce caspase-dependent cell death in cholangiocarcinoma cells. (**A**) Mz-ChA-1 cells were treated with embelin for 24 hours and caspase 3/7 activity measured biochemically. Untreated cells were used for comparison and caspase activity in untreated cells was normalized at 1.0. (**B**) BDEneu cells were treated with embelin (48 hours) and caspase 3/7 activity measured. (**C**) Apoptosis was measured after 4 hours treatment with vehicle, embelin (15 μM) or staurosporine (1 μg/mL) in Mz-ChA-1, KMCH, and HuCCT cells to test for early caspase 3/7 activation. (**D**) BDEneu cells treated with 50 μM embelin for 48 hours were assayed for DAPI-positive nuclei with and without co-treatment with caspase inhibitor Z-VAD-fmk (50 μM). DAPI-positive nuclei are presented as percent of total cells, n=3, mean +/− SEM. The % DAPI-positive nuclei between embelin and embelin + Z-VAD-fmk was not significantly different. Panels A, B, C & D are a mean of 3 or 4 experiments +/− SEM; ** $p<0.01$, *** $p<0.001$ vs vehicle, n.s.=not significantly different, ANOVA with Bonferroni correction. (**E**) Mz-ChA-1 cells were treated with embelin (5–15 μM) in DMSO or DMSO alone (Veh) for 24 hours. Whole-cell lysates were blotted for PARP. Actin was included as a loading control. Apparent molecular mass for each protein is indicated to the right.

Embelin has been shown to inhibit cell proliferation in cancer cells [326-328]. We tested the effect of embelin on Mz-ChA-1 cell growth, using the MTT assay. Growth was significantly reduced, initially apparent as no increase in cell number at 24 or 48 hours, followed by a significant reduction in the number of viable cells at 72 hours in the presence of 15 μM embelin (**Figure 3.4A**). Growth inhibition was also apparent in KMCH cells at 24-72 hours, though to a smaller extent than in Mz-ChA-1 cells. HuCCT cells were found to be resistant to the growth-inhibitory effects of embelin, similar to the lack of effect of embelin on XIAP protein content in these cells (see **Figure 3.1B**). To further analyze the effect of embelin on proliferation, investigation of cell cycle progression was performed using propidium iodide staining followed by flow cytometry. Mz-ChA-1 cells were chosen based on their response to embelin treatment in growth assays. In vehicle-treated cells (DMSO), 76% of cells were in the G0/G1 phase (2N), with the remaining cells divided between S phase and G2/M (4N). Treatment with 15 μM embelin caused cell cycle arrest and an increase in the percentage of cells in G2/M as well as an increase in the percentage of cells in S phase. Correspondingly, a decrease in the number of cells in G0/G1 was observed (**Figures 3.4B & C**).

Figure 3.4 Inhibition of proliferation and cell cycle arrest by embelin

A.

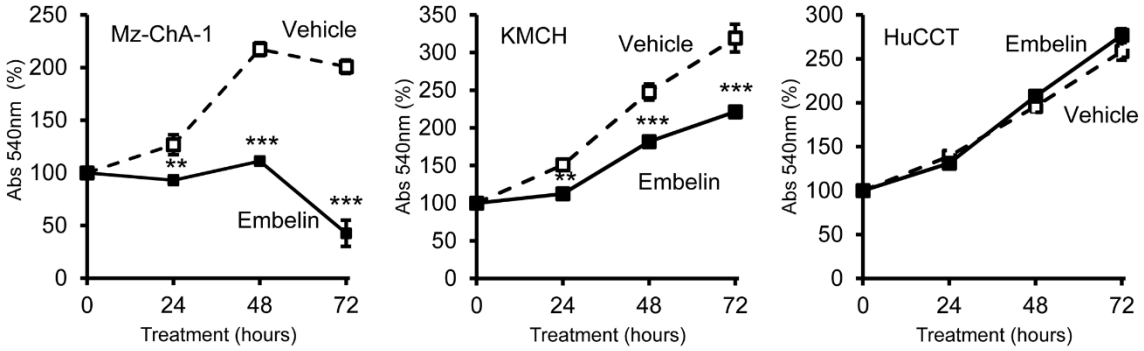

B.

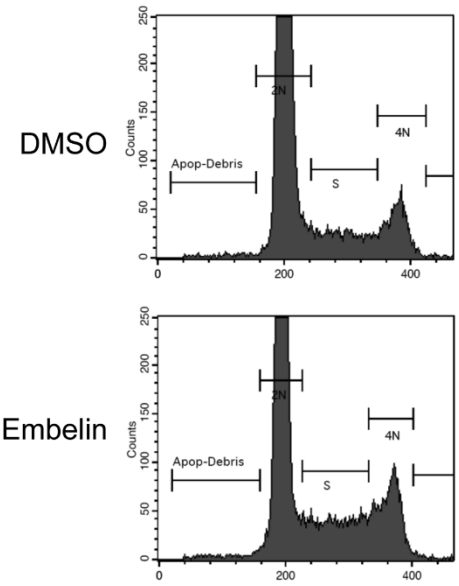

C.

	2N	4N	S
Untreated	75	12	11
DMSO	76	11	12
Embelin	61	18	19

Figure 3.4. Inhibition of proliferation and cell cycle arrest by embelin. (**A**) Cell proliferation was measured by MTT and cell number measured by absorbance at 540 nm (Abs 540 nm). Signal represents the mean (n=4) +/− standard error of the mean, normalized to the starting value (day 0, set at 100%). Cells treated with embelin (15 μM) are plotted with a solid line and filled symbols and vehicle-treated cells are plotted with a dashed line and open symbols. ** $p<0.01$ and *** $p<0.001$ versus vehicle at the same time point, ANOVA with Bonferroni correction. Values for HuCCT were not significantly different at any time point. (**B**) Cell cycle analysis of Mz-ChA-1 cells was performed by propidium iodide staining followed by flow cytometry. A histogram of propidium iodide-stained cells is shown for DMSO-treated and embelin-treated cells (15 μM, 24 hours). (**C**) Quantitation of the percentage of cells with 2N or 4N nuclear DNA content, and cells that are in S phase (DNA content intermediate between 2N and 4N). Representative experiment of 3 independent treatments.

Discussion

The results of this study relate to effects on proliferation of cholangiocarcinoma cells upon embelin treatment. Our results demonstrated that embelin decreased cellular XIAP protein levels, caused a caspase-independent change in nuclear morphology, decreased proliferation, and slowed progression through the cell cycle. Each of these findings will be discussed below.

Embelin has been described to have numerous activities, including antifertility [329] and analgesia [330] functions. Recently, embelin has received attention as an antitumor agent that promotes apoptosis [318, 320, 331, 332] and decreases proliferation [319, 327, 333, 334]. In a computational screen for structures that bind XIAP, embelin was selected for further characterization. Embelin could compete with SMAC for XIAP binding and, in prostate tumor cells (PC3), caused loss of cell growth, increased apoptosis (defined as annexin V-positive, propidium iodide-positive cells), and an increased percentage of cells with activated caspase 9 [318]. In a pancreatic cancer cell line, combined treatment with an antisense oligonucleotide to cFLIP, embelin, and TRAIL decreased cell viability compared to cFLIP antisense and TRAIL alone in a tetrazolium-based assay [331]. Because XIAP has a strong effect in cholangiocarcinoma cell lines to protect against cell death, we tested the effect of embelin on XIAP protein levels in human cholangiocarcinoma cell lines and found that embelin caused a reduction in XIAP in Mz-ChA-1 and KMCH cells.

The differential effect of embelin treatment on XIAP protein levels depending on the cell line tested is consistent with literature reports. Embelin treatment of the leukemia cell line HL 60 caused a reduction in XIAP protein levels and increased cleavage of caspase 3 and caspase 9 [319]. However, in glioma cell lines, embelin did not significantly alter XIAP protein levels [332]. In a breast cancer cell line overexpressing ErbB2, embelin alone decreased the viability of cells (tetrazolium), although siRNA to XIAP did not. Combined treatment with trastuzumab (an antagonistic ErbB2 antibody) and embelin had no effect while siRNA to XIAP plus trastuzumab increased apoptosis, suggesting that embelin does not simply mimic loss of XIAP [335]. Embelin treatment of PC3 prostate cancer cells did not decrease XIAP protein levels, and did not increase caspase 9 activation (alone or combined with ionizing radiation), although there was an increase in annexin V and propidium iodide double-positive cells [327]. Thus, the effect of embelin on XIAP protein depends on the context. Similarly, the effect on cell viability of embelin alone or in combination treatments varies.

We next sought evidence of a direct interaction of embelin with XIAP in our cells. We utilized the recently described cellular thermal shift assay [304] to assess the stability of XIAP in the presence or absence of embelin. In our experiments, however, embelin did not reproducibly alter the stability of XIAP. Thus, we were unable to confirm direct binding. This can be interpreted either as a lack of direct binding, or that binding does not significantly stabilize XIAP structurally. In previous heteronuclear single quantum coherence spectroscopy experiments, embelin was found to alter the spectrum of the XIAP BIR3 domain, suggesting a physical interaction [318]. The lack of stabilization in

the complex cell lysate (this study) does not rule out a direct interaction, and similarly, observation of a direct binding interaction in a single-component system does not answer the question of binding in the cellular environment.

Based on the role of XIAP in preventing cholangiocarcinoma cell apoptosis, we hypothesized that embelin would increase cell death in combination with TRAIL. Initial experiments indeed showed that an increased percentage of cells had altered nuclear morphology upon embelin treatment, measured by the DNA dye DAPI. However, careful analysis confirmed that the altered morphology did not reflect increased apoptotic nuclei. Binding of DAPI to DNA is known to result in increased fluorescent signal over soluble unbound DAPI [336]. Altered nuclear morphology is a hallmark of apoptosis, and can be easily visualized by DAPI staining as increased fragmentation, compaction of the nuclear signal, and increased staining intensity. Indeed, an advantage of using DAPI as a DNA stain in apoptosis measurement is the observation that many viable cells exclude the dye but dying cells take up DAPI and fluoresce brightly, thus providing a strong signal with low background staining of viable nuclei. Notably, some living cells take up DAPI, possibly through the transporters organic cation transporter-1 (OCT1) [337] and multidrug and toxin extrusion proteins (MATE1 and MATE2) [338], and most cells will gradually accumulate DAPI over time. Thus, a brightly stained nucleus is not definitive evidence of apoptosis. Additional morphological features can be used then to distinguish brightly stained living cells from brightly stained apoptotic cells, including fragmentation and condensation of the nucleus. Altered nuclear morphology is also observed during different phases of the mitotic or meiotic cell cycle

(e.g., see [339] and [340]) and with different chromatin state (heterochromatin versus euchromatin). Thus, an alternate measure of apoptosis is important, such as DNA fragmentation, biochemical assessment of caspase activity, and immunoblot analysis of cleaved PARP levels. Importantly, in our cells, embelin treatment did not induce DNA fragmentation and caused inhibition, not activation of caspases, and did not increase the levels of cleaved PARP. Further, inhibition of caspase activity did not alter embelin-induced nuclear staining. Thus, we interpret the altered nuclear morphology to reflect nuclear changes unrelated to apoptosis, possibly due to altered cell cycle or increased cellular DAPI uptake.

Despite decreasing XIAP, embelin treatment did not increase cell death. It is possible that XIAP levels were not sufficiently decreased to allow for disinhibition of apoptosis. Alternatively, embelin may have pleiotropic effects on cell death that mask sensitization. Moreover, XIAP may not play a dominant role in apoptosis protection in these cholangiocarcinoma cell lines. This latter explanation seems less likely based on our previous experiments showing that siRNA against XIAP caused increased apoptosis and increased caspase activity in KMCH cholangiocarcinoma cells [313].

Cholangiocarcinoma cell lines exhibited growth inhibition upon treatment with embelin. In Mz-ChA-1 and KMCH cells, this was manifested initially as growth arrest at 24 hours. Mz-ChA-1 cells failed to proliferate after this arrest and eventually viability was lost. In KMCH, after the initial 24 hours, the rate of proliferation remained lower than vehicle-treated cells but was not completely halted. HuCCT cells appeared to be

resistant to embelin-induced growth arrest. This pattern of strong inhibition in Mz-ChA-1, intermediate inhibition in KMCH, and no effect in HuCCT cells parallels the data on XIAP protein levels. Cell cycle analysis of Mz-ChA-1 cells confirmed an effect of embelin on cell cycle progression, and revealed more cells in S and G2/M phases. This effect is similar to the growth inhibition in PC3 cells where embelin caused a reduction in cells in G0/G1 and increased numbers in S phase and G2/M phase [327]. An increase in the number of cells in the later stages of the cell cycle can be consistent with either increased proliferation, or decreased proliferation due to a late-stage block or slowing in the cell cycle. For instance, cells treated with topoisomerase inhibitor have decreased proliferation and an increased percentage of cells are in both S phase and G2/M (e.g., [341]), consistent with activation of a late checkpoint.

In conclusion, our results demonstrated sensitivity of cholangiocarcinoma cells to treatment with embelin, which resulted in inhibition of cell cycle progression and slowed proliferation. We did not observe increased spontaneous or TRAIL-induced apoptosis in embelin-treated cells, despite reduced XIAP protein levels. In this regard, embelin did cause an alteration in nuclear staining that was initially taken by us to reflect apoptosis. Additional studies on caspase activation as well as cell-by-cell analysis of staining instead revealed altered staining but no increase in characteristic apoptotic nuclear features. Embelin may cause altered cellular uptake of DAPI, as untreated healthy cells did not take up this DNA-binding dye. In addition, the effect of embelin to delay cell cycle progression may have resulted in a higher percentage of nuclei in various stages of mitosis manifesting altered nuclear morphology. The late loss of cells

that was observed in tetrazolium-based proliferation assays (e.g., **Figure 3.4A,** at 72 hours) may reflect mitotic collapse, apoptosis, or necrosis. Taken together, our data suggest that embelin may have a growth inhibitory effect in cholangiocarcinoma, but to promote tumor cell apoptosis additional treatments are required.

Embelin inhibits *in vitro* cell proliferation of cholangiocarcinoma cells and slows cell cycle progression but does not have an effect on apoptosis despite its ability to reduce XIAP protein levels. These modest results of growth inhibition but lack of cell death induction make embelin a less attractive candidate for pursuit as a therapeutic agent *in vivo*. This led us to investigate other targets for the potential treatment of cholangiocarcinoma, namely, the oncogenic microRNA 106b. Extensive studies of miR-106b in cholangiocarcinoma cells and tumors were performed and will be discussed in the next chapter.

Chapter 4 - miR-106b-responsive gene landscape identifies regulation of Krüppel-like factor family[2]

Cody J. Wehrkamp
Sathish Kumar Natarajan
Ashley M. Mohr
Mary Anne Phillippi
Justin L. Mott

[2]Adapted from: Wehrkamp CJ, Natarajan SK, Mohr AM, Phillippi MA, Mott JL. (2018) miR-106b-responsive gene landscape identifies regulation of Kruppel-like factor family. *RNA Biol* 15(3):391-403. With minor modifications for continuity and clarity.

Abstract

MicroRNA dysregulation is a common feature of cancer and, due to the promiscuity of microRNA binding, this can result in a wide array of genes whose expression is altered. MiR-106b is an oncomiR overexpressed in cholangiocarcinoma, and its upregulation in this and other cancers often leads to repression of anti-tumorigenic targets. The goal of this study was to identify the miR-106b-regulated gene landscape in cholangiocarcinoma cells using a genome-wide, unbiased mRNA analysis. Through RNA-Seq, we found 112 mRNAs significantly repressed by miR-106b. The majority of these genes contain the specific miR-106b seed-binding site. We have validated 11 genes from this set at the mRNA level and demonstrated regulation by miR-106b of 7 proteins. Combined analysis of our miR-106b-regulated mRNA data set and published reports indicate that miR-106b binding is anchored by G:C pairing in and near the seed. Novel targets Krüppel-like factor 2 (KLF2) and KLF6 were verified both at the mRNA level and at the protein level. Further investigation showed regulation of four other KLF family members by miR-106b. We have discovered coordinated repression by miR-106b of multiple members of the KLF family that may play a role in cholangiocarcinoma tumor biology.

Introduction

MiR-106b has been established as an oncogenic microRNA with increased expression in many cancers, including cholangiocarcinoma [68-72], and prostate [62], gastric [64], and hepatocellular carcinoma [65]. Some functions of miR-106b include increased proliferation by miR-106b-mediated reduction of the transcription factor E2F1 [342] and the tumor suppressor RB1 [73]. Additionally, miR-106b increased migration through targeting of the phosphatase PTEN [343], and reduced apoptosis by regulating the BH3-containing protein Bim [58].

MicroRNAs function to dampen the expression of their targets [344-346]. This is accomplished both through reduction in mRNA transcript level as well as by repression of translation. While both mechanisms contribute to reduced target protein expression, the effect of mRNA reduction may dominate [41], in part, because each message is used as a transcript for synthesis of many protein molecules; still, the magnitude of change in mRNA expression is low. A focused description of the binding characteristics and targets of individual microRNAs is feasible and desirable.

Targeting of mRNAs by microRNA is a sequence-driven process. The seed region is a 7-8 nucleotide sequence at its 5′ end, which is essential for recognition of its specific mRNA binding partners. The complementary seed-binding site is more or less conserved among targets, allowing for broad transcript-expression dampening effects from a single microRNA. Seed-binding sites are highly enriched in the 3′ untranslated region (UTR) of transcripts [347]. There is also evidence that supports non-canonical,

non-seed mRNA target interactions between microRNAs and their targets [348, 349]. The traditional seed for miR-106b is located at nucleotides 1-8 on its 5′ end, corresponding to the microRNA sequence 5′UAAAGUGC.

In this study, we sought to define the genome-wide target set of miR-106b and found that miR-106b binding relied on sequences between bases 2-10, tolerating a G:U wobble in the seed region. We found 112 transcripts that were regulated at the mRNA level in cholangiocarcinoma cells. Finally, we demonstrated that members of the KLF family of transcription factors are coordinately repressed by miR-106b. Comparison of our data in cholangiocarcinoma cells with data in Flp-In T-REx 293 human embryonic kidney-derived cells [349] revealed that the microRNA-responsive gene set is largely cell type-specific.

Results

RNA-Seq to determine miR-106b targets

To determine miR-106b targets, we experimentally manipulated miR-106b levels in human Mz-ChA-1 cholangiocarcinoma cells (**Figure 4.1A**). Total RNA from each condition, miR-106b and LNA-106b, was sequenced. Messages with decreased counts in miR-106b-transfected samples compared to LNA-106b-transfected samples were defined as repressed by miR-106b, while mRNAs that had increased counts were defined to be increased by miR-106b. More genes were repressed by miR-106b than increased, with 112 mRNAs repressed and 17 increased (**Figure 4.1B**). Based on the RefSeq sequences, we searched the two data sets—genes with decreased expression and those with increased expression—for the miR-106b seed-binding site. Specifically, we sought perfect 8-mer binding sites and either 7-mer with a match at position 8 (m8) or 7-mer with an A opposite position 1 (A1). The seed sequence of miR-106b is 5'UAAAGUGC and the corresponding 8-mer binding site is 5'GCACUUUA. Of the 112 mRNAs with decreased expression, 81 had either an 8-mer or a 7-mer binding site (72.3%), and 31 had at least one perfect 8-mer binding site (27.7%; **Figure 4.1C**). Conversely, of the 17 mRNAs with increased expression in cells transfected with miR-106b, only one mRNA contained a 7-mer binding sequence (5.9%) and none had a perfect 8-mer site (**Figure 4.1C**). The enrichment of seed-binding sites suggested that our technique was effective in detecting miR-106b targets.

SylArray analysis

The entire gene set was analyzed by SylArray [300] to detect enrichment of microRNA binding sites. We confirmed the enrichment of the miR-106b 7-mer m8 seed-binding site, 5'GCACTTT (red line) in the sequences that were significantly altered by miR-106b (genes were ranked by significance with most significant to the left on the plot; **Figure 4.1D**). Notably, this analysis also revealed enrichment of a 7-nucleotide sequence complementary to nucleotides 3-9 of miR-106b (5'AGCACTT, blue line).

Figure 4.1 miR-106b targets in cholangiocarcinoma cells predominantly contain a seed-binding site

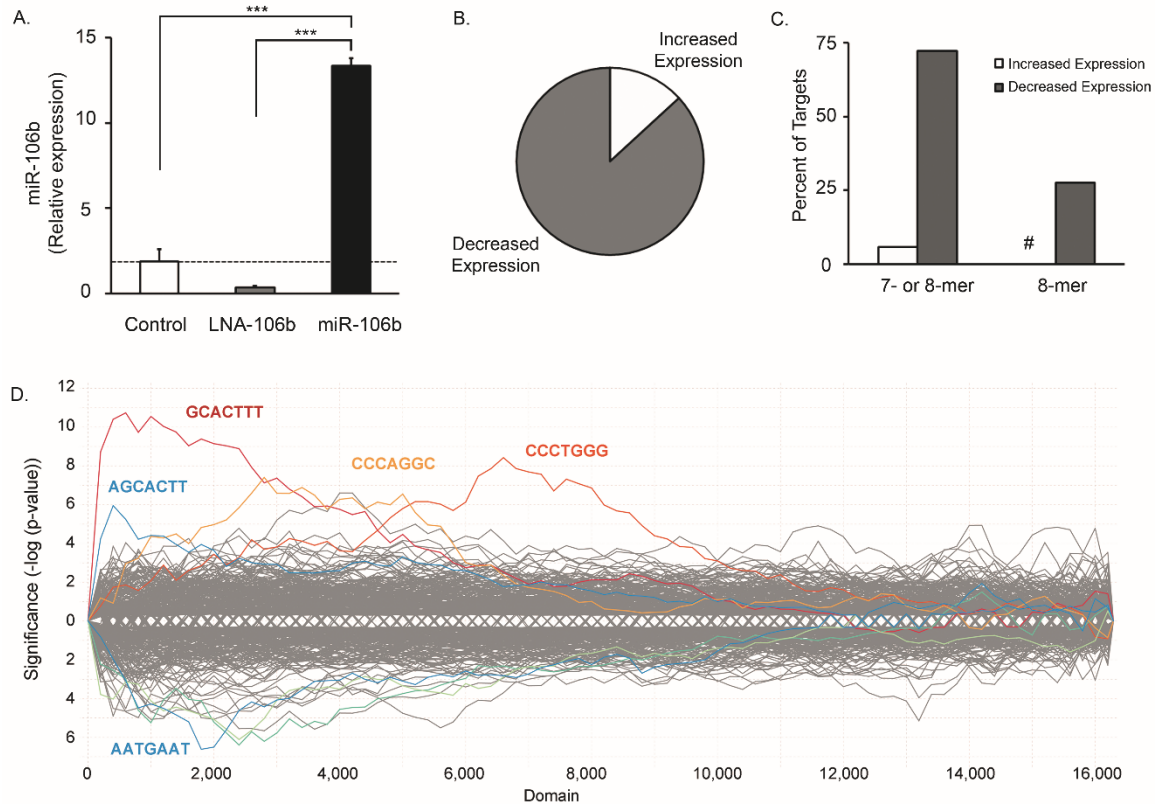

Figure 4.1. miR-106b targets in cholangiocarcinoma cells predominantly contain a seed-binding site. (**A**) miR-106b RNA levels were measured by qRT-PCR after transfection of Mz-ChA-1 cells with control LNA (Control), antagonist to miR-106b (LNA-106b), or miR-106b. Expression was normalized to Z30 and plotted as relative level. The dashed horizontal line indicates the mean of miR-106b in Control cells. Data are mean +/- SEM for three samples each. ***$p < 0.001$ using ANOVA with *post hoc* correction. (**B**) Following RNA-Seq of the LNA-106b and miR-106b samples from panel A, significantly altered transcripts were categorized as increased (13.2%) or decreased (86.8%) by miR-106b. (**C**) A majority of decreased transcripts contained one or more miR-106b seed-binding sites (7-mer or 8-mer) while only one increased transcript contained a 7-mer binding site. None of the increased transcripts contained an 8-mer binding site (#). (**D**) All transcripts identified by RNA-Seq were sorted by statistical significance of differential expression between miR-106b and LNA-106b. This sorted list (plotted on the horizontal axis) was analyzed by SylArray to identify microRNA binding sites that are over-represented, shown by colored traces. Over-representation of seed-binding sites is indicated on the vertical axis above zero, plotted on a log scale. Underrepresented sequences are plotted below zero.

Sequence determinants of miR-106b targeting

Using previously published data [349], we determined that 76.2% of miR-106b target interactions employed 7 or more consecutive miR-106b bases in the microRNA-mRNA binding hybrid. Because a high proportion of interactions contained at least 7 consecutive bases, we determined which of the miR-106b 7- or 8-mer binding sites were favored in our target gene set. We searched the 112 significant mRNA sequences for all 65,536 possible 8-mer sequences and plotted the frequency of occurrence of each 8-mer (count) versus the number of 8-mers in each bin (**Figure 4.2A**). Approximately 50% of all possible 8-mers were observed with a frequency of between 1 and 10 occurrences, while 5,020 8-mers were not observed at all (count = 0). Notably, the perfect 8-mer binding site 5'GCACTTTA was present 63 times and the overlapping 8-mer (2-9) was present 81 times. The two most over-represented 8-mers were 5'AAAAAAAA (1,987 times) and 5'TTTTTTTT (830 times). The analogous k-mer data set was developed for all possible 7-mer sequences (16,384 possible 7-mers) within the significant gene set (**Figure 4.2B**). Again the most common sequences were 5'AAAAAAA and 5'TTTTTTT. Forty-nine 7-mers were absent in the data set. The sequence complementary to bases 1-7 of miR-106b was observed 121 times, the 2-8 sequence was observed 170 times, and the 3-9 sequence was observed 147 times.

Each of the possible miR-106b-complementary 8-mers were tiled from 5' to 3' (i.e., 1-8, 2-9, 3-10, etc.). The 8-mer opposite bases 2-9 was somewhat more frequent that the 1-8 complement (**Figure 4.2C**). A similar plot of the frequency of all complementary

7-mers tiled from 5′ to 3′ showed that over-represented sequences again favored the 5′ end of miR-106b, especially the classical seed (**Figure 4.2D**). We used an unrelated, control microRNA let-7a; the same plot of tiled 8- and 7-mer sequences showed that none of these sequences were found in the top 10 percentile (**Figures 4.2C & D**).

To determine the tolerance for single-base differences within the seed sequence, we started from a perfect 1-8 sequence and systematically searched for one-off variants. For example, the 1-8 binding site 5′GCACTTTA was observed 63 times while the sequence 5′ACACTTTA occurred 26 times, thus, in the plot in **Figure 4.2E**, G is in the 8th position at a count of 63, while A is at 26. The sequence 5′GCATTTTA contains a single base difference opposite position 5 of miR-106b and was observed 40 times (96th percentile). Compare this result to the sequence 5′GCAGTTTA which was observed only 13 times (66th percentile). We plotted the counts for each of these one-off sequences as a function of the position in the miR-106b binding site (**Figure 4.2E**). The most tolerance was observed opposite position 1 of miR-106b. The next most tolerated substitution was a T at position 5, which would result in a G:U wobble base instead of a G:C pair.

The raw count for each sequence may not indicate over-representation, but rather may indicate frequently encountered 8-mers (e.g., 5′AAAAAAAA within the poly-A tail). Thus, we sought to determine the statistical significance of a number of sequences commonly observed in our set of 129 significant genes. This set contained 191 sequences due to some genes having multiple forms. To correct for natural frequency variation, we generated 1,000 additional sets of mRNAs each containing 191 random

transcript sequences and compared the frequency of the miR-106b binding sequence and related sequences. The 8-mer sequence 5'GCACTTTA was over-represented in our gene set and this finding was highly statistically significant ($p = 0$). Similarly, each of the 7-mer sequences was statistically different in our set ($p = 0$). The two C's within the miR-106b binding sequence were reassigned as T's to search for seed-binding sites including a G:U wobble, C5 and C7. The wobble at the 5th position, 5'GCATTTTA, was highly significant, as was the double wobble, 5'GTATTTTA. Tolerance for a G:U wobble at position 7 only, 5'GTACTTTA, was not as highly significant ($p = 0.022$, **Figure 4.2F**).

RNA hybrid analysis

Although the perfect complement is likely preferred, our data indicated that related sequences were also commonly overrepresented. We sought to identify the characteristics of the most thermodynamically stable miR-106b binding site in our significantly repressed genes. We used RNAhybrid to determine the microRNA:mRNA pairing with the lowest free energy for each repressed target. Next, these predicted miR-106b binding sites were analyzed using MEME Suite to identify the most common motif. The resulting sequence motif includes 6 nucleotides that align with the predicted miR-106b binding site from bases 5-10 (**Figure 4.2G; upper**). This sequence does not include the triplet U at positions 2-4, possibly because A:T pairs have less favorable free energy than G:C pairs and the query set was limited by the lowest free energy binding site from RNAhybrid.

Comparison to CLASH data

Supplemental data from a previous study [349] included 143 target mRNAs physically bound by miR-106b, including the sequence at the region of interaction. To validate the miR-106b binding characteristics we have described, we searched for sequence motifs in this published CLASH (crosslinking ligation and sequencing of hybrids) data set using MEME Suite. Within the 143 sequences, 138 contained a sequence highly related to 5'CTGTCAGCACTTTC. This is the complement of the 5' end of miR-106b from bases 2-14 (with 'C' opposite the first position of miR-106b slightly favored over the expected 'A'). The most frequently observed region of this meme is 5'CAGCA, complementary to miR-106b bases 6-10 (**Figure 4.2G; lower**). Comparing the two motifs, the sequence from bases 6-10 is most important with some contribution from flanking bases and tolerance for substitution opposite position 5 (allowing a G:U wobble). The two data sets are mostly in agreement and indicate that binding of miR-106b is anchored by G:C pairing in and near the seed.

Figure 4.2. Preferential miR-106b target binding via the 5′ end of the microRNA.
(**A**) Histogram of the distibution of 8-mers found in miR-106b-regulated sequences. The horizontal axis depicts the frequency each 8-mer was observed and the vertical axis represents the number of 8-mers at each count. The bins containing the miR-106b 1–8 and 2–9 perfect binding sequences are indicated. (**B**) Data are as in panel A except that 7-mers were analyzed. Bins containing the miR-106b 1–7, 2–8, and 3–9 perfect binding sequences are indicated. (**C**) The count of each possible 8-mer binding site in the miR-106b-regulated sequences is indicated (left). Sequences are ordered as they occur along miR-106b. The horizontal dashed line represents the count corresponding to the 90th percentile of all 8-mers (i. e., only the top 10 percent occur more frequently). The same plot except using 8-mers derived from let-7a is displayed on the right. (**D**) Counts in the miR-106b-regulated sequences of each possible 7-mer along miR-106b (left) are indicated. The horizontal dashed line represents the count corresponding to the 90th percentile of all 7-mers. The same plot except using 7-mers derived from let-7a is displayed on the right. (**E**) Single-base substitutions within the 8-base miR-106b binding site were queried for their frequency, compared to the perfect 8-mer (observed 63 times) and plotted as the nucleotide frequency (count) at each position when the other 7 positions were a perfect miR-106b match. For example, the single substitution of a 'U' opposite position 5 (forming a G:U wobble) was observed 40 times while the favored 'C' (forming a G:C pair) was found 63 times. (**F**) k-mer analysis of the count of miR-106b binding sites in the miR-106b-regulated gene set compared to 1,000 randomly chosen similarly-sized gene sets. (**G**) The binding motif for miR-106b is shown over the sequence of the microRNA (antiparallel). Taller letters indicate greater representation of that nucleotide in determining the motif. The upper motif was generated using RNA-Seq data and hybrid prediction from the current study. The analysis was performed separately on CLASH data from Helwak et al., 2013 [349], shown in the lower motif.

Figure 4.2 Preferential miR-106b target binding via the 5′ end of the microRNA

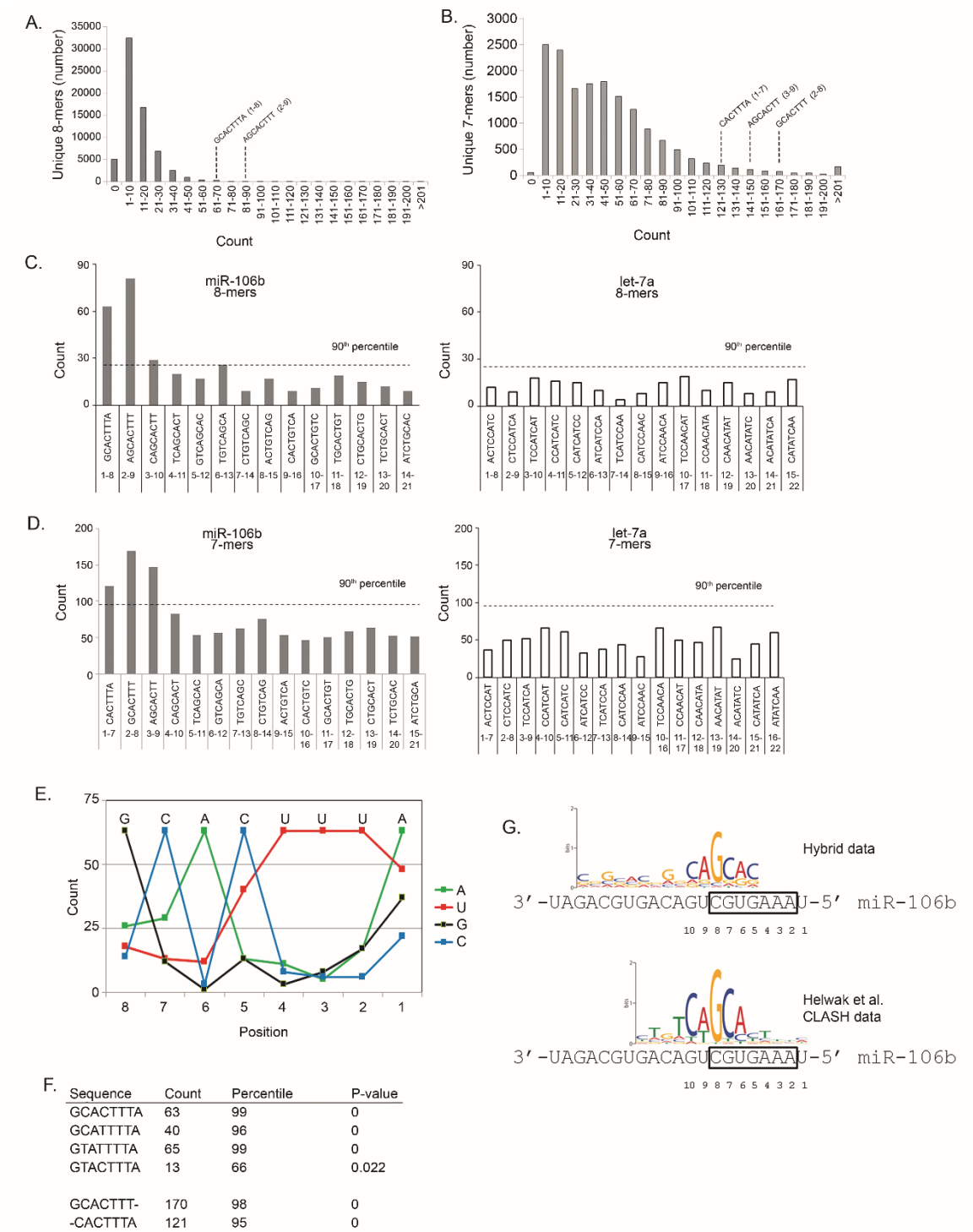

F.

Sequence	Count	Percentile	P-value
GCACTTTA	63	99	0
GCATTTTA	40	96	0
GTATTTTA	65	99	0
GTACTTTA	13	66	0.022
GCACTTT-	170	98	0
-CACTTTA	121	95	0

Genome-wide target identification

Next, the identified transcripts in our RNA-Seq data set were plotted by change in expression versus statistical significance (volcano plot). The relative expression changes between miR-106b and LNA-106b samples were plotted on the horizontal axis as log2 of the fold-change, against the statistical significance plotted as -log of the p value on the vertical axis (**Figure 4.3A**). Targets were considered significant if the -log p value was above 3.35 (e.g., $p < 4.2 \times 10^{-4}$) and this significance cutoff is indicated by the horizontal dashed line. Transcripts with decreased expression by miR-106b are to the left of zero, increased expression to the right. Expression change suppressed significant genes ranged between -1.16- to -2.22-fold reduced expression and +1.15- to +1.47-fold increased expression. Selected targets are indicated (for a complete list of the significant targets, see **Table 4.1**). Known target genes *RB1* and *IL-8* were significantly repressed [73, 350]. Among the novel targets identified in our genome-wide analysis were members of the Krüppel-like factor family, *KLF2* and *KLF6*. These targets were significantly repressed by miR-106b with a p value of $1.72*10^{-7}$ and $2.85*10^{-4}$, respectively.

Table 4.1 List of genes with differential expression by miR-106b modulation

Table 4.1: Gene Name, Downregulated	Fold Change	log2(fold change)	p value	q value
tubulin, alpha 1a (TUBA1A), transcript variants 2, 3, and 1	0.45	-1.16	0.0E+00	0.0E+00
pleckstrin and Sec7 domain containing 3 (PSD3), transcript variants 1 and 2	0.64	-0.65	1.5E-05	5.9E-03
Kruppel-like factor 2 (lung) (KLF2)	0.65	-0.63	1.7E-07	1.7E-04
centromere protein Q (CENPQ)	0.66	-0.60	4.9E-05	1.3E-02
interleukin 8 (IL8)	0.67	-0.58	0.0E+00	0.0E+00
cyclin E2 (CCNE2)	0.69	-0.53	1.3E-04	2.2E-02
abhydrolase domain containing 13 (ABHD13)	0.69	-0.53	1.6E-07	1.6E-04
transmembrane protein 64 (TMEM64), transcript variants 1 and 2	0.70	-0.52	1.5E-11	4.3E-08
epiregulin (EREG)	0.71	-0.50	0.0E+00	0.0E+00
osteopetrosis associated transmembrane protein 1 (OSTM1)	0.71	-0.50	2.1E-04	3.0E-02
BTG family, member 3 (BTG3), transcript variants 1 and 2	0.71	-0.50	2.0E-05	7.1E-03
FBJ murine osteosarcoma viral oncogene homolog (FOS)	0.71	-0.50	3.2E-10	5.2E-07
thioredoxin-related transmembrane protein 3 (TMX3)	0.72	-0.48	3.8E-10	5.5E-07
zinc finger protein 367 (ZNF367)	0.72	-0.48	4.1E-11	1.0E-07
LysM, putative peptidoglycan-binding, domain containing 3 (LYSMD3)	0.73	-0.46	1.1E-05	4.8E-03
cathepsin S (CTSS), transcript variants 2 and 1	0.73	-0.45	2.6E-05	8.4E-03
chromosome 2 open reading frame 69 (C2orf69)	0.73	-0.44	1.7E-06	1.2E-03
mitogen-activated protein kinase kinase kinase 2 (MAP3K2)	0.74	-0.44	5.6E-05	1.3E-02
FtsJ methyltransferase domain containing 1 (FTSJD1), transcript variants 2 and 1	0.74	-0.43	5.4E-05	1.3E-02
interferon-induced protein with tetratricopeptide repeats 5 (IFIT5)	0.74	-0.43	2.2E-04	3.1E-02
OTU domain containing 1 (OTUD1)	0.75	-0.42	4.3E-05	1.1E-02
ArfGAP with coiled-coil, ankyrin repeat and PH domains 2 (ACAP2)	0.76	-0.40	6.5E-06	3.5E-03
coagulation factor III (thromboplastin, tissue factor) (F3), transcript variants 2 and 1	0.76	-0.39	1.7E-10	3.1E-07
discoidin, CUB and LCCL domain containing 2 (DCBLD2)	0.76	-0.39	5.4E-11	1.1E-07
neutral cholesterol ester hydrolase 1 (NCEH1), transcript variants 1, 3, 4, and 2	0.77	-0.39	1.1E-08	1.4E-05
zinc finger and BTB domain containing 6 (ZBTB6)	0.77	-0.38	7.3E-05	1.5E-02
early endosome antigen 1 (EEA1)	0.77	-0.38	6.5E-05	1.5E-02
breast cancer metastasis-suppressor 1-like (BRMS1L)	0.77	-0.37	2.1E-05	7.2E-03
centrosomal protein 152kDa (CEP152), transcript variants 1 and 2	0.78	-0.37	9.3E-05	1.8E-02

nuclear protein, ataxia-telangiectasia locus (NPAT)	0.78	-0.36	2.2E-04	3.0E-02
RAB27B, member RAS oncogene family (RAB27B)	0.78	-0.36	1.6E-06	1.2E-03
tankyrase, TRF1-interacting ankyrin-related ADP-ribose polymerase 2 (TNKS2)	0.78	-0.36	9.1E-06	4.4E-03
family with sequence similarity 3, member C (FAM3C), transcript variants 2 and 1	0.78	-0.36	2.1E-07	2.0E-04
EF-hand calcium binding domain 14 (EFCAB14)	0.78	-0.36	1.9E-06	1.2E-03
trans-golgi network vesicle protein 23 homolog B (S. cerevisiae) (TVP23B)	0.78	-0.36	6.8E-06	3.5E-03
RMI1, RecQ mediated genome instability 1, homolog (S. cerevisiae) (RMI1)	0.78	-0.36	1.9E-04	2.8E-02
receptor accessory protein 3 (REEP3)	0.78	-0.35	9.0E-05	1.8E-02
transmembrane protein 245 (TMEM245)	0.78	-0.35	3.0E-08	3.4E-05
TBC1 domain family, member 9 (with GRAM domain) (TBC1D9)	0.79	-0.35	3.3E-05	9.8E-03
Ewing tumor-associated antigen 1 (ETAA1)	0.79	-0.34	2.4E-05	8.0E-03
twinfilin, actin-binding protein, homolog 1 (Drosophila) (TWF1), transcript variants 1 and 2	0.79	-0.34	1.6E-08	1.9E-05
transmembrane protein 167A (TMEM167A)	0.79	-0.33	2.0E-06	1.2E-03
TruB pseudouridine (psi) synthase homolog 1 (E. coli) (TRUB1)	0.80	-0.33	7.6E-05	1.6E-02
glyoxalase I (GLO1)	0.80	-0.32	3.7E-07	2.8E-04
ribonucleotide reductase M2 (RRM2), transcript variant 1	0.80	-0.32	2.3E-07	2.0E-04
integrin, alpha 2 (CD49B, alpha 2 subunit of VLA-2 receptor) (ITGA2), transcript variant 1	0.80	-0.32	3.3E-07	2.7E-04
thioredoxin domain containing 9 (TXNDC9)	0.80	-0.31	1.1E-04	2.0E-02
RAB22A, member RAS oncogene family (RAB22A)	0.80	-0.31	9.3E-06	4.4E-03
UDP-GlcNAc:betaGal beta-1,3-N-acetylglucosaminyltransferase 5 (B3GNT5)	0.80	-0.31	3.9E-04	4.6E-02
retinoblastoma 1 (RB1)	0.80	-0.31	3.0E-05	9.0E-03
ankyrin repeat domain 22 (ANKRD22)	0.81	-0.31	8.2E-06	4.1E-03
fatty acyl CoA reductase 1 (FAR1)	0.81	-0.31	3.8E-05	1.0E-02
LIM domain kinase 1 (LIMK1), transcript variants 2 and 1	0.81	-0.31	1.1E-04	2.0E-02
ubiquitin specific peptidase 1 (USP1), transcript variants 2, 3, and 1	0.81	-0.31	2.4E-05	8.0E-03
polo-like kinase 2 (PLK2), transcript variants 2 and 1	0.81	-0.31	3.5E-04	4.3E-02
deoxycytidine kinase (DCK)	0.81	-0.30	1.6E-04	2.6E-02
receptor accessory protein 5 (REEP5)	0.81	-0.30	1.4E-05	5.7E-03
CD46 molecule, complement regulatory protein (CD46), transcript variants a,d,n,c,e,f,b,l	0.81	-0.30	6.2E-06	3.5E-03
aryl hydrocarbon receptor nuclear translocator-like 2 (ARNTL2), transcript variants 2,3,4,5,1	0.81	-0.30	1.4E-04	2.3E-02
WD repeat domain 36 (WDR36)	0.81	-0.30	7.3E-05	1.5E-02
paraoxonase 2 (PON2), transcript variants 1 and 2	0.82	-0.29	1.1E-04	2.0E-02
soc-2 suppressor of clear homolog (C. elegans) (SHOC2), transcript variants 2 and 1	0.82	-0.29	2.3E-04	3.2E-02

mannose-6-phosphate receptor (cation dependent) (M6PR), transcript variants 2 and 1	0.82	-0.29	2.0E-06	1.2E-03
protein phosphatase 3, regulatory subunit B, alpha (PPP3R1)	0.82	-0.29	3.0E-05	9.0E-03
protein phosphatase 1, regulatory subunit 15B (PPP1R15B)	0.82	-0.29	3.1E-05	9.1E-03
TMED7-TICAM2 readthrough (TMED7-TICAM2), transcript variants 1 and 2	0.82	-0.28	7.1E-05	1.5E-02
fatty acid binding protein 5 (psoriasis-associated) (FABP5)	0.82	-0.28	3.1E-04	3.9E-02
transmembrane emp24 protein transport domain containing 5 (TMED5), transcript variants 2 and 1	0.82	-0.28	1.4E-04	2.3E-02
Kruppel-like factor 6 (KLF6), transcript variants B, C, and A	0.82	-0.28	2.8E-04	3.7E-02
ciliary neurotrophic factor (CNTF); ZFP91 zinc finger protein (ZFP91), transcript variants 2 and 1	0.82	-0.28	6.7E-05	1.5E-02
COP9 signalosome subunit 2 (COPS2), transcript variants 2 and 1	0.83	-0.28	2.4E-04	3.2E-02
dynein, cytoplasmic 1, light intermediate chain 2 (DYNC1LI2)	0.83	-0.28	1.1E-05	4.7E-03
karyopherin alpha 3 (importin alpha 4) (KPNA3)	0.83	-0.27	3.9E-04	4.6E-02
structural maintenance of chromosomes flexible hinge domain containing 1 (SMCHD1)	0.83	-0.27	3.6E-05	1.0E-02
glia maturation factor, beta (GMFB)	0.83	-0.27	2.8E-04	3.7E-02
dynein, light chain, Tctex-type 3 (DYNLT3)	0.83	-0.27	3.2E-04	4.1E-02
MLF1 interacting protein (MLF1IP)	0.83	-0.27	1.8E-04	2.8E-02
dickkopf 1 homolog (Xenopus laevis) (DKK1)	0.83	-0.27	5.0E-05	1.3E-02
integrin, alpha 6 (ITGA6), transcript variants 2 and 1	0.83	-0.27	5.9E-05	1.4E-02
thioredoxin-related transmembrane protein 1 (TMX1)	0.83	-0.26	5.6E-05	1.3E-02
YTH domain family, member 3 (YTHDF3)	0.83	-0.26	1.1E-04	2.0E-02
UDP-N-acetyl-alpha-D-galactosamine:polypeptide N-acetylgalactosaminyltransferase 3 (GalNAc-T3) (GALNT3)	0.83	-0.26	1.6E-05	6.1E-03
reticulocalbin 2, EF-hand calcium binding domain (RCN2), transcript variants 2 and 1	0.83	-0.26	7.4E-05	1.5E-02
RAB12, member RAS oncogene family (RAB12)	0.83	-0.26	3.9E-04	4.6E-02
v-yes-1 Yamaguchi sarcoma viral oncogene homolog 1 (YES1)	0.83	-0.26	8.6E-05	1.8E-02
eukaryotic translation initiation factor 2, subunit 1 alpha, 35kDa (EIF2S1)	0.84	-0.26	1.5E-05	5.9E-03
transmembrane protein 123 (TMEM123)	0.84	-0.26	1.1E-05	4.7E-03
epithelial cell transforming sequence 2 oncogene (ECT2), transcript variants 1, 2, and 3	0.84	-0.25	3.5E-05	1.0E-02
ATPase family, AAA domain containing 2 (ATAD2)	0.84	-0.25	1.8E-05	6.4E-03
RNA binding motif (RNP1, RRM) protein 3 (RBM3)	0.84	-0.25	1.3E-04	2.3E-02
transmembrane protein 30A (TMEM30A), transcript variants 2 and 1	0.84	-0.25	4.0E-04	4.6E-02
family with sequence similarity 91, member A1 (FAM91A1)	0.84	-0.25	2.0E-04	3.0E-02
ATP-binding cassette, sub-family E (OABP), member 1 (ABCE1), transcript variants 2 and 1	0.84	-0.25	1.9E-04	2.8E-02
integrin, alpha V (ITGAV), transcript variants 2, 3 and 1	0.84	-0.25	1.2E-04	2.1E-02

RAD18 homolog (S. cerevisiae) (RAD18)	0.84	-0.25	3.3E-04	4.1E-02
cytidine monophosphate (UMP-CMP) kinase 1, cytosolic (CMPK1), transcript variants 2 and 1	0.84	-0.25	3.8E-05	1.0E-02
signal peptidase complex subunit 3 homolog (S. cerevisiae) (SPCS3)	0.84	-0.24	9.1E-05	1.8E-02
ERO1-like (S. cerevisiae) (ERO1L)	0.84	-0.24	4.2E-04	4.7E-02
ras homolog family member B (RHOB)	0.85	-0.24	2.8E-04	3.7E-02
alkylglycerone phosphate synthase (AGPS)	0.85	-0.24	4.1E-04	4.6E-02
nuclear fragile X mental retardation protein interacting protein 2 (NUFIP2)	0.85	-0.24	3.0E-04	3.9E-02
ubiquitin protein ligase E3C (UBE3C)	0.85	-0.24	6.0E-05	1.4E-02
prostaglandin-endoperoxide synthase 2 (prostaglandin G/H synthase and cyclooxygenase) (PTGS2)	0.85	-0.23	2.3E-04	3.2E-02
potassium channel tetramerisation domain containing 9 (KCTD9)	0.85	-0.23	4.0E-04	4.6E-02
poly(A) polymerase alpha (PAPOLA), transcript variants 2, 3, and 1	0.85	-0.23	3.6E-04	4.4E-02
solute carrier family 25 (mitochondrial carrier; phosphate carrier), member 24 (SLC25A24), transcript variants 1 and 2	0.85	-0.23	3.6E-04	4.4E-02
eukaryotic translation initiation factor 1A, X-linked (EIF1AX)	0.85	-0.23	9.8E-05	1.9E-02
nicotinamide phosphoribosyltransferase (NAMPT)	0.85	-0.23	3.0E-04	3.9E-02
lysophospholipase I (LYPLA1)	0.85	-0.23	1.9E-04	2.8E-02
DEK oncogene (DEK), transcript variants 2 and 1	0.85	-0.23	3.7E-04	4.4E-02
CD55 molecule, decay accelerating factor for complement (Cromer blood group) (CD55), transcript variants 1 and 2	0.86	-0.22	2.1E-04	3.0E-02
solute carrier family 38, member 2 (SLC38A2)	0.86	-0.22	1.9E-04	2.8E-02

Gene Name, Upregulated	**Fold Change**	**log2(fold change)**	**p value**	**q value**
lipocalin 2 (LCN2)	1.16	0.21	2.7E-04	3.7E-02
FK506 binding protein 8, 38kDa (FKBP8)	1.17	0.23	1.7E-04	2.6E-02
biliverdin reductase B (flavin reductase (NADPH)) (BLVRB)	1.17	0.23	3.9E-04	4.6E-02
ribosomal protein S28 (RPS28)	1.18	0.24	9.3E-05	1.8E-02
pancreatic progenitor cell differentiation and proliferation factor homolog (zebrafish) (PPDPF)	1.19	0.25	5.6E-05	1.3E-02
phosphoglycerate dehydrogenase (PHGDH)	1.19	0.25	2.0E-04	2.9E-02
mevalonate (diphospho) decarboxylase (MVD)	1.20	0.26	1.1E-04	2.0E-02
mucin 5B, oligomeric mucus/gel-forming (MUC5B)	1.21	0.27	5.6E-06	3.3E-03
ribosomal protein L28 (RPL28), transcript variants 2, 1, 3, 4, and 5	1.21	0.28	1.3E-04	2.3E-02
(Unassigned; overlap with mucin 5AC, oligomeric mucus/gel-forming (MUC5AC))	1.22	0.29	2.9E-05	9.0E-03
N-myc downstream regulated 1 (NDRG1), transcript variants 1,3, 4, and 2	1.24	0.31	1.5E-04	2.4E-02
RNA, 5.8S ribosomal 5 (RNA5-8S5), ribosomal RNA	1.25	0.32	1.5E-04	2.4E-02

phosphoenolpyruvate carboxykinase 2 (mitochondrial) (PCK2), transcript variants 2 and 1	1.26	0.33	1.1E-04	2.0E-02
DNA-damage-inducible transcript 4 (DDIT4)	1.31	0.39	1.4E-11	4.3E-08
mucin 2, oligomeric mucus/gel-forming (MUC2)	1.36	0.44	1.6E-05	6.0E-03
ubiquitin domain containing 1 (UBTD1)	1.43	0.52	6.8E-05	1.5E-02
LY6/PLAUR domain containing 2 (LYPD2)	1.48	0.56	1.7E-04	2.6E-02

Table 4.1. List of genes with differential expression by miR-106b modulation. RNA-Seq results tabulated here list the 129 genes that had a significant expression differential between miR-106b-transfected and LNA-106b-transfected cells. The 112 downregulated genes are listed first, followed by the 17 upregulated genes. Annotated genes are listed in the leftmost column, and followed to the right by the fold change in expression, then the log2 of fold change. Significance is given in the next two columns as a p-value and false discovery rate-corrected q-value.

Figure 4.3. miR-106b target discovery by RNA-Seq. (**A**) Volcano plot of gene expression by RNA-Seq. miR-106b RNA levels were altered by transfection of Mz-ChA-1 cells with LNA-106b or miR-106b and the resulting differential expression of all genes was evaluated. Transcripts are plotted as log2 of expression fold change on the horizontal axis versus –log of the p value on the vertical axis. Gene expression change was considered significant at –log p > 3.35 and this cutoff is indicated by the dashed line. Significantly altered transcripts were either decreased (left of 0) or increased (right of 0). Labeled genes are those that have been evaluated for modulation by miR-106b through additional experiments. (**B**) Venn diagram demonstrating overlap of our RNA-Seq miR-106b target repression results with microRNA target prediction databases TargetScan and Micro-T. Our data contained 35 novel targets not predicted by either program.

Figure 4.3 miR-106b target discovery by RNA-Seq

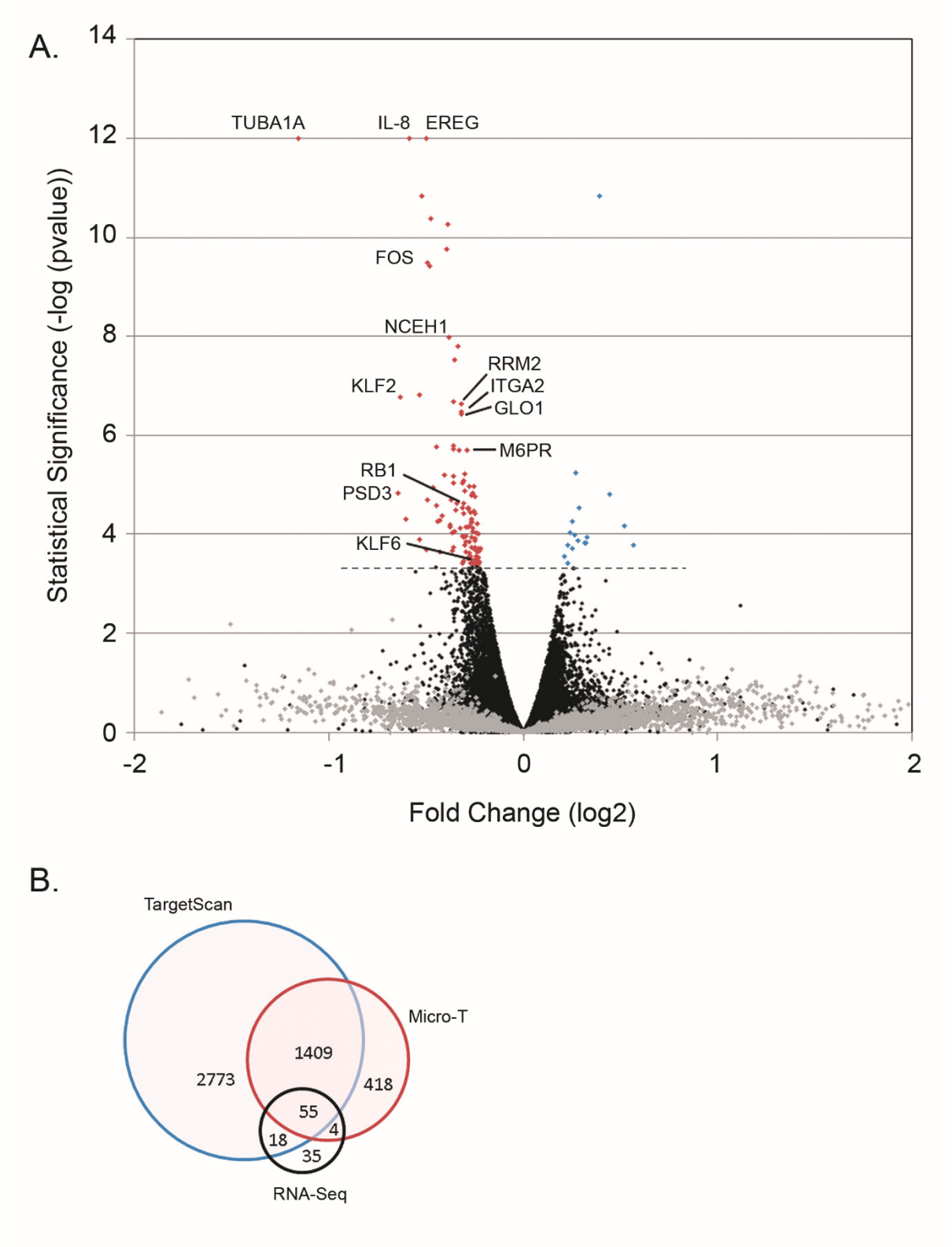

We compared our experimentally determined set of 112 repressed mRNAs, labeled "RNA-Seq," to the genes predicted by TargetScan [351] or Micro-T [352], and compared the two prediction programs to each other as well. **Figure 4.3B** shows a Venn diagram of the number of shared targets in these data sets. The majority of genes contained in our data set were predicted by one or both programs, though 35 experimentally identified targets were not predicted by either program (**Figure 4.3B**). We have also compared our target list with the genes confirmed by CLASH and find that only *ERO1L, FAM91A1,* and *YES1* were identified as miR-106b targets both in our data and that of Tollervey and colleagues [349].

Target validation

A subset of the 112 significant targets identified by RNA-Seq was chosen in part based on both statistical significance and difference in expression. Next, we performed a literature search to identify candidates that may affect tumor cell behavior and we included targets for validation that may play a role in the cancer phenotype. We transfected Mz-ChA-1 cells with negative control LNA, miR-106b, or LNA-106b and isolated total RNA. Transcript levels of selected targets were determined by quantitative RT-PCR and normalized to 18S rRNA. Targets confirmed by RT-PCR include *EREG*, *RRM2*, *ITGA2*, *RB1*, *GLO1*, *M6PR*, and *PSD3*. We also evaluated non-target negative controls *ITGA3* and *HRAS* and found no change by LNA-106b compared to negative control LNA. (**Figure 4.4A**). *NCEH1* was a target identified by RNA-Seq that had a trend towards increased mRNA expression upon miR-106b antagonism, but the change was

not statistically significant ($p = 0.07$). We did not observe a change in mRNA level in RNA-Seq target *FOS* by RT-PCR. Many of these putative miR-106b-regulated mRNAs showed altered levels upon miR-106b transfection in KMCH and HuCCT cholangiocarcinoma cell lines (**Supplemental Figures 1A & 2A**, see end of chapter). Not all miR-106b targets will be identified by the current method, specifically those that do not have a decrease in mRNA levels. We have not exhaustively attempted to determine the identity of such targets, but did recognize TRAIL death receptor DR5 (TNFRSF10B) as a predicted miR-106b target by TargetScan. Because miR-106b is clustered with miR-25, and miR-25 regulates cell death by targeting (DR4) [71], we tested whether miR-106b decreased the functionally related DR5 protein. Transfection with miR-106b decreased DR5 protein levels (**Figure 4.4B**), potentially acting to complement miR-25-mediated DR4 repression and promote TRAIL resistance. Additionally, we tested regulation of RB1 and E2F1 proteins, both known miR-106b targets. Transfection of miR-106b into Mz-ChA-1 cells decreased RB1 and E2F1 protein expression (**Figure 4.4B**).

We used biotinylated miR-106b in order to demonstrate a physical interaction with targets by affinity binding and capture. Mz-ChA-1 cells were transfected with either biotinylated miR-106b or biotinylated *C. elegans* miR-67 (Cel-miR-67) as a control. Biotin-bound RNA was isolated and RT-PCR was performed for *IL-8* and *KLF2*. We observed significant enrichment of *IL-8* and *KLF2* transcripts with biotinylated miR-106b pull-down versus control Cel-miR-67 pull-down (**Figure 4.4C**).

Figure 4.4. RNA-Seq target validation. (**A**) qRT-PCR for nine candidate targets from RNA-Seq. Relative expression is significantly increased for LNA-106b compared to miR-106b in seven of the genes. There was a trend towards increased expression for LNA-106b compared to miR-106b for NCEH1 but it was not statistically significant ($p = 0.07$). FOS did not have significant change in expression by qRT-PCR. Dotted line represents expression level for scrambled control LNA. ITGA3 and HRAS are non-target negative control genes which show no significant expression change. Relative expression is given on the left y-axis and fold change is shown on the right y-axis. (**B**) Immunoblot showing transfection with miR-106b decreased protein levels of DR5, RB1, and E2F1 in Mz-ChA-1 cells. (**C**) Schematic of experimental design for capture of mRNA targets using biotinylated microRNA. Briefly, Mz-ChA-1 cells were transfected for 24 hours with either mature human miR-106b or *C. elegans* miR-67 which had been biotinylated. Cells were lysed and incubated with streptavidin-bound beads to capture biotinylated microRNA and associated mRNAs. Total RNA was isolated and relative expression of target mRNAs KLF2 and IL-8 was measured for enrichment by qRT-PCR. 18S rRNA was used as a control RNA. $*p < 0.05$; $**p < 0.01$; $***p < 0.001$; using ANOVA with *post hoc* correction.

Figure 4.4 RNA-Seq target validation

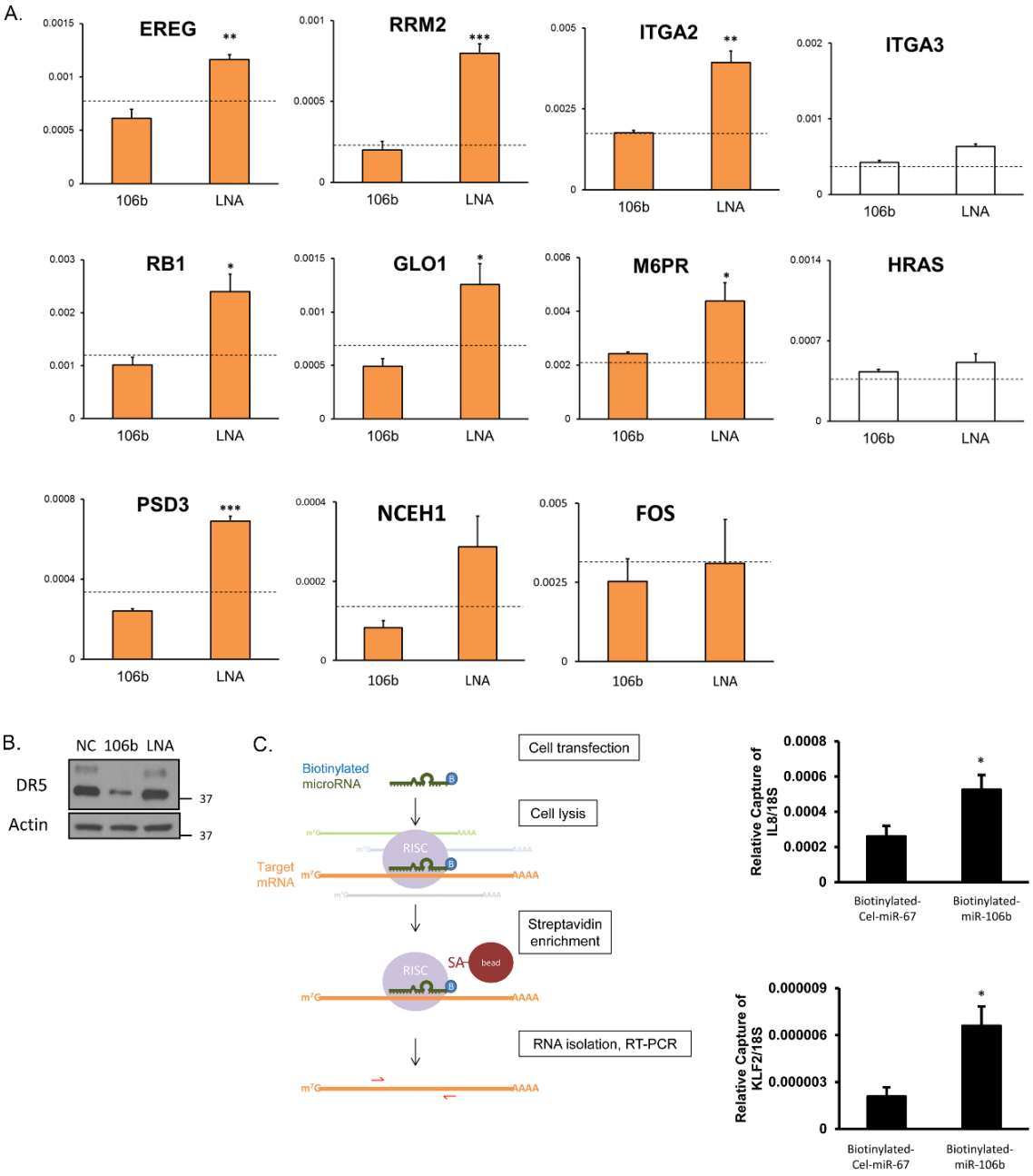

MiR-106b targets multiple KLF family members

Based on the observed decrease in *KLF2* and *KLF6* in the RNA-Seq data set, we tested the effects of miR-106b on additional KLF family members. KLFs represent a large family of transcription factors, of which many act as tumor suppressors and are often downregulated in cancer [228, 353]. We confirmed that *KLF2* and *KLF6* mRNAs were regulated by miR-106b and found other KLF family members *KLF4*, *KLF10*, *KLF11* and *KLF13* to have increased expression when cells were transfected with LNA-106b (**Figure 4.5A**). Many of these KLFs showed altered mRNA levels upon miR-106b transfection in KMCH and HuCCT cholangiocarcinoma cell lines (**Supplemental Figures 1B & 2B**, see end of chapter). Additionally, we examined the effects of miR-106b on protein expression of KLFs by immunoblot in Mz-ChA-1 cells. We observed decreased expression of KLF2, KLF4, KLF6, and KLF10 after 24 hours of transfection with miR-106b compared to negative control LNA and a slight increase in expression with LNA-106b (**Figure 4.5B**).

Figure 4.5 miR-106b regulates multiple KLF family members

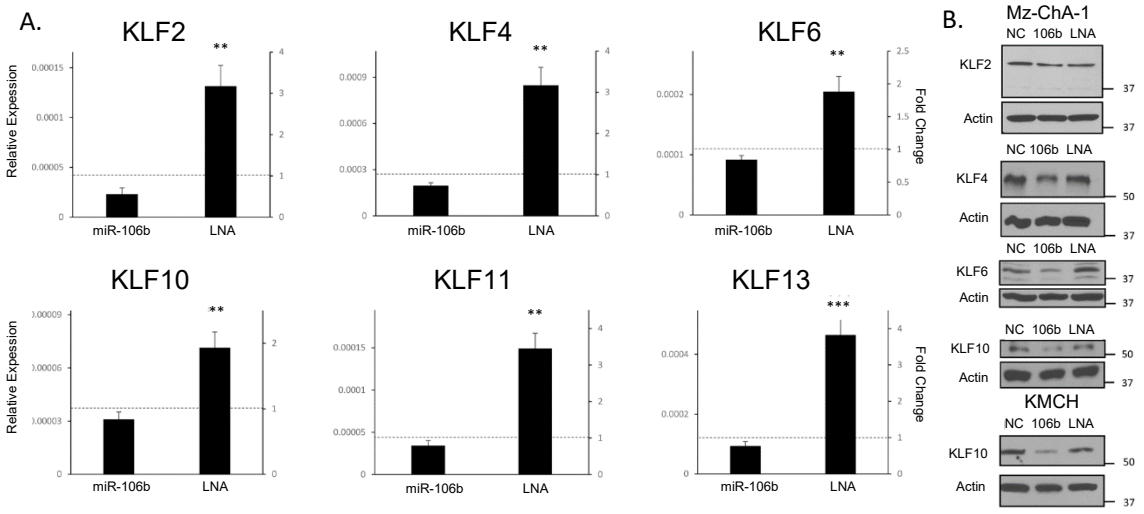

Figure 4.5. miR-106b regulates multiple KLF family members. (**A**) qRT-PCR for candidate miR-106b targets KLF2 and 6 confirmed regulation at the mRNA level. KLF transcript expression was increased by miR-106b antagonism with LNA-106b compared to miR-106b. Additional members KLF4, 10, 11, and 13 were evaluated and showed the same pattern of expression increase with LNA-106b antagonism compared to miR-106b treatment. Relative expression is given on the left y-axis and fold change is shown on the right y-axis. (**B**) Immunoblots show repression of KLFs 2, 4, 6 and 10 by miR-106b at the protein level. 24 hour transfection of Mz-ChA-1 or KMCH cells with control LNA, miR-106b, or LNA-106b led to decrease in KLF protein expression by miR-106b compared to control LNA or LNA-106b. Actin was probed as a loading control. *$p < 0.05$; **$p < 0.01$; ***$p < 0.001$; using ANOVA with *post hoc* correction.

Proliferation

To investigate the role of miR-106b in proliferation of cholangiocarcinoma cells, we assessed the change in cell number over time using the MTT assay. Mz-ChA-1, KMCH, and BDEneu cholangiocarcinoma cells were transfected with miR-106b, LNA-106b or negative control LNA for 24 hours. Cells were then allowed to grow for up to 72 hours. We did not observe any significant difference in cell proliferation upon alteration of miR-106b levels. To eliminate the possibility of a long-term effect on cell growth, we repeated the assay over a one-week course in Mz-ChA-1 cells and again observed no change in proliferation (data not shown). Therefore, although RB1 and E2F1 were confirmed as miR-106b-regulated proteins, there was no effect on proliferation indicating that RB1 and E2F1 may not have a dominant role in cholangiocarcinoma cell proliferation.

MiR-106b protects against apoptosis

KLF2, KLF6 and KLF10 were all regulated by miR-106b and are known to promote apoptosis [217, 354, 355]. Our data demonstrated additionally that DR5, a pro-apoptotic death receptor, was regulated by miR-106b. Thus, we reasoned that miR-106b may protect against apoptosis in cholangiocarcinoma cells. H69, KMCH, and Mz-ChA-1 cells were transfected with miR-106b, LNA-106b or negative control followed by treatment with either TRAIL or staurosporine to induce cell death. We observed a decrease in apoptotic nuclei by DAPI staining upon transfection with miR-106b and an

increase in apoptotic nuclei upon transfection with LNA-106b (**Figure 4.6**). Thus, miR-106b acts in part to protect cholangiocarcinoma cells from apoptosis.

Figure 4.6 miR-106b protects against TRAIL- or staurosporine-induced apoptosis in cholangiocarcinoma cells

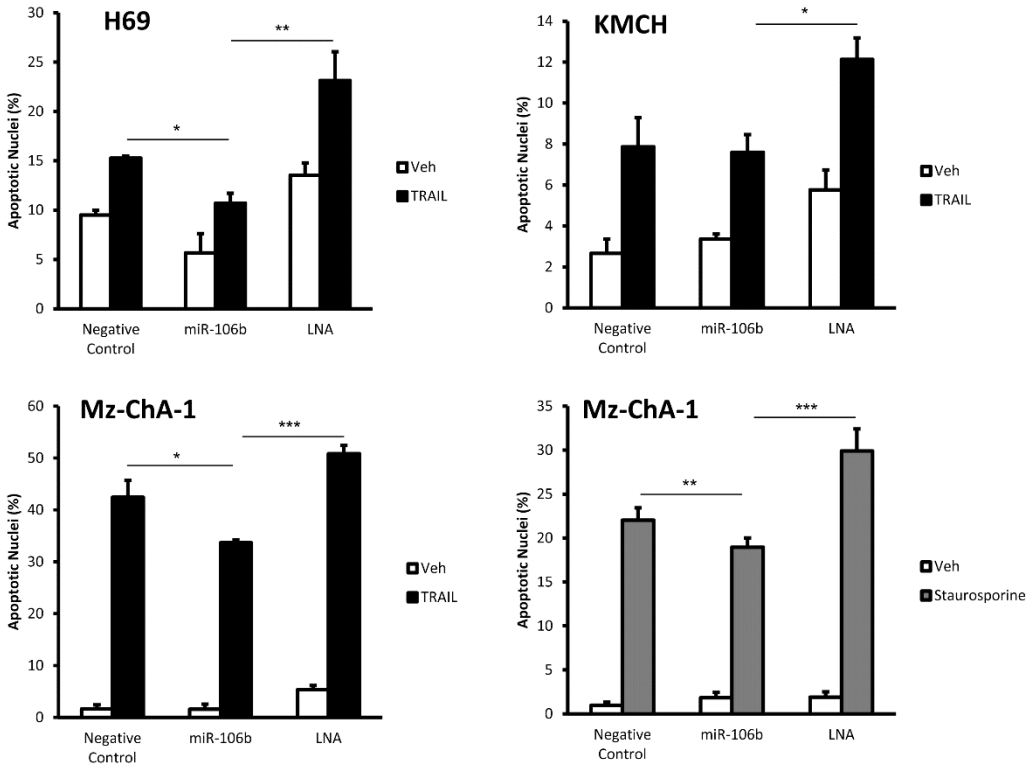

Figure 4.6. miR-106b protects against TRAIL- or staurosporine-induced apoptosis in cholangiocarcinoma cells. H69, KMCH or Mz-ChA-1 cells were transfected with control LNA (Negative Control), miR-106b or LNA-106b (LNA) for 24 hours followed by treatment with either TRAIL or staurosporine to induce apoptosis. Vehicle controls (Veh) were water for TRAIL experiments and DMSO for staurosporine experiments. We observed a decrease in apoptotic nuclei by DAPI staining upon transfection with miR-106b and an increase in apoptotic nuclei upon transfection with LNA-106b. DAPI-positive nuclei were counted and expressed as a percent of total nuclei. Data are a mean of three experiments +/− SEM. *$p < 0.05$; **$p < 0.01$; ***$p < 0.001$; using ANOVA with *post hoc* correction.

Discussion

The data presented herein relate to mRNAs regulated by miR-106b in cholangiocarcinoma cells. A number of cancer types overexpress miR-106b, which increases the potential value of the miR-106b target gene set to include tumors beyond cholangiocarcinoma. The principal findings reported here show: (i) miR-106b repressed 112 mRNA targets; (ii) most target genes contained a 7- or 8-mer seed-binding site; (iii) multiple KLF family proteins are targeted by miR-106b; and (iv) miR-106b promoted tumor cell survival in cholangiocarcinoma cells. Each of these findings will be discussed below.

Our study has revealed 112 mRNAs that were negatively regulated by miR-106b. Some known miR-106b-regulated genes (e.g., *RB1, IL-8, F3, YES1, FAM91A1*, and *ERO1L*) were identified and several novel targets were uncovered as well. Our experiments did not further investigate a functional role for these known targets. Not all previously identified miR-106b-regulated genes were significantly altered in our study. Specifically, we did not observe any change in the mRNA levels of *PTEN, E2F1*, or *BCL2L11* (Bim). A lack of change in expression of these mRNAs may reflect cell line-specific differences in microRNA targeting, changes in mRNA levels below the threshold of detection, or post-transcriptional effects that do not change mRNA levels. Reduced E2F1 protein expression, for example, was observed upon miR-106b induction, demonstrating that not all targets have altered mRNA levels. Previously unknown genes that were regulated at the mRNA level include KLF family members, which are discussed below.

MicroRNA binding depends on sequence complementarity. The degree of complementarity and length of consecutive bases can vary, resulting in refinement of rules of binding [356] and definition of new types or classes of microRNA:mRNA interactions [349]. Classes I-III interactions involve complementarity within the seed region. Class IV interactions show complementarity in a more central region, described as centered pairing [348]. Finally, Class V interactions exhibited distributed pairing, where discrete continuous regions of complementarity were not observed [349]. These data are consistent with a role for microRNAs in regulating expression of mRNAs based on sequence complementarity but not strictly limited to seed pairing. Our expression change data support direct targeting of candidate mRNAs. However, binding was presumed to be direct as evidenced by target sequence complementarity and functional effects. Physical binding was experimentally tested through pull-down of mRNAs bound to biotinylated miR-106b, performed for KLF2 and IL8. Perhaps not surprisingly, the GC content of microRNA binding motifs, representing the average or commonly identified binding site over many mRNAs, was higher than the GC content of microRNA seed regions in general [349]. Thus, binding energy may be more important than binding position, a concept incorporated into the microRNA target prediction algorithm RNAhybrid [301].

Over 70% of mRNAs that were decreased contained either a 7-mer or 8-mer miR-106b binding site. Analysis of all 8-mers or 7-mers in miR-106b-regulated sequences demonstrated that the sequences at or near the seed, including up to nucleotide 10, were

over-represented. This over-representation of the 7-mer and 8-mer sequences was highly statistically significant when compared to the expected distribution of the same sequences in a thousand random gene sets of the same size. The seed sequence tolerated a 'U' in the place of 'C' (resulting in G:U wobble pairing) opposite positions 5, 7, or both. Two hydrogen bonds connect the G:U pair while three hydrogen bonds stabilize the G:C pair, suggesting there may be a thermodynamic cost to miR-106b binding sites with G:U wobbles. Alternatively, the exocyclic amino group of 'G' is available for additional interactions when 'G' is paired with 'U' [357], allowing for the possibility of compensatory stabilizing hydrogen bonds to functional groups within the RISC polypeptides.

Based on both the CLASH dataset [349] and our own, we found that the sequence 5'U<u>CAGCAC</u>U represents an 'average' sequence motif serving as a binding site for miR-106b, with the best evidence for the central 6-mer (underlined, complementary to miR-106b based 5-10). While this is the average binding sequence, the most prevalent 7-mer was 5'GCACUUU and the most common 8-mer was 5'AGCACUUU. The difference between the average and the most prevalent sequences is that the average (in our data set) was determined using the single-most-stable predicted binding site, as identified by RNAhybrid. Such a filter will bias against the triplet UUU. Still, the agreement between our average binding motif and the motif generated from CLASH data where this potential bias is not relevant suggests that this filter is not unreasonable. Overall, we find good evidence that binding favors complementarity near

the 5′ end of the microRNA, consistent with the seed model, as well as evidence that the sequence tolerates a slight shift toward the center of miR-106b.

Comparison of our data set of modulated genes and that obtained by CLASH showed a striking near-absence of overlap in the mRNAs identified. Indeed, of the 143 mRNAs in the CLASH set and 112 genes down regulated in our experiment, only three mRNAs were on both lists: *ERO1L*, *YES1*, and *FAM91A1*. None of these contains an 8-mer binding site. *YES1* and *FAM91A1* each have a single copy of the 7-mer-m8 binding site and *YES1* has an additional 7-mer-A1 binding site. The cell lines used in the two studies are very different, Flp-In T-REx 293 embryonic kidney-derived cells versus Mz-ChA-1 biliary tract cancer-derived cells. The techniques used are also different. Finally, data from the CLASH study reflect steady-state interactions of all detected microRNAs and their targets, while the current study assessed acute changes to mRNA targets after manipulation of only miR-106b. It is likely that different cell types will have a different microRNA target landscape, and that identification of these targets by several methods will allow a detailed understanding of mRNA regulation and binding by microRNAs.

An important finding in the current study was the coordinated regulation of multiple KLF family members. The seventeen members of the KLF family of transcription factors are involved in a diverse range of biological functions and aberrations can lead to disorders such as cardiovascular and respiratory disease, obesity, inflammatory diseases and cancer [155]. Many KLF family members have been implicated in some aspect of cancer cell biology including growth, apoptosis,

differentiation, and migration [215]. We have revealed regulation of six KLF members by miR-106b in our study. Two members, *KLF2* and *KLF6*, were significantly repressed genes in our RNA-Seq experiment. Additionally, *KLF4*, *KLF10*, and *KLF11* were somewhat near the cutoff for significance ($p = 0.024$, 0.038, and 0.032 respectively), while *KLF13* mRNA in the RNA-Seq data did not suggest regulation ($p = 0.81$). These six KLFs were demonstrated to be miR-106b-responsive genes by qRT-PCR. In particular, the result for *KLF13* was surprising as this gene was included as a control under the expectation it would not be responsive to miR-106b. The coordinated modulation of these six family members may indicate a functional aspect of miR-106b biology that was not previously appreciated. Each of the KLFs regulated by miR-106b in our study has tumor-suppressive function in one or several cancers. KLF2 has been shown to induce apoptosis and to be a tumor suppressor in prostate and breast cancer cell lines as well as in xenograft mice [228]. In pancreatic cancer cells, KLF2 expression is decreased and its enforced expression leads to inhibition of growth and metastasis [221]. KLF4 regulates proliferation and differentiation of lung cancer cells and its deletion in a mouse is enough to generate tumors [358]. KLF6 reduced tumorigenic features in osteosarcoma cells [359] and its expression is reduced in human and mouse prostate cancer [360]. Loss of KLF6 expression results in increased liver mass, decreased cyclin-dependent kinase inhibitor p21, and correlated with low p21 in liver cancer [361]. Mice deficient in *KLF10* exhibit increased skin tumorigenesis when exposed to carcinogens [362]. Knockdown of *KLF11* in leiomyoma cells leads to increased proliferation and its expression is lower in tumor tissue compared to normal [363]. KLF13 is shown to repress anti-apoptotic Bcl-2

in acute lymphoblastic leukemia [364]. These varied and overlapping anti-tumorigenic features of KLFs in cancer make them attractive potential targets for future study in cholangiocarcinoma.

Resistance to apoptosis is a characteristic of cholangiocarcinoma cells. Several studies implicate KLFs in the regulation of apoptosis in tumor cells but their role in cholangiocarcinoma cell death is unknown. Overexpression of KLF2 in hepatocellular carcinoma cell lines led to increased cell death [365]. KLF6 has dual roles in apoptosis as its wildtype form is pro-apoptotic [366], while the splice variant SV1, which is overexpressed in cancer [367], is anti-apoptotic. KLF10 promotes cell death in human leukemia cells through upregulation of pro-apoptotic proteins Bim and Bax [355]. We have shown regulation of six KLFs by miR-106b. Antagonism of miR-106b with LNA led to increased apoptosis sensitivity in cholangiocarcinoma cells. In part, this effect could be through derepression of pro-apoptotic KLFs. Alternatively, apoptosis could be controlled through other miR-106b targets either regulated at the levels of mRNA or protein. We have not functionally tested which miR-106b targets regulate apoptosis.

In summary, we reveal a landscape of miR-106b-responsive genes in cholangiocarcinoma cells and report on the particular seed-binding character of this microRNA with its target transcripts. Several members of the KLF family of transcription factors were discovered to be modulated by miR-106b. Finally, we showed that miR-106b is protective against apoptosis in cholangiocarcinoma cells.

In-depth study of miR-106b and its target landscape in cholangiocarcinoma cell lines provided candidates of interest for further investigation. For instance, some of the responsive KLFs have been implicated as tumor suppressors in multiple cancers. This suggested that the coordinate repression of these transcription factors could have possible overlapping or compounding effects on tumor biology. However, the degree of KLF suppression by miR-106b is mild. Therefore, more direct means of KLF manipulation in cholangiocarcinoma were desired in order to examine functional changes with more robust modulations in KLF expression. We chose to investigate the potential tumor suppressive role of KLF2 in particular. These studies are the basis of the following chapter.

Figure 4.7 *Supplemental Figure 1, miR-106b modulation of candidate target genes in KMCH cells*

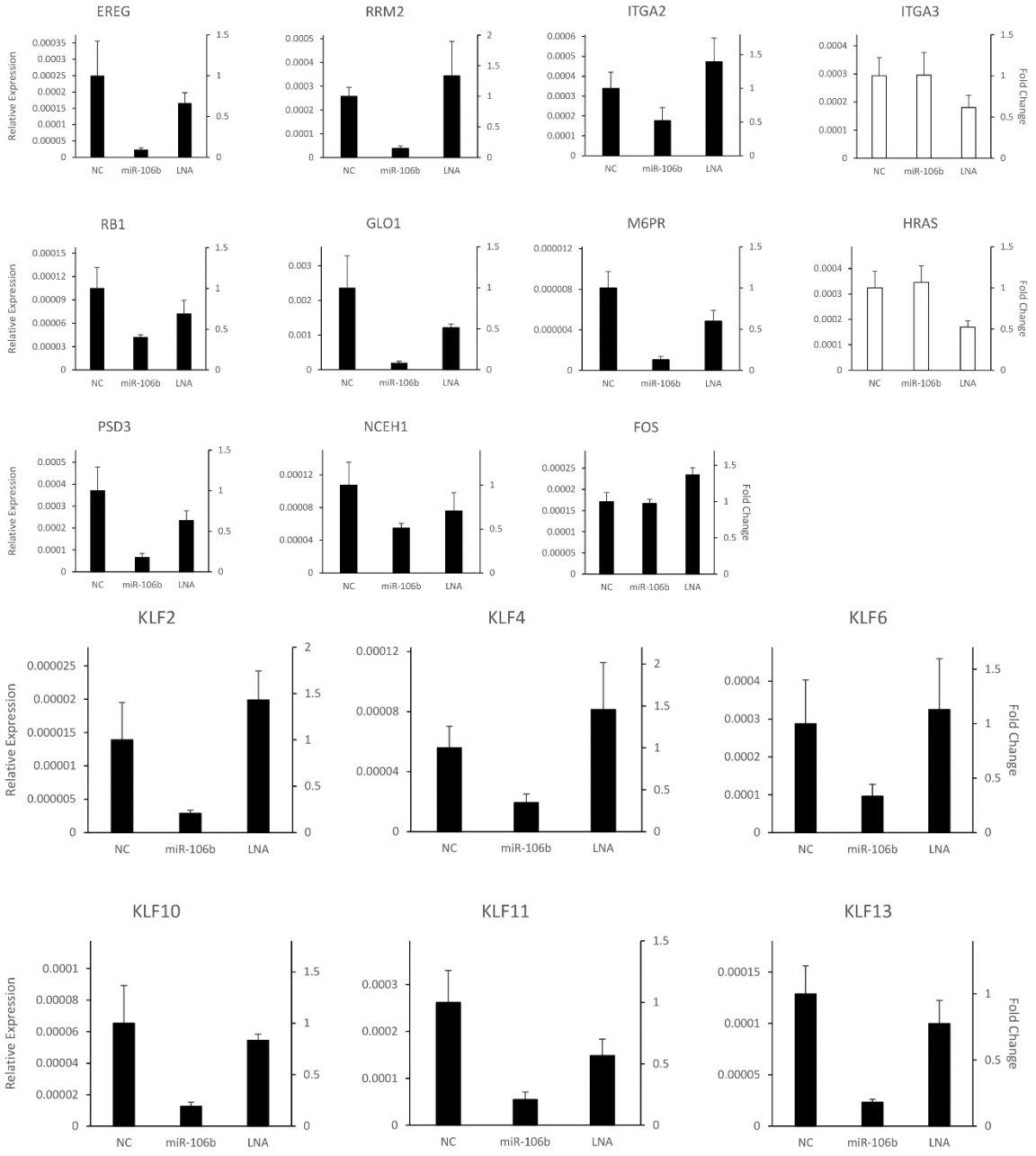

Supplemental Figure 1. miR-106b modulation of candidate target genes in KMCH cells. KMCH cells were transfected with negative control LNA (NC), miR-106b, or antisense LNA against miR-106b (LNA) for 48 hours. Total RNA was collected and gene expression normalized to 18S rRNA. Relative expression is depicted on the left y-axis and fold change is on the right y-axis. KMCH cells showed a marked reduction in candidate gene expression for miR-106b-treated samples compared to control and LNA conditions. Non-target negative controls did not display this same trend (**A**). The same conditions were used to test for KLF expression and again showed miR-106b decreased the mRNA levels for these selected KLFs (**B**).

Figure 4.8 *Supplemental Figure 2, miR-106b modulation of candidate target genes in HuCCT cells*

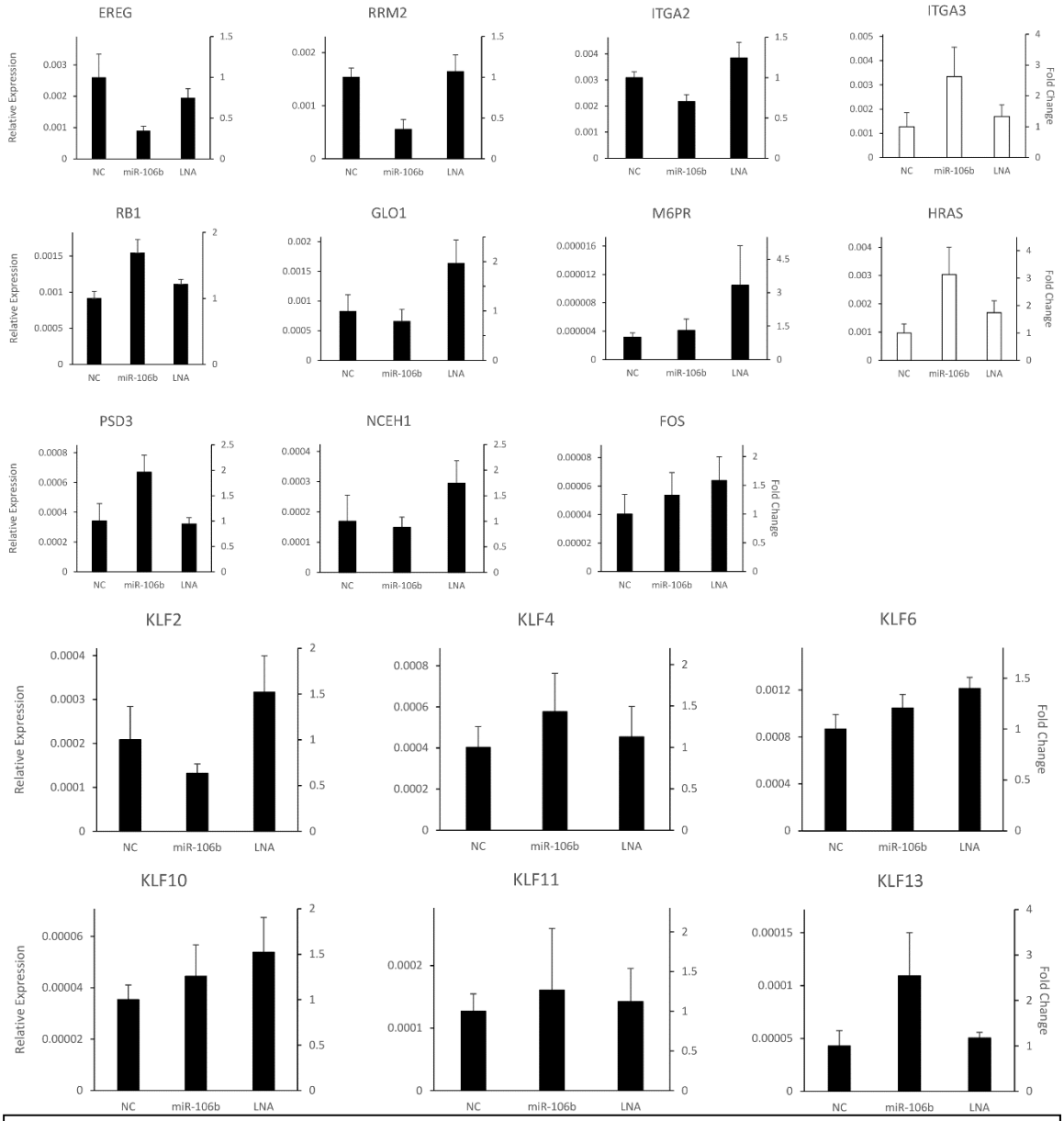

Supplemental Figure 2. miR-106b modulation of candidate target genes in HuCCT cells. Selected gene target mRNA expression levels were determined by quantitative RT-PCR. HuCCT cells were transfected with negative control LNA (NC), miR-106b, or LNA against miR-106b (LNA) for 48 hours. Total RNA was collected and gene expression normalized to 18S rRNA. Relative expression is depicted on the left y-axis and fold change is on the right y-axis. In HuCCT cell line, not all candidate target expression levels were changed by miR-106b expression or repression. However, some candidate targets exhibited repression by miR-106b, including EREG, RRM2, ITGA2 and GLO1. (**A**). The KLFs tested also generally did not show regulation by miR-106b in HuCCT cells. (**B**). These results are indicative of variation in target landscape across different cell lines.

Chapter 5 - The primary cilium-KLF2 signaling axis in bile duct cells

Abstract

Cholangiocarcinoma is a solid tumor formed in the bile duct epithelium, and often, therefore, becomes a physical obstruction, causing impaired or stopped bile flow (cholestasis). Normal cholangiocytes detect bile flow in the ductal lumen with an extension of the apical membrane called the primary cilium. However, these sensory organelles are often lost in malignant cells. Krüppel-like factor 2 (KLF2) is an important flow-sensitive transcription factor involved in shear stress response in endothelial cells, and has anti-proliferative, anti-inflammatory, and anti-angiogenic effects. The potential role of KLF2 in cholangiocyte flow detection and in cholangiocarcinoma is unknown. We sought to elucidate functional effects of KLF2 and posited regulation of proliferation, migration and apoptosis in cholangiocarcinoma cells. We hypothesized that reduced bile flow may contribute to malignant features in cholangiocarcinoma through regulation of KLF2 signaling. Additionally, investigated cilia-mediated KLF2 expression in cholangiocytes as we consider a potential connection between these flow-responsive signaling mechanisms and reduced bile flow in cholangiocarcinoma. We observed that primary cilia were expressed in normal cholangiocytes but were absent in malignant cells. Coordinately, KLF2 expression was higher in normal cells compared to malignant. Depletion of cilia in normal cells led to a decrease in KLF2 expression and increased cilia number (by serum-deprivation) was associated with increased KLF2. Enforced KLF2 expression inhibited cell proliferation and migration while also decreasing cell death induction in malignant cells. Applied flow over cholangiocytes caused an increase in KLF2 and cilia depletion completely blocked flow-induced KLF2 expression. This flow-

induced KLF2 expression was unchanged in the presence of a calcium chelator, indicating calcium is likely not the second messenger involved in flow-induced KLF2 signaling in cholangiocytes. Disruption of filamentous actin decreased KLF2 expression, suggesting the cilium may communicate through a cytoskeletal mechanotransduction pathway. The repression of proliferation and migration in addition to decrease in induced cell death upon enforced KLF2 expression reflects an overall more quiescent phenotype. Our studies here demonstrate that cilia positively regulated KLF2 protein levels and increased fluid flow also induced KLF2. More study is needed to identify how cilia transduce a signal to increase KLF2 in bile duct cells.

Introduction

Cholangiocarcinoma is an aggressive epithelial neoplasm of the biliary tree associated with inflammation, injury, and bile duct obstruction. This cancer is often diagnosed at a late stage due to its silent character, and unresectable tumors are uniformly lethal. The five-year survival is less than 15%, and intrahepatic cholangiocarcinoma is the most aggressive subtype with a five-year survival of 6% [15]. The asymptomatic nature of this disease portends a reduced opportunity for surgical resection, with only approximately 35% of patients considered eligible for surgery with curative intent [368]. Absent resection, the current standard of care is chemotherapy; however, cholangiocarcinoma is characteristically chemoresistant and these therapies are palliative only [369, 370]. Cholangiocarcinoma tumors are particularly heterogeneous, due to the diversity of anatomical location, varied predisposing risk factors, and wide assortment of associated genetic alterations [371]. These features contribute to a narrow range of treatment options, and at the same time, create a need for expansion of understanding of the specific molecular pathways exploited by this cancer.

Biliary obstruction is the most common cause of the presenting symptoms of cholangiocarcinoma [372]. Bile duct obstruction can arise either from conditions that predispose to cancer, such as primary sclerosing cholangitis (PSC) or intrahepatic cholelithiasis, or from tumor-induced ductal blockage. Premalignant inflammation (PSC or liver fluke infestation) can limit bile flow through strictures that narrow the lumen [373, 374]. Intrahepatic bile stones, while not a common cause, can induce both

obstructive cholestasis and cholangiocarcinoma [375, 376]. The tumor itself can decrease or block flow through compression of the bile duct by mass expansion effect. To recapitulate this feature of human disease, several of the existing cholangiocarcinoma animal models induce cholestasis with bile duct ligation [377]. Moreover, the cholestatic environment in combination with chemical carcinogen treatment in some models is required for carcinogenesis [378, 379]. Additionally, in an orthotopic [380] or oncogenic transduction [381] model, induced cholestasis by bile duct ligation significantly increased tumor progression. In the healthy biliary system, cholangiocytes sense and maintain the regular flow of bile. Reduced flow can induce cholangiocyte proliferation contributing to some cholangiopathies including polycystic liver disease [382]. The mechanism(s) by which cholestasis promotes cholangiocarcinoma are not fully defined.

The primary cilium has been well documented as an important signaling organelle in many cell types in the human body [249, 253]. Functioning as a sensory antenna for the cell, the primary cilium is responsive to mechanical, chemical, and osmotic stimuli. Its significance in various biological processes is revealed by the pathologies to which its dysfunction or absence can be associated, or directly attributed. Often, cancer cells lack or have defective primary cilia compared to their non-malignant counterparts [383-386]. This is also true for biliary epithelial cells. Normal cholangiocytes possess primary cilia, with which they can detect bile flow in the ductal lumen; however, primary cilia are lost in cholangiocarcinoma cells [283, 284].

Krüppel-like factor 2 (KLF2) is a member of a large family of transcription factors that direct a range of cellular processes including proliferation [220], apoptosis [217], differentiation [166], inflammation [154], and migration [219]. It is not surprising then that the expression or function of many KLFs is dysregulated in cancer [216, 217, 228]. Separately, considerable study has established KLF2 as a key factor involved in shear stress response to flow in non-malignant endothelial cells, where under normal, undisturbed flow conditions, KLF2 expression exerts anti-proliferative and anti-inflammatory protective effects [187, 199]. The status and function of KLF2 in cholangiocarcinoma is not yet known. Furthermore, the capacity of KLF2 as a mediator of flow response in a non-endothelial cell type has not been described.

Results

Expression of primary cilia

We sought to determine the presence of primary cilia in cultured cholangiocyte and cholangiocarcinoma cell lines. Previous reports have shown a reduced frequency or absence of cilia in malignant cells compared to non-malignant cells [283, 384, 387]. Serum deprivation (also termed serum starvation) was demonstrated to induce ciliogenesis and is a commonly used practice to promote cilia formation *in vitro* [275, 388]. We cultured non-malignant cholangiocyte cell lines, NHC and H69, and malignant cholangiocarcinoma cells, Mz-ChA-1, KMCH, and HuCCT, in serum-free medium for 24 hours. Cells were then assessed by fluorescence microscopy for presence of cilia. Specifically, we detected ADP-ribosylation factor-like protein 13B (Arl13b), a cilia-localized protein that assists in cilia formation and maintenance [389]. Imaging revealed significant expression of cilia in normal cholangiocyte cells (**Figures 5.1A & B**), while cholangiocarcinoma cells expressed essentially none (**Figures 5.1C, D & E**). These data demonstrate that malignant cholangiocarcinoma cells lack primary cilia.

Figure 5.1. Normal but not malignant cholangiocytes express primary cilia. Upper panels. Normal cholangiocyte cells NHC (**A**) and H69 (**B**) were fixed and probed for the ciliary marker Arl13b (green) and visualized by confocal fluorescence microscopy. Lower panels. Cholangiocarcinoma cells Mz-ChA-1 (**C**), KMCH (**D**), and HuCCT (**E**) were probed with anti-Arl13b (red). Nuclei were stained with DAPI. Scale bar = 50 μm (**A**). All images are at the same scale. Inserts: each insert is a 3-fold magnification of a subsection of the respective image.

Figure 5.1 Normal but not malignant cholangiocytes express primary cilia

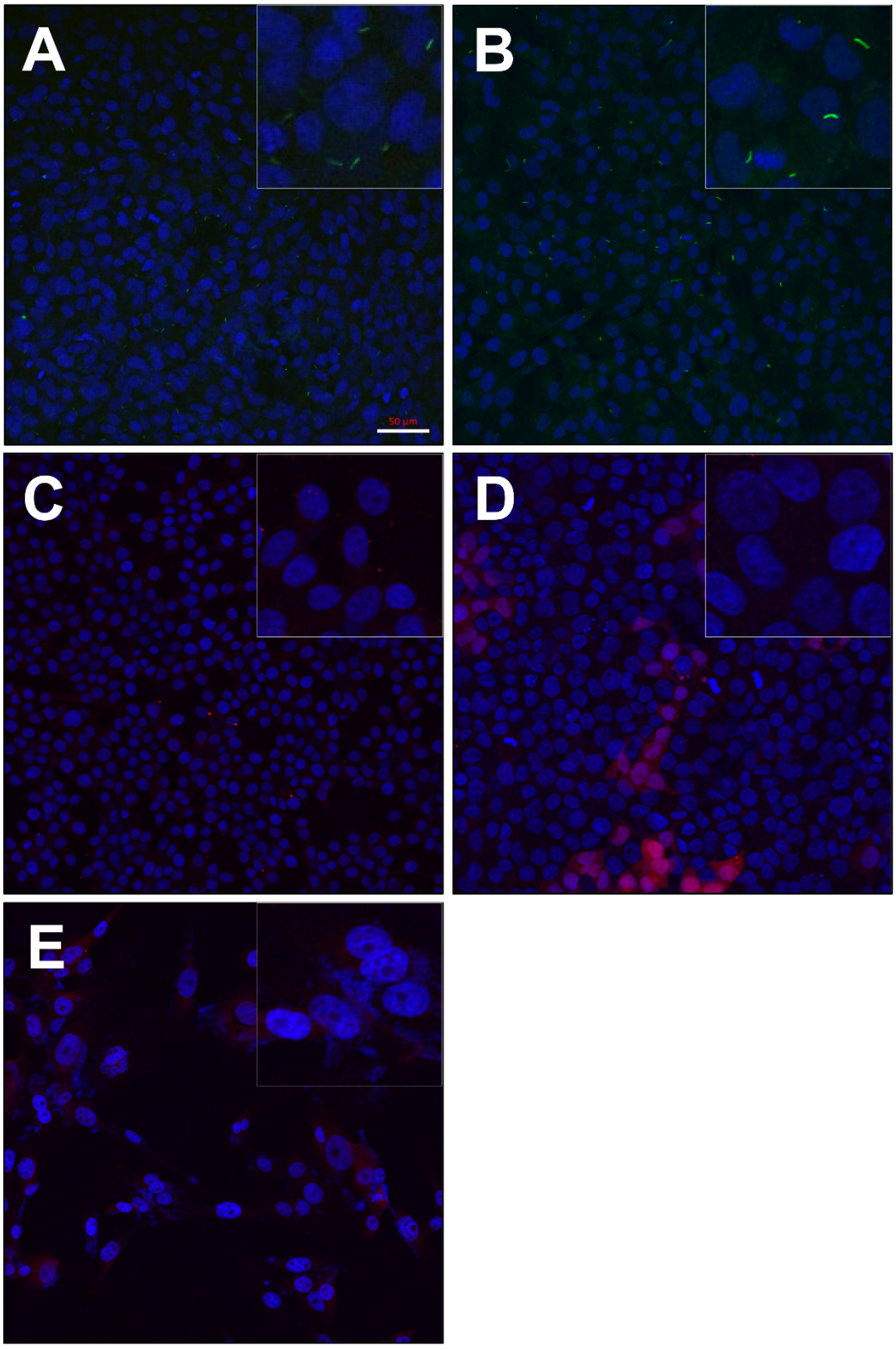

Expression of KLF2 is decreased in cholangiocarcinoma

We considered that cilia may regulate the transcription factor KLF2 and examined the expression of KLF2 in normal cholangiocyte cells and malignant cholangiocarcinoma cells. KLF2 protein expression was higher in normal H69 and NHC cells compared to cholangiocarcinoma cell lines HuCCT and KMCH (**Figure 5.2A**), as well as OZ and EGI-1 (not shown). We expanded our analysis of KLF2 expression status in malignant cells by sampling recently derived cell lines from four cholangiocarcinoma patients. These cells, ICC2, ICC3, ICC8, and ICC11, exhibited lower KLF2 protein expression compared to normal NHC cells (**Figure 5.2B**). Additionally, human tissue samples were obtained from three normal livers, from three normal, cholangiocarcinoma-adjacent livers, and from 14 cholangiocarcinoma tumors. We probed for KLF2 protein by immunoblot and probed for actin as an expression control. We quantified the relative KLF2 protein signal versus actin and calculated the mean relative KLF2 expression between samples. KLF2 expression in normal tissue was significantly higher than in tumors. We also observed a decrease KLF expression in the tumor-adjacent normal liver tissue, but this did not reach statistical significance (**Figure 5.2C**). Together, these data demonstrate a consistent decrease in KLF2 expression in cholangiocarcinoma.

Figure 5.2 Expression of KLF2 is decreased in cholangiocarcinoma

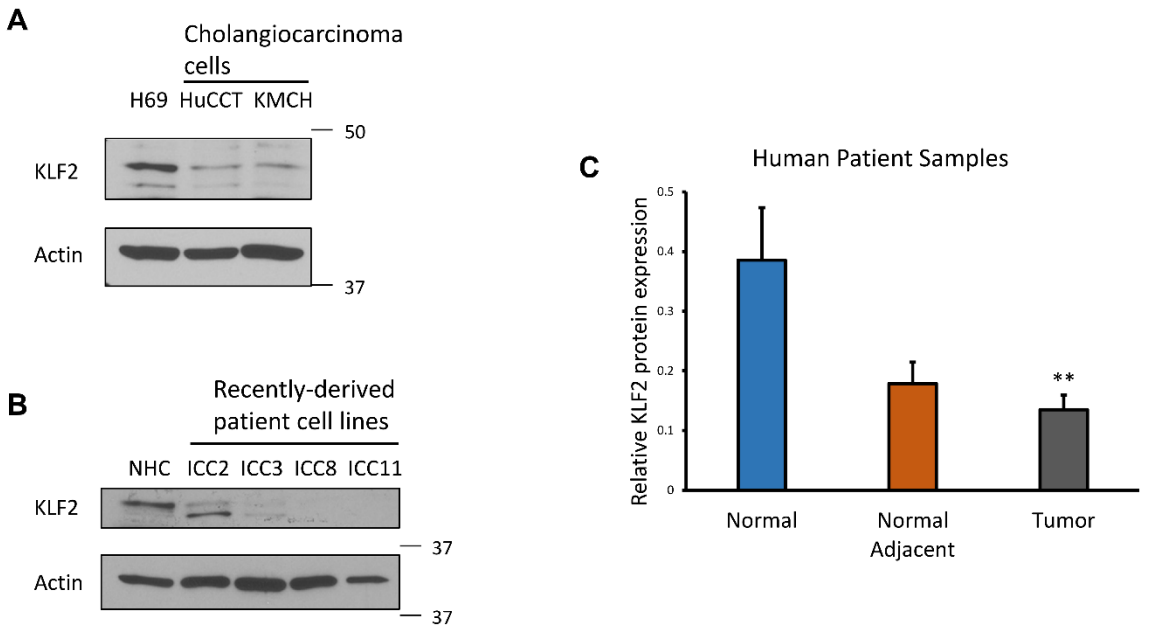

Figure 5.2. Expression of KLF2 is decreased in cholangiocarcinoma. Normal cholangiocyte cell line H69 has higher KLF2 protein expression than cholangiocarcinoma cell lines HuCCT and KMCH (**A**). Patient-derived cholangiocarcinoma cells have decreased KLF2 expression compared to normal cholangiocyte cell line NHC (**B**). Relative KLF2 protein expression compared to actin loading control was measured by signal on immunoblot. Normal human liver tissue expressed significantly higher KLF2 protein than cholangiocarcinoma tumors. ** $p < 0.01$, using ANOVA with *post hoc* correction.

Primary cilia and KLF2 expression are correlated

To investigate the expression pattern and potential link between the cholangiocyte primary cilium and KLF2, we experimentally ablated cilia in cholangiocyte cells. This was accomplished with RNAi suppression of intraflagellar transport 88 (IFT88), a ciliary transport protein necessary for the biogenesis and maintenance of primary cilia [283, 390]. Data published by our collaborators showed that knockout of IFT88 in cholangiocyte cell lines H69 and NHC resulted in complete loss of primary cilia expression [283, 288]. Deciliation of NHC and H69 cells caused a decrease in KLF2 protein (**Figures 5.3A & B**). An established means of promoting ciliogenesis in epithelial cells is by serum deprivation (starvation). This is based on the reciprocal link between ciliogenesis and the cell cycle [391-393]. Serum starvation for 48 hours resulted in a significant increase in the percentage of ciliated cholangiocytes compared to cells grown in serum-containing medium (**Figure 5.3C**). Serum-starved cells also showed a robust increase in KLF2 protein compared to controls (**Figure 5.3D**). These results indicate a positive correlation between the presentation of primary cilia and the expression of KLF2 in cholangiocytes.

Figure 5.3 Primary cilia and KLF2 expression are correlated

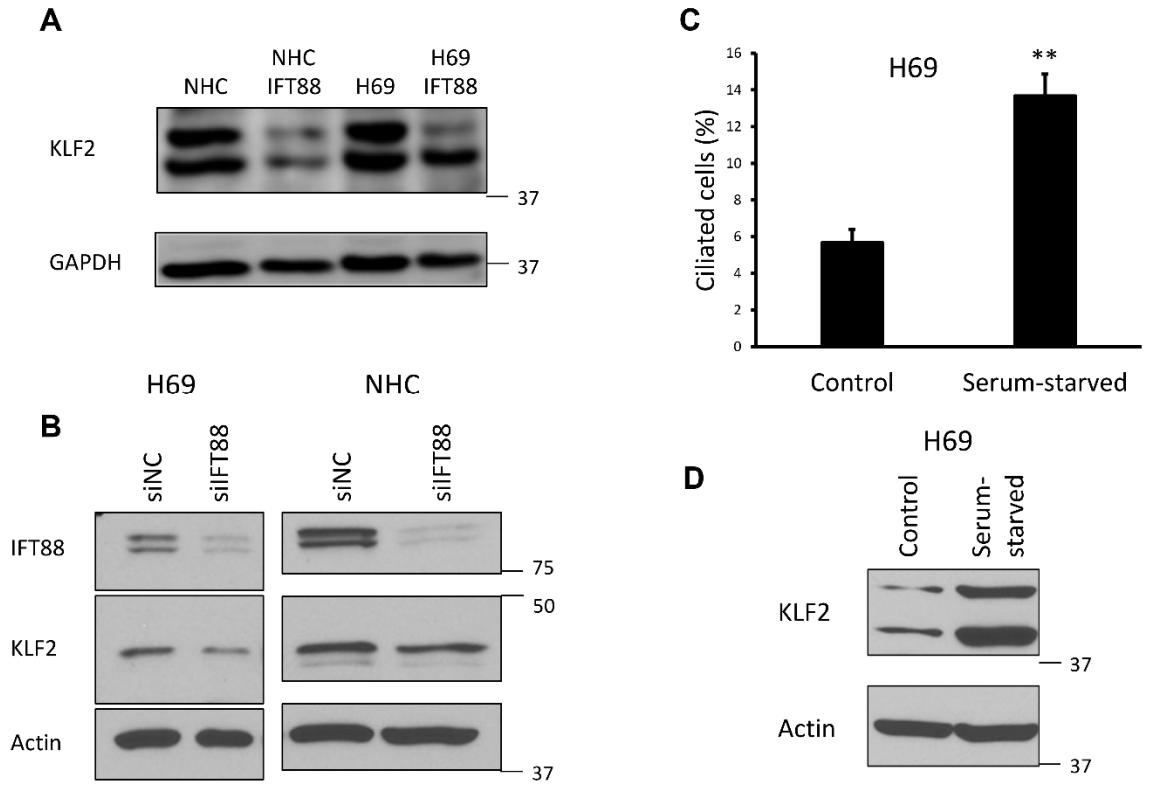

Figure 5.3. Primary cilia and KLF2 expression are correlated. Cilia-expressing NHC and H69 cells had higher KLF2 expression than cells with cilia knocked down by treatment with siRNA against IFT88, a protein required for ciliogenesis and maintenance (**A**). IFT88 protein was knocked down by siRNA in cholangiocytes and KLF2 protein expression decreased (**B**). Normal cholangiocytes were serum-starved for 48 hours, which led to an increase in percentage of ciliated cells (**C**), and an increase in KLF2 expression compared to cells grown in serum-containing medium (**D**). Quantification of ciliated cells by confocal microscopy is based on the average of three separate high-powered fields. Actin or GAPDH were probed as loading controls. ** $p < 0.01$, Student's *t*-test.

KLF2 overexpression decreases proliferation and apoptosis

The functional implications of KLF2 regulation were determined by directly manipulating KLF2 expression. Cells were transfected with a KLF2 expression construct that contained a puromycin resistance cassette and dsRed fluorescent marker for selection of stable clones. Selected clonal KMCH cells (**Figure 5.4A**) and HEK293T cells (**Figure 5.4B**) stably overexpressed KLF2 at the mRNA and protein levels. KLF2-overexpressing cells proliferated at a slower rate that became significant beginning at 24 hours for KMCH (**Figure 5.5A**) and 48 hours for HEK293T (**Figure 5.5B**) and continued through 72 hours. We also tested the effect of KLF2 overexpression on resistance to apoptosis. In KMCH cells, treatment with TRAIL to induce cell death revealed decreased sensitivity in KLF2-overexpressing cells versus control. This effect on apoptosis was observed when measured by activation of effector caspases 3 and 7 (**Figure 5.5C**) or by nuclear morphology changes seen with retention and condensation of DAPI stain (**Figure 5.5D**). HEK293T cells were found to be TRAIL-insensitive, possibly because they are not malignant cells, thus staurosporine was employed to induce apoptosis. Induction of cell death in HEK293T cells resulted in an increase in apoptosis for both control and KLF2-overexpressing cells that was not significantly different between them (**Figure 5.5E**). These data indicate that KLF2 caused reduced apoptosis in cholangiocarcinoma cells, but may not have the same apoptosis-suppressing effect in non-malignant cells. Alternatively, cell line-specific effects may be unrelated to the malignant status, a possibility that remains to be determined.

Figure 5.4 Stable KLF2 expression clones

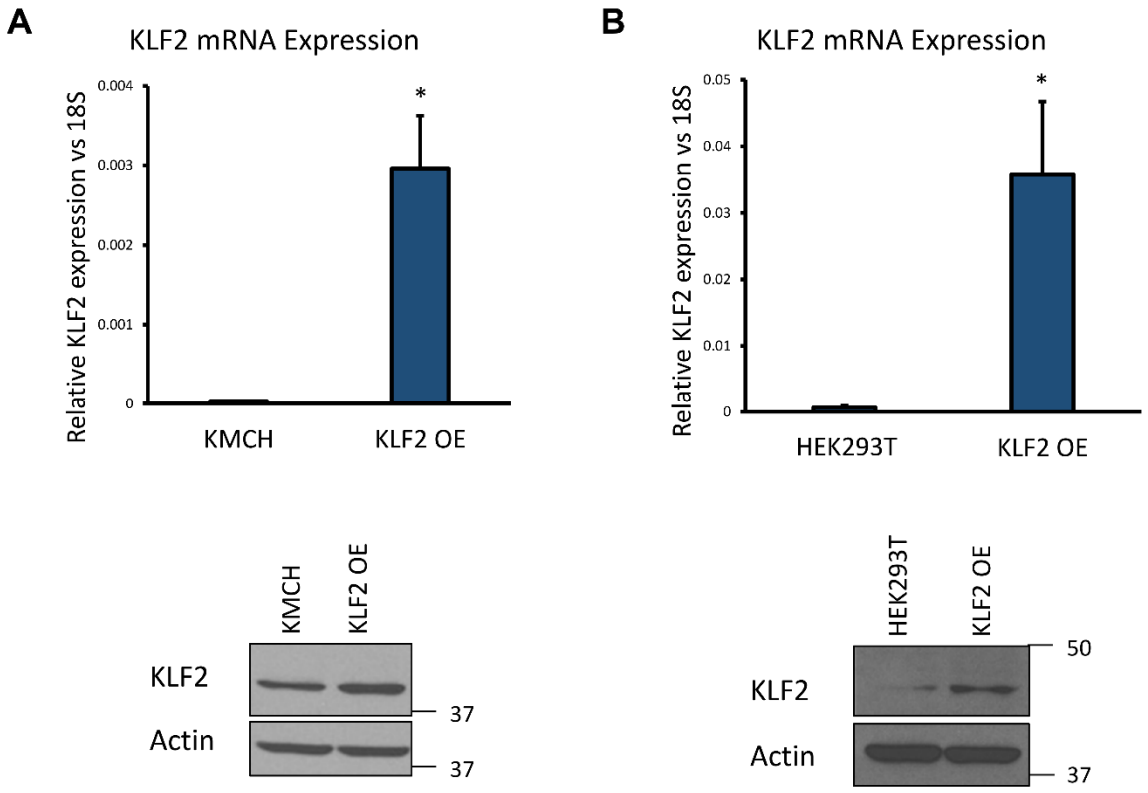

Figure 5.4. Stable KLF2 expression clones. Stable transfection with a KLF2 expression plasmid of KMCH (**A**) or HEK293T (**B**) cells generated overexpression (OE) clones with increased KLF2 as measured by qRT-PCR or immunoblot. 18S rRNA was used as a control RNA for qRT-PCR, and actin as a loading control for western blot. * $p < 0.05$, Student's *t*-test.

Figure 5.5 KLF2 decreases proliferation and apoptosis

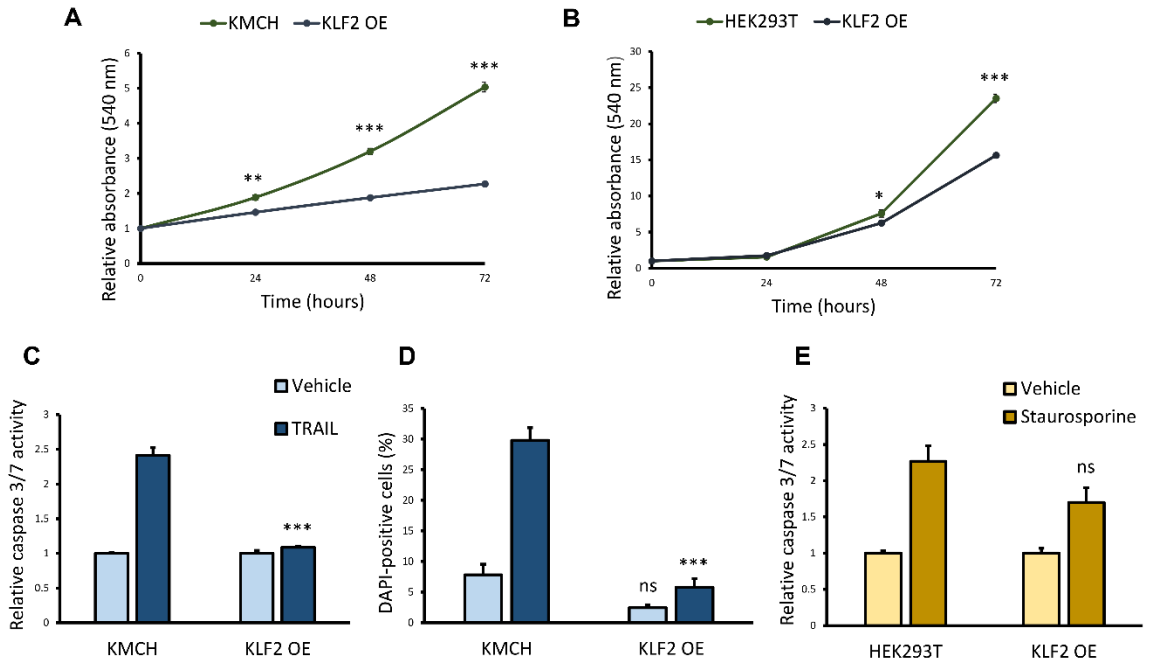

Figure 5.5. KLF2 decreases proliferation and apoptosis. Proliferation was significantly decreased in KLF2 overexpression (OE) clones compared to parental KMCH (**A**) and HEK293T (**B**) cells as measured by MTT assay over 72 hours. KLF2-normal or -overexpressing KMCH cells were treated with vehicle or 50 ng/mL TRAIL to induce cell death and HEK293T cells were treated with vehicle or 5 μg/mL staurosporine. TRAIL-induced apoptosis was decreased in KLF2-overexpressing cells when measured by caspase 3/7 activity assay (**C**) or DAPI staining and nuclear morphology (**D**). KLF2 overexpression in HEK293T cells did not significantly affect staurosporine-induced apoptosis compared to KLF2-normal cells as measured by caspase 3/7 activity (**E**). * $p < 0.05$, ** $p < 0.01$, *** $p < 0.001$, ns = not significant; using ANOVA with *post hoc* correction.

KLF2 inhibits migration

We then tested the role of KLF2 in cell migratory activity using a transwell assay. Identical numbers of cells were seeded in serum-free medium in the upper chamber separated by a porous membrane from the lower chamber. The lower chamber contained FBS in the medium as a chemoattractant. Cells that migrated through the membrane were fixed and stained with DAPI and counted by fluorescence microscopy. There was a significant suppression of migratory potential in KLF2-overexpressing clones compared to control cells (**Figures 5.6A & B**). Overall, enforced expression of KLF2 in malignant cholangiocarcinoma cells decreased proliferation, apoptosis, and migration, consistent with a more quiescent state.

Figure 5.6 KLF2 inhibits migration

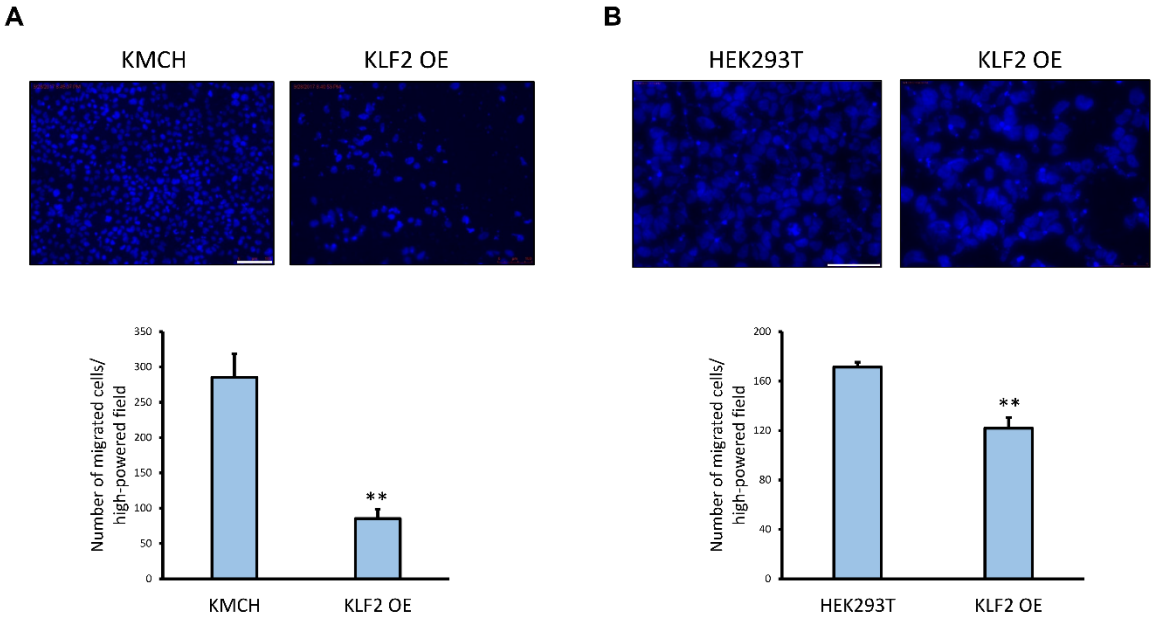

Figure 5.6. KLF2 inhibits migration. Cell migratory potential was measured using a transwell assay. Fewer KLF2-expression cells migrated compared to KLF2-normal cells over 72 hours for KMCH (**A**) or 48 hours for HEK293T (**B**). Upper panels are representative images of transwell membranes with fixed cells stained by DAPI. The quantification data in the lower graphs are a mean of three experiments +/- SEM. Scale bars = 100 μm for KMCH, = 75 μm for HEK293T. ** $p < 0.01$, Student's *t*-test.

Flow-induced KLF2 in cholangiocytes

Because KLF2 is known to be responsive to shear stress generated by fluid flow in endothelial cells, we wanted to simulate this effect and test if it is a flow-responsive gene in cholangiocytes. First, we tested our orbital flow model in the human endothelial cell line HUVEC and observed a robust increase in KLF2 mRNA expression with the application of 18 dyne/cm^2 shear stress over 48 hours (**Figure 5.7A**). Cholangiocyte epithelial cells were more tolerant to a slower flow rate than HUVECs; therefore, the level of shear stress was reduced to 9.8 dyne/cm^2. Cholangiocyte cells responded similarly as endothelial cells, and flow induced a significant increase in KLF2 mRNA compared to static controls (**Figures 5.7B & C**). This is the first demonstration of KLF2 regulation by fluid flow in cholangiocytes.

Fluid flow can induce opening of mechanosensitive ion channels, including the cilium-localized PC2 calcium channel [272]. To investigate if calcium is acting as a second messenger in the flow-induced signal transduction of KLF2, we used the cell-permeant calcium chelating molecule 1,2-bis(2-aminophenoxy)ethane-N,N,N′,N′-tetraacetic acid tetrakis(acetoxymethyl ester) (BAPTA-AM) to scavenge cytosolic calcium and again exposed cells to fluid flow. There was an increase in KLF2 expression in flow-treated cells as before, but no significant difference in KLF2 induction when calcium was chelated (**Figure 5.7D**). This suggests that the KLF2 flow response is not significantly dependent on calcium in cholangiocytes, and that another signaling mechanism is likely at play.

Figure 5.7 Flow-induced KLF2 expression is not dependent on cytoplasmic calcium in cholangiocytes

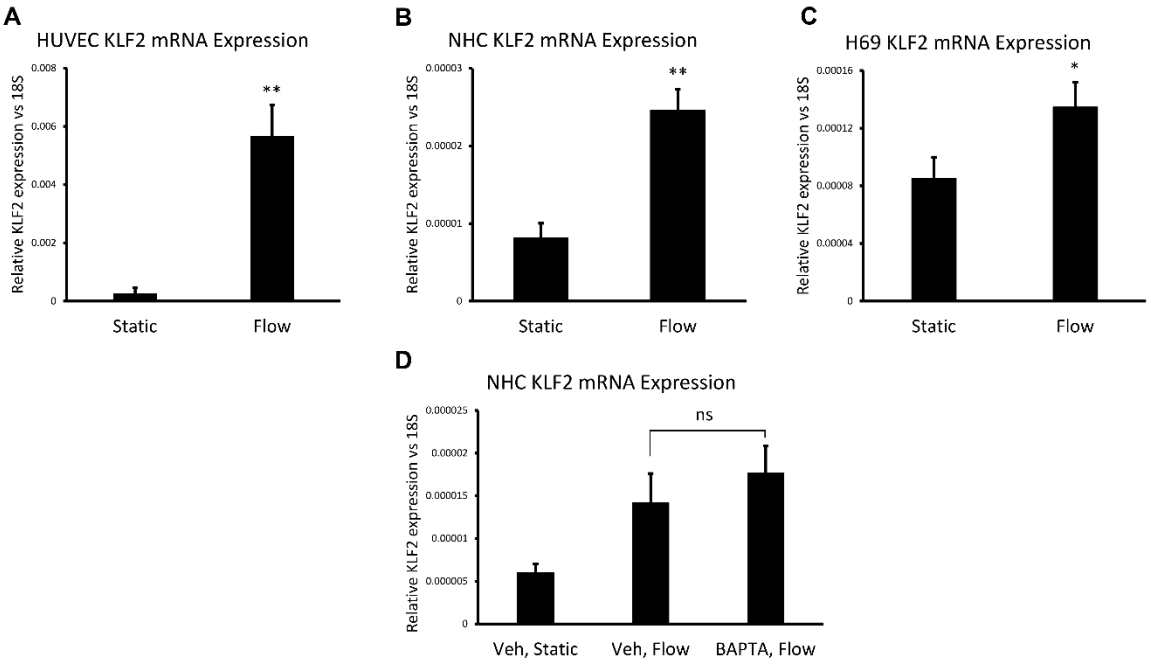

Figure 5.7. Flow-induced KLF2 expression is not dependent on cytoplasmic calcium in cholangiocytes. Cells were subjected to shear stress and compared to cells with no flow (static). Fluid shear stress induced a significant increase in KLF2 mRNA in endothelial cells (HUVEC) (**A**), and cholangiocytes (**B**, **C**), as measured by qRT-PCR. Flow-induced KLF2 expression was not significantly affected in cholangiocytes that were treated with the calcium chelator BAPTA, compared to vehicle-treated cells (**D**). HUVEC flow (shear stress) treatments were 18 dyne/cm^2, and NHC and H69 were 9.8 dyne/cm^2. 18S rRNA was used as a control RNA. * $p < 0.05$, ** $p < 0.01$, ns = not significant; using ANOVA with *post hoc* correction.

To further characterize the KLF2 flow response in cholangiocytes, it was necessary to evaluate the primary cilium as a candidate mediator, as this organelle is also a flow responder. Toward this end, we again employed siRNA knockdown of IFT88 to generate deciliated cells and then measured KLF2 expression under static or flow conditions. NHC cells were transfected with control siRNA (siNC) or siIFT88 for 16 hours and then incubated under static or flow (9.8 dyne/cm^2) conditions for an additional 48 hours. Shear stress caused an increased fold-change of KLF2 mRNA in siNC-transfected cells; however, this increase was abolished in cells with cilia ablation by siIFT88 (**Figure 5.8A**). Fluid flow in siNC control cells induced KLF2 protein expression. In NHC cells under static conditions, removal of cilia with siIFT88 led to a drop in KLF2 compared to control. Moreover, IFT88 knockdown prevented flow induction of KLF2 protein expression (**Figure 5.8B**). The KLF2 flow response could be completely abolished by removal of primary cilia, placing KLF2 downstream of primary cilia signaling and revealing a ciliary-dependent mechanism of KLF2 flow response in cholangiocyte cells.

Figure 5.8 KLF2 induction by flow is ciliary-dependent

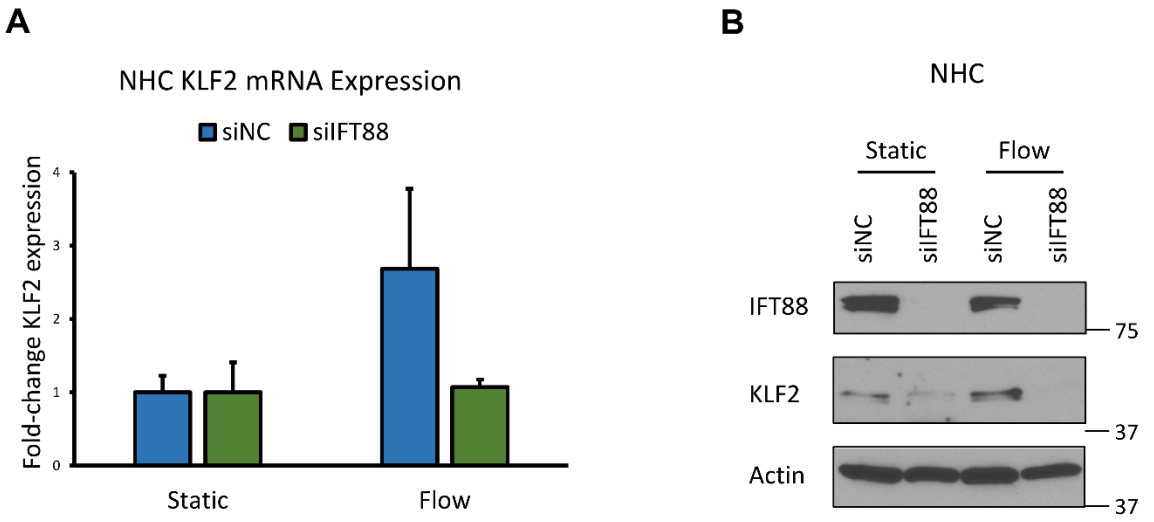

Figure 5.8. KLF2 induction by flow is ciliary-dependent. NHC cells were transfected with control siRNA (siNC) or siIFT88 to remove cilia and then incubated under static or flow (9.8 dynes/cm^2) conditions. Fold-change of KLF2 mRNA increased by flow with siNC but this induction was abolished with siIFT88 transfection (**A**). Similarly, knockdown of IFT88 protein decreased KLF2 protein under static conditions, and IFT88 knockdown prevented induction of KLF2 protein expression by flow (**B**). 18S rRNA was used as a control RNA and actin as a protein loading control.

Actin disruption uncouples primary cilia and KLF2 expression

The ciliary axoneme communicates with the actin cytoskeleton, and depolymerization of cytoplasmic actin can induce increased cilia formation [394, 395]. We postulated that the increase in cilia induced by the actin-depolymerizing small molecule cytochalasin D would cause an increase in KLF2 as well. We treated H69 cells with vehicle (DMSO) or 100 μM cytochalasin D for 24 hours, then probed for cilia-specific marker Arl13b and visualized by fluorescence confocal microscopy. Vehicle-treated cells displayed typical morphology and cilia expression (**Figure 5.9A**). Treatment with cytochalasin D caused a change in cell shape, likely due to disruption of the actin cytoskeleton, and also caused an increase in the number of cells expressing cilia, as well as a qualitative increase in the length of cilia in these cells (**Figure 5.9B**). Quantification of cilia-expressing cells compared to the total cell number showed a significant increase in cilia expression with actin filament disruption (**Figure 5.9C**). Under the same conditions to promote actin cytoskeleton destabilization, there was an unexpected decrease in KLF2 protein (**Figure 5.9D**) and mRNA levels (**Figure 5.9E**). Thus, disruption of actin filaments blocked the signal from cilia to increase KLF2. Additional experiments will be necessary to determine if mechanotransduction of a ciliary signal through the actin cytoskeleton induces KLF2, but such a signaling pathway has been described for other transcription factors, reviewed by Mammoto et al. [396].

Figure 5.9 Actin disruption increased cilia and decreased KLF2

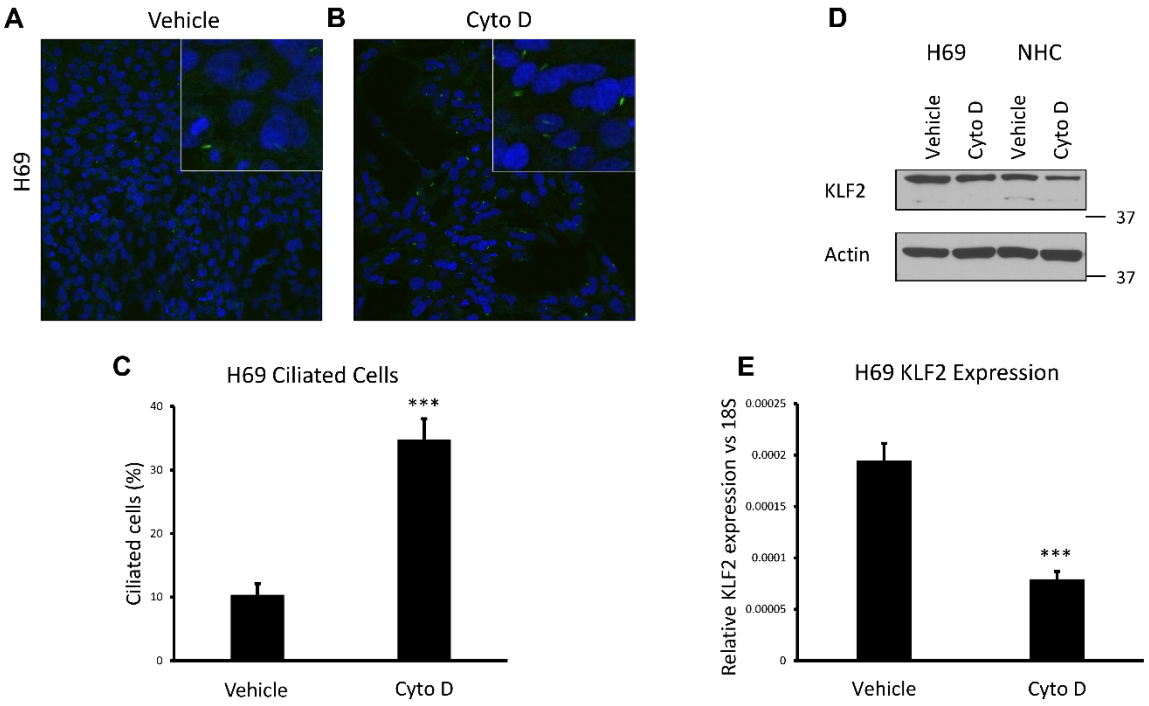

Figure 5.9. Actin disruption increased cilia and decreased KLF2. Normal cholangiocytes were treated with vehicle (**A**) or 100 μM cytochalasin D (Cyto D), an inhibitor of filamentous actin polymerization (**B**), for 24 hours and primary cilia were imaged by confocal fluorescence microscopy.The percentage of ciliated cells was increased by cytochalasin D treatment (**C**). Actin filament disruption caused a decrease in KLF2 protein expression (**D**) and mRNA expression (**E**). 18S rRNA was used as a control RNA and actin as a protein loading control. *** $p < 0.001$, Student's *t*-test.

Primary cilia and KLF2 signaling in bile duct epithelia

KLF2 decreased proliferation and migration as well as increased resistance to apoptosis, which together reflect its promotion of a more quiescent phenotype. KLF2 is regulated through multiple upstream pathways. MiR-106b inhibits KLF2 expression in malignant cells [77]. Shear stress by flow increased KLF2 in cholangiocytes and this induction was removed upon knockdown of cilia. Primary cilia and KLF2 expression response were dissociable with the disruption of actin filaments, which points to a intermediate messenging function for the actin cytoskeleton between these flow responders. The presence of primary cilia is correlated with KLF2 expression in bile duct epithelial cells and they might be linked in cholangiocarcinoma, as there is decreased KLF2 expression in malignant cells compared to normal, and ablation of cilia results in a decrease in KLF2 (**Figure 5.10**).

Figure 5.10 Primary cilia and KLF2 signaling in bile duct epithelia

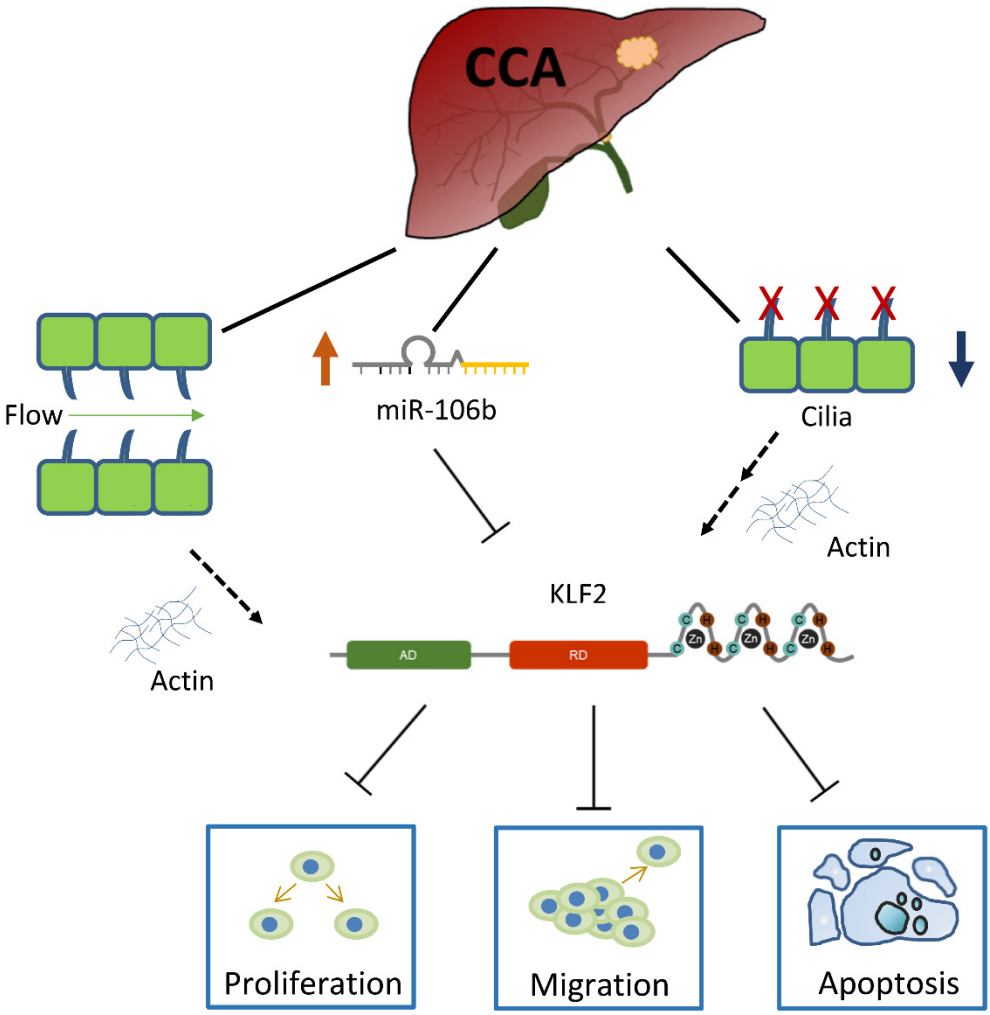

Figure 5.10. Primary cilia and KLF2 signaling in bile duct epithelia. KLF2 decreases proliferation and migration increases resistance to apoptosis, reflecting an overall more-quiescent phenotype. The expression of KLF2 is decreased in cholangiocarcinoma cells and tumors. Primary cilia incidence is correlated with KLF2 expression in bile duct epithelial cells. KLF2 is regulated by miR-106b in malignant cells and induced by flow in normal cells. This flow-induced KLF2 expression is abolished upon knockdown of primary cilia, indicating that the KLF2 flow response is ciliary-dependent. Disruption of actin filaments uncouples the primary cilium-KLF2 pattern of coordinate expression, implicating the actin cytoskeleton as a potential intermediate for the primary cilium-KLF2 signaling axis in cholangiocytes.

Discussion

The principal findings of this study relate to the role of KLF2 in cholangiocarcinoma and the signaling dynamics of both cholangiocyte primary cilia and KLF2, as they relate to flow response. Here we showed that: (i) KLF2 and cilia expression are positively correlated in cholangiocytes and are decreased in cholangiocarcinoma cells; (ii) KLF2 inhibited proliferation, migration, and cell death induction; (iii) fluid flow increased expression of KLF2 in cholangiocytes and this flow response was ciliary-dependent; and (iv) disruption of actin filaments dissociated the positive expression relationship between primary cilia and KLF2. These findings are further discussed below.

The primary cilium is expressed on nearly all non-hematological cell types in the body. The diminished presence or function of cilia is commonly reported in cancer. For instance, in glioblastoma cells, ciliogenesis is inhibited and very few cells express cilia [397]. In pancreatic cells, not only are cilia lost, but disruption of ciliogenesis could sensitize normal cells switch to malignant transformation [398]. In addition, inhibition of ciliogenesis led to increased tumor formation and aggressiveness in breast cancer, through disinhibition of Hedgehog signaling [399]. It seems that cilia loss may not be sufficient as a tumor initiator, but rather cooperates and synergizes with additional oncogenic signaling. Moreover, it could be that cilia loss acts as one of two or more needed “hits”, predisposing a cell to transformation. We found that cilia are absent from cholangiocarcinoma cells but present in normal cholangiocyte cells and these observations are consistent with the literature [283, 284]. While we did not directly test

the tumorigenic or transforming effect of inhibition of ciliogenesis in normal cells or induction of ciliogenesis in cholangiocarcinoma cells, the primary cilium was described as a tumor suppressor in these cells [118, 283, 288].

Cholangiocarcinoma commonly presents with cholestasis. This obstruction of the bile ducts can arise from conditions that predispose to cancer such as PSC and intrahepatic cholelithiasis, or directly from blockage by the tumor mass and associated desmoplastic stroma. Whatever the direct cause, the result is diminished or stoppage of regular luminal flow. Cholangiocytes are responsive to this change. Here we report a positive correlation between two flow responders, primary cilia and KLF2, in cholangiocytes. Furthermore, there is a coordinate decrease in both cilia presence and KLF2 expression in cholangiocarcinoma.

After its discovery and characterization within the last few decades [167, 168, 173], human KLF2 was shortly thereafter demonstrated to control T-cell quiescence [151, 152] and was identified as a master regulator of transcriptional flow response in endothelial cells [184, 187, 400]. While lymphocyte and vascular biology have long had the majority claim on KLF2 function, reports of its role as a tumor suppressor have grown in number since the first few descriptions around 15 years ago [217, 220]. The function of KLF2 as a suppressor of cancer hallmarks is observed in multiple cell types, but in cholangiocarcinoma, its potential influence has not been investigated. Here we showed that increased expression of KLF2 decreased proliferation and migration in normal HEK293T cells. Moreover, in cholangiocarcinoma cells, proliferation and

migration were repressed by KLF2 expression, and these cells showed decreased sensitivity to TRAIL-induced apoptosis. Thus, in cholangiocarcinoma cells, KLF2 could decrease cell growth and migratory potential, but they were also more resistant to extrinsic cell death, possibly imparting a net effect of increased quiescence.

We demonstrated a correlative expression pattern for cilia and KLF2 in normal and malignant cholangiocytes. Deciliated cells showed a decrease in KLF2 expression, and it was presumed that KLF2 is downstream of ciliary signaling. Our data have suggested that the KLF2 flow response is dependent on the cholangiocyte primary cilium, and we have therefore uncovered a link between these two flow-responsive signal transducers. The intermediary messaging remains unclear, however. Calcium was a likely candidate as it has been shown to be a second messenger in kidney cell ciliary signaling. Fluid shear stress caused calcium-induced calcium release (CICR) via the cilia-localized mechanosensor PC1 and cation channel PC2 [401]. Luminal flow activated these same receptors on the cholangiocyte cilium to increase intracellular calcium as well [272]. Also, disruption of calcium signaling inhibited flow induction of KLF2 mRNA in endothelial cells [194]. Furthermore, the purinergic receptor P2X4, an ATP-driven calcium channel, could mediate KLF2 response to shear stress [402]. Surprisingly, modulation of intracellular calcium levels by chelation in cholangiocytes did not result in a repression of KLF2 induction by shear stress. Under fluid flow conditions, the increased KLF2 expression compared to static controls was not significantly different with or without calcium chelation. Studies to date that describe calcium-mediated KLF2

signaling have all been performed in endothelial cells. It is possible that the KLF2 signaling axis in epithelial cells or even biliary cells specifically, employs different biochemical participants. An important caveat is the question of true depletion of intracellular calcium levels in our experiments. Though the cell-permeant calcium chelator BAPTA-AM is a commonly used reagent with demonstrated ability to decrease cell calcium levels [403-405], it will be important for us to confirm an experimental decrease in intracellular calcium, by direct measurement with a calcium indicator, such as fura-2. An obvious candidate for future query is cyclic AMP. cAMP signaling has been shown to be involved in the ciliary mechano-response in cholangiocytes. In bile ducts *in vitro*, luminal flow elicited a cAMP signal response, specifically through regulation of adenylyl cyclase 6 (AC6) activity [272, 277]. However, the flow-induced decrease in cAMP was further shown to be secondary to calcium, which could inhibit AC6. Therefore, if the cAMP response in ciliary-mediated mechanosensation is downstream of calcium, we become skeptical of its role as an intermediary molecule in flow-induced KLF2 signaling.

In pursuit of other candidate signaling intermediates, we considered the actin cytoskeleton based on reports of its role in primary cilium assembly/disassembly [395, 406] and signal transduction [407]. When we manipulated the expression of cilia by preventing actin polymerization, we observed an expected increase in number of cilia. We observed an unexpected decrease in KLF2 expression however. Cilia morphology changed as well, with a presentation of longer cilia with cytoskeleton rearrangement.

The unexpected change in KLF2 expression could partially be attributed to differential cilia signaling, as long cilia signal differently than short cilia. These data could be the result of a differential response to cytoskeletal rearrangement based on cilia morphology. More importantly, these preliminary data imply that the disruption of the actin cytoskeleton causes an uncoupling of the positive expression pattern of primary cilia and KLF2. This finding indicates that actin is a potential intermediate messenger in the primary cilium-KLF2 signaling axis that warrants further investigation in cholangiocyte biology. In summary, in cholangiocytes shear stress and cilia positively affect KLF2 expression. Bile flow and cilia are decreased in cholangiocarcinoma and we found KLF2 was also decreased in tumors. KLF2 seems to regulate tumor-related features of migration, proliferation, and cell death.

Chapter 6 – Conclusions

A PubMed search for the term "cancer" returned a little over 27,000 publications in 1977, while the number has expanded to over 150,000 thus far in 2018. Granted, this metric is not the most accurate means of quantifying the growth of cancer research (one would likely consider NIH/NCI spending as a useful barometer). It does reflect increased studies, and understanding. Successive and recursive cancer studies over time have culminated in the establishment of fundamental tumor characteristics, or hallmarks of cancer [408] that are now augmented with additional keystone cancer-enabling mechanisms [409]. With the expansion of inquiry, there has been a concomitant growth in the complexity of cancer biology as we understand it. In order to make therapies more effective, scientist will have to search for creative ways to target the tumor. We know now that tumor heterogeneity is such that a tumor is actually a diverse assemblage of cell subpopulations, each with different molecular and mutational profiles that impart varied susceptibilities to treatment. This contributes to the ongoing difficulty in finding real cures. We must continue to learn.

The focus of this dissertation is cholangiocarcinoma, which, unlike the combined trend for all cancer types, has seen an increase in age-adjusted incidence and mortality and meager improvement in survival with treatment [15]. This cancer is particularly deadly and therapeutic response is dismal. Surgery is not an option for most patients, and the chemotherapies that are available to these patients are palliative only. A deeper understanding is necessary of the malignant features of cholangiocarcinoma that make it

such an obstinate tumor. Herein I investigated the regulation of some of these features, such as proliferation, migration, and resistance to cell death, and endeavored to identify and characterize molecules and mechanisms with importance in cholangiocarcinoma biology. In the following pages, I will address my studies on (i) a purported small-molecule XIAP antagonist; (ii) my primary and collaborative work on microRNAs and anti-microRNA antagonists; and (iii) my identification of KLF2 dysregulation in cholangiocarcinoma. The latter of these three areas of study has not yet resulted in a therapeutic strategy, but has identified new biological signaling pathways.

Resistance to apoptosis is a signature feature of cholangiocarcinoma. Anti-apoptotic proteins including XIAP and members of the Bcl-2 family such as Mcl-1 and Bcl-X_L are increased in cholangiocarcinoma. Strategies to overcome the protection provided by these proteins include treatment with small-molecule inhibitors and RNAi. If we are able to overcome cell death resistance by shutting down these cytoprotective proteins, tumor cells become more vulnerable to drugs that activate apoptosis pathways. Other means of killing the tumor cell include increased sensitivity to immune surveillance pathways. TRAIL is expressed in normal cells, especially NK and NK-T innate immune cells, which are responsible for tumor surveillance. TRAIL activates the extrinsic apoptosis pathway in malignant, but not healthy, cells. Thus, an attractive strategy for cancer therapy is restoration of TRAIL sensitivity, thereby allowing it to specifically kill cancer cells without cytotoxic side effects in normal cells. Puzzlingly, cholangiocarcinoma tumor cells express TRAIL, which would be expected to induce

paracrine/juxtacrine apoptosis of neighboring malignant cells. Cholangiocarcinoma cells have therefore developed pro-survival signaling and methods of apoptosis resistance that allow them to propagate in the presence of a functioning immune system and neighboring TRAIL-expressing tumor cells.

Chemotherapeutic drugs typically activate apoptotic signaling. Therefore, if we create a background of apoptosis sensitivity by repressing anti-apoptotic proteins, it would be expected that these agents would have increased efficacy. Note the similarity in strategy here to enhancing TRAIL-mediated death, now with a chemical inducer. We investigated embelin for its ability to enhance apoptotic signaling. We found that this small-molecule inhibitor of XIAP was unlikely to be therapeutically effective in this framework. Though embelin reduced the proliferative capacity of cholangiocarcinoma cells, it did not promote cell death, nor did it increase apoptosis sensitivity to TRAIL. Staining with the DNA-binding fluorescent dye DAPI is a common practice to visually measure apoptosis in cell culture. Its utility as a cell death indicator in live cell imaging is due to the relatively low concentration in healthy cells (mostly due to drug efflux mechanisms and partly due to the relative impermeability of DAPI through the healthy plasma membrane). This results in selective, bright staining of apoptotic cells with decreased membrane integrity and impaired efflux capacity. Additionally, nuclear condensation and fragmentation are morphologic changes inherent to apoptosis that can be easily detected on fluorescent imaging of a DAPI-stained nucleus. Embelin treatment of cholangiocarcinoma cells increased nuclear staining for DAPI, but did not cause

characteristic nuclear fragmentation, and it did not induce DNA laddering or caspase activation. It appeared then, that embelin caused an increase in the uptake of DAPI in non-apoptotic, otherwise healthy cells. We concluded that embelin was not promising as an inducer of therapeutic apoptosis, thus, we did not further pursue it as a treatment drug.

In continuation of our investigation of factors involved in apoptosis signaling in cholangiocarcinoma, we turned to microRNAs. First recognized as a conserved class of regulatory molecules at the turn of the century, the aberrant regulation of, and by, these non-coding RNAs has since been implicated in every cancer hallmark. The biological functions of microRNAs are manifested through negative regulation of the expression levels of gene targets. Often, microRNAs act to fine-tune expression of their mRNAs, of which there are often several to hundreds. Messenger RNA transcripts themselves can be targeted by multiple different microRNAs. This regulatory interplay and collective post-transcriptional honing provides a buffering system for fluctuations in gene expression, and grants robustness in biological processes [410]. MicroRNA expression is frequently altered in cancer cells upsetting this homeostasis. Commonly in malignant cells, the upregulation of oncomiRs causes inhibition of target tumor suppressor genes. Alternatively, downregulation of tumor suppressor microRNAs releases oncogenes from inhibition.

MicroRNA function and dysregulation in cancer have garnered interest in developing microRNA-based therapies. There is a large amount of promising pre-

clinical data demonstrating effective strategies to silence oncomiRs in tumors [411]. Increasingly, restoration of silenced tumor suppressor microRNAs has seen compelling results as well [412]. Despite all the effort and progress, a relative few microRNA-based therapies have made it through clinical trials [413]. Notably, the first RNAi drug recently received FDA approval, and moreover, six additional RNAi drugs are currently in phase III clinical trials [414].

I investigated the role of miR-106b in modulating cancer hallmarks in cholangiocarcinoma cells. The goal of this study was to identify the miR-106b-regulated gene landscape in cholangiocarcinoma cells by measuring genome-wide changes in mRNA abundance. Through RNA-Seq, I found 112 mRNAs significantly repressed by miR-106b. Although we validated a number of the genes from this set at the mRNA and protein levels as genuine miR-106b targets, remarkably, few were shared with other studies that included miR-106b targets. This suggests that individual cell or tumor types may have a characteristic set of microRNA targets, depending on target splice form, abundance, and availability for microRNA binding.

Effective microRNA delivery is a key challenge for treatment and in the development of microRNA therapeutic drugs. A free-floating, exogenous microRNA is labile in extracellular space compared to endogenous microRNAs, which are protected from degradation by association with ribonucleoprotein complexes like RISC and controlled transport in membrane-bound vesicles [78]. Several strategies have been developed to maintain microRNA stability during treatment and increase target cell

delivery. The development of polyelectrolyte complexes of nucleic acids with polycations (polyplexes), offer a nanoparticle-based system of stable delivery of siRNA/microRNA [415]. We collaborated with nanomedicine researchers to test the effect of a polyplex of a CXCR4-inhibiting polymer (PCX) with a miR-200c mimic [143]. Both CXCR4 and miR-200c have observed roles in regulating cholangiocarcinoma cell migration and metastasis, so it was reasoned that a combination of CXCR4 antagonism with miR-200c delivery would enhance inhibition of cholangiocarcinoma migratory potential. Indeed, treatment with PCX/miR-200c polyplex resulted in a cooperative inhibition of cell migration that was more effective than either treatment alone [143].

Another method of microRNA delivery is via exosomes. These small extracellular vesicular bodies are secreted by all cells and function in either paracrine or endocrine signaling by transfer of nucleic acids, proteins, and lipids [416]. As with all signaling pathways, exosomes can be repurposed by cholangiocarcinoma cells to nurture a favorable microenvironment and promote pathogenesis [417]. However, advances have been made recently to exploit this tumor exosomal dysregulation. Positive efforts to establish signature expression profiles of exosomal cargos in PSC and cholangiocarcinoma patients offers some promise for these vesicles as biomarkers in biliary disease [418]. Additionally, exosomes can be isolated and subsequently loaded with endogenous or exogenous cargo, including microRNAs, and used to selectively deliver encapsulated therapeutic molecules to target cells [416]. This method of nucleic acid delivery into cells is reminiscent of liposome transfection, which is also based on

phospholipid membrane encapsulation. By aggregating negatively charged nucleic acids (e.g., microRNA) with cationic lipids, cargo nucleic acids are packaged in vesicles that are able to efficiently fuse with the phospholipid bilayer of a transfected cell and release their contents to the intracellular space. We routinely modify microRNA levels in cholangiocarcinoma cells with liposomal transfection to deliver either microRNA mimics or antisense locked nucleic acid (LNA) inhibitors to the cell's interior. LNAs are RNAs modified with a methylene linkage between the 2'-O and 4'-O of the ribose ring. This structural alteration improves LNA oligos as therapeutic agents in two ways: first, the constraint from the methylene linkage locks the LNA in a conformation that coordinates cognate binding with high affinity, and second, the backbone promotes a much higher *in vivo* stability [419, 420]. The invention of LNA technology has provided a useful tool to suppress microRNAs.

We again worked with the Oupický team and tested their PCX-based nanoparticle as a therapeutic delivery system, however this time in a complex with LNA antagonist against miR-210. PCX/anti-miR-210 treatment *in vitro* caused a significant increase in apoptosis in cholangiocarcinoma cells. Cell stemness features including soft agar growth, tumor spheroid formation, and expression of the stem cell marker ALDH were all decreased by PCX/anti-miR-210. Following up on the effectiveness of PCX/anti-miR-210 as an anticancer agent in cultured cells, we next explored the delivery ability of nanoparticles to tumors. Biodistribution studies showed significant accumulation of fluorescent nanoparticles in the tumor. Finally, in a cholangiocarcinoma xenograft

mouse model, PCX/anti-miR-210-treated mice displayed reduced tumor growth compared to control and compared to Gemcitabine/Cisplatin. Combination treatment of PCX/anti-miR-210 with Gemcitabine/Cisplatin caused a striking chemosensitization and these subcutaneous tumors had no mass increase over the 22-day post-tumor inoculation [108]. These results demonstrated the potential of multi-pronged treatment strategies and are encouraging for future studies to promote clinical translation of PCX/anti-miR-210 as antitumor therapies.

Based on my studies showing miR-106b targeted KLF family members, I searched for publications implicating the KLF family in cholangiocarcinoma cell function. There is a limited amount of literature on this topic and thus I began studies to investigate KLF2 in cholangiocarcinoma signaling. KLF2 is an important flow-sensitive transcription factor in endothelial cells, where it has anti-proliferative effects. The potential role of KLF2 in cholangiocarcinoma is unknown. Tumor suppressive functions are reported in other cancer types, and we therefore posited that KLF2 might regulate proliferation, migration and apoptosis in cholangiocarcinoma cells. Built on the rationale that: 1) KLF2 and primary cilia are responsive to fluid flow, 2) reduced KLF2 and primary cilia are observed in cancer, and 3) cholangiocarcinoma tumors do not express cilia and have reduced bile flow, we hypothesized that KLF2 is induced by fluid flow through a ciliary-dependent mechanism, and cilia loss and cholestasis in cholangiocarcinoma decrease KLF2.

We hypothesized that bile flow may contribute to malignant features in cholangiocarcinoma through regulation of KLF2 signaling. Additionally, we investigated cilia-mediated KLF2 expression in cholangiocytes as we considered a potential connection between these flow-responsive signaling mechanisms and reduced bile flow in cholangiocarcinoma. My data demonstrated that KLF2 repressed proliferation and migration in cholangiocarcinoma cells. Additionally, there was a decrease in induced cell death upon enforced KLF2 expression. Together, these features suggest an overall more quiescent phenotype. The presence of primary cilia was associated with increased KLF2 levels, and both may play a role in mechanosensation. My studies herein have also demonstrated that increased fluid flow induced KLF2. In cholangiocarcinoma, there is a decrease in bile flow due to cholestasis, and a loss of primary cilia in malignant cells. Both of these factors may act to decrease KLF2 expression. Because KLF2 seems to encourage cell quiescence, loss of fluid flow and primary cilia may promote aggressiveness in biliary tumors.

The maintenance of physiological homeostasis in any organ or tissue type is not contingent on the activity of one isolated signaling pathway, or the expression of a single master molecular regulator. There is no magic bullet. The elegant orchestrated signaling of the normal cell is malformed to an entangled jazz of dysregulation in the cancer cell. There are many players on many paths. So how do we best treat cholangiocarcinoma? We still don't know. Our data implicate changes in the targets miR-106b, KLFs, and primary cilia signaling in the tumor; future work will be necessary to translate these to

therapeutics. These basic science studies of cholangiocarcinoma features required a dedicated concerted effort to uncover their role and I hope the results presented here will help form new therapies. Overall, this dissertation sought deeper understanding of biochemical and molecular features of cholangiocarcinoma in order to find molecular targets to improve treatment. I have added to our understanding of microRNAs and mechanosensory pathways.

References

1. Alpini G, Roberts S, Kuntz SM, Ueno Y, Gubba S, Podila PV, LeSage G, LaRusso NF. (1996) Morphological, molecular, and functional heterogeneity of cholangiocytes from normal rat liver. *Gastroenterology* 110(5):1636-1643.

2. Hall C, Sato K, Wu N, Zhou T, Kyritsi K, Meng F, Glaser S, Alpini G. (2017) Regulators of Cholangiocyte Proliferation. *Gene Expr* 17(2):155-171.

3. Bogert PT & LaRusso NF. (2007) Cholangiocyte biology. *Curr Opin Gastroenterol* 23(3):299-305.

4. Tavoloni N. (1987) The intrahepatic biliary epithelium: an area of growing interest in hepatology. *Semin Liver Dis* 7(4):280-292.

5. Forker EL. (1967) Two sites of bile formation as determined by mannitol and erythritol clearance in the guinea pig. *J Clin Invest* 46(7):1189-1195.

6. Esteller A. (2008) Physiology of bile secretion. *World J Gastroenterol* 14(37):5641-5649.

7. Arrese M & Accatino L. (2002) From blood to bile: recent advances in hepatobiliary transport. *Ann Hepatol* 1(2):64-71.

8. Trauner M & Boyer JL. (2003) Bile salt transporters: molecular characterization, function, and regulation. *Physiol Rev* 83(2):633-671.

9. Boyer JL. (2013) Bile formation and secretion. *Compr Physiol* 3(3):1035-1078.

10. Meier PJ & Stieger B. (2002) Bile salt transporters. *Annu Rev Physiol* 64:635-661.

11. Erlinger S & Dhumeaux D. (1974) Mechanisms and control of secretion of bile water and electrolytes. *Gastroenterology* 66(2):281-304.

12. Nathanson MH & Boyer JL. (1991) Mechanisms and regulation of bile secretion. *Hepatology* 14(3):551-566.

13. Sathe MN & Freeman AJ. (2016) Gastrointestinal, Pancreatic, and Hepatobiliary Manifestations of Cystic Fibrosis. *Pediatr Clin North Am* 63(4):679-698.

14. Lazaridis KN, Strazzabosco M, Larusso NF. (2004) The cholangiopathies: disorders of biliary epithelia. *Gastroenterology* 127(5):1565-1577.

15. Mukkamalla SKR, Naseri HM, Kim BM, Katz SC, Armenio VA. (2018) Trends in Incidence and Factors Affecting Survival of Patients With Cholangiocarcinoma in the United States. *J Natl Compr Canc Netw* 16(4):370-376.

16. Endo I, Gonen M, Yopp AC, Dalal KM, Zhou Q, Klimstra D, D'Angelica M, DeMatteo RP, Fong Y, Schwartz L, Kemeny N, O'Reilly E, Abou-Alfa GK, Shimada H, Blumgart LH, Jarnagin WR. (2008) Intrahepatic cholangiocarcinoma: rising frequency, improved survival, and determinants of outcome after resection. *Ann Surg* 248(1):84-96.

17. Rizvi S, Khan SA, Hallemeier CL, Kelley RK, Gores GJ. (2018) Cholangiocarcinoma - evolving concepts and therapeutic strategies. *Nat Rev Clin Oncol* 15(2):95-111.

18. Valle J, Wasan H, Palmer DH, Cunningham D, Anthoney A, Maraveyas A, Madhusudan S, Iveson T, Hughes S, Pereira SP, Roughton M, Bridgewater J. (2010) Cisplatin plus gemcitabine versus gemcitabine for biliary tract cancer. *N Engl J Med* 362(14):1273-1281.

19. Razumilava N & Gores GJ. (2014) Cholangiocarcinoma. *Lancet* 383(9935):2168-2179.

20. DeOliveira ML, Cunningham SC, Cameron JL, Kamangar F, Winter JM, Lillemoe KD, Choti MA, Yeo CJ, Schulick RD. (2007) Cholangiocarcinoma: thirty-one-year experience with 564 patients at a single institution. *Ann Surg* 245(5):755-762.

21. Saha SK, Zhu AX, Fuchs CS, Brooks GA. (2016) Forty-Year Trends in Cholangiocarcinoma Incidence in the U.S.: Intrahepatic Disease on the Rise. *Oncologist* 21(5):594-599.

22. Rizvi S & Gores GJ. (2013) Pathogenesis, diagnosis, and management of cholangiocarcinoma. *Gastroenterology* 145(6):1215-1229.

23. Bergquist A, Ekbom A, Olsson R, Kornfeldt D, Loof L, Danielsson A, Hultcrantz R, Lindgren S, Prytz H, Sandberg-Gertzen H, Almer S, Granath F, Broome U. (2002) Hepatic and extrahepatic malignancies in primary sclerosing cholangitis. *J Hepatol* 36(3):321-327.

24. Burak K, Angulo P, Pasha TM, Egan K, Petz J, Lindor KD. (2004) Incidence and risk factors for cholangiocarcinoma in primary sclerosing cholangitis. *Am J Gastroenterol* 99(3):523-526.

25. Tyson GL & El-Serag HB. (2011) Risk factors for cholangiocarcinoma. *Hepatology* 54(1):173-184.

26. Batts KP. (1998) Ischemic cholangitis. *Mayo Clin Proc* 73(4):380-385.

27. Pennacchietti S, Michieli P, Galluzzo M, Mazzone M, Giordano S, Comoglio PM. (2003) Hypoxia promotes invasive growth by transcriptional activation of the met protooncogene. *Cancer Cell* 3(4):347-361.

28. Chang Q, Jurisica I, Do T, Hedley DW. (2011) Hypoxia predicts aggressive growth and spontaneous metastasis formation from orthotopically grown primary xenografts of human pancreatic cancer. *Cancer Res* 71(8):3110-3120.

29. Zhou F, Xu J, Ding G, Cao L. (2014) Overexpressions of CK2beta and XIAP are associated with poor prognosis of patients with cholangiocarcinoma. *Pathol Oncol Res* 20(1):73-79.

30. Yamagiwa Y, Marienfeld C, Meng F, Holcik M, Patel T. (2004) Translational regulation of x-linked inhibitor of apoptosis protein by interleukin-6: a novel mechanism of tumor cell survival. *Cancer Res* 64(4):1293-1298.

31. Wehrkamp CJ, Gutwein AR, Natarajan SK, Phillippi MA, Mott JL. (2014) XIAP antagonist embelin inhibited proliferation of cholangiocarcinoma cells. *PLoS One* 9(3):e90238.

32. Ishimura N, Isomoto H, Bronk SF, Gores GJ. (2006) Trail induces cell migration and invasion in apoptosis-resistant cholangiocarcinoma cells. *Am J Physiol Gastrointest Liver Physiol* 290(1):G129-136.

33. Tanaka S, Sugimachi K, Shirabe K, Shimada M, Wands JR. (2000) Expression and antitumor effects of TRAIL in human cholangiocarcinoma. *Hepatology* 32(3):523-527.

34. Fromm B, Billipp T, Peck LE, Johansen M, Tarver JE, King BL, Newcomb JM, Sempere LF, Flatmark K, Hovig E, Peterson KJ. (2015) A Uniform System for the Annotation of Vertebrate microRNA Genes and the Evolution of the Human microRNAome. *Annu Rev Genet* 49:213-242.

35. Friedman RC, Farh KK, Burge CB, Bartel DP. (2009) Most mammalian mRNAs are conserved targets of microRNAs. *Genome Res* 19(1):92-105.

36. Lewis BP, Burge CB, Bartel DP. (2005) Conserved seed pairing, often flanked by adenosines, indicates that thousands of human genes are microRNA targets. *Cell* 120(1):15-20.

37. Rodriguez A, Griffiths-Jones S, Ashurst JL, Bradley A. (2004) Identification of mammalian microRNA host genes and transcription units. *Genome Res* 14(10a):1902-1910.

38. Lin S & Gregory RI. (2015) MicroRNA biogenesis pathways in cancer. *Nat Rev Cancer* 15(6):321-333.

39. Liu J, Carmell MA, Rivas FV, Marsden CG, Thomson JM, Song JJ, Hammond SM, Joshua-Tor L, Hannon GJ. (2004) Argonaute2 is the catalytic engine of mammalian RNAi. *Science* 305(5689):1437-1441.

40. Huntzinger E & Izaurralde E. (2011) Gene silencing by microRNAs: contributions of translational repression and mRNA decay. *Nat Rev Genet* 12(2):99-110.

41. Guo H, Ingolia NT, Weissman JS, Bartel DP. (2010) Mammalian microRNAs predominantly act to decrease target mRNA levels. *Nature* 466(7308):835-840.

42. Eichhorn SW, Guo H, McGeary SE, Rodriguez-Mias RA, Shin C, Baek D, Hsu SH, Ghoshal K, Villen J, Bartel DP. (2014) mRNA destabilization is the dominant effect of mammalian microRNAs by the time substantial repression ensues. *Mol Cell* 56(1):104-115.

43. Eulalio A, Huntzinger E, Nishihara T, Rehwinkel J, Fauser M, Izaurralde E. (2009) Deadenylation is a widespread effect of miRNA regulation. *RNA* 15(1):21-32.

44. Wu L, Fan J, Belasco JG. (2006) MicroRNAs direct rapid deadenylation of mRNA. *Proc Natl Acad Sci U S A* 103(11):4034-4039.

45. Jonas S & Izaurralde E. (2015) Towards a molecular understanding of microRNA-mediated gene silencing. *Nat Rev Genet* 16(7):421-433.

46. Fabian MR & Sonenberg N. (2012) The mechanics of miRNA-mediated gene silencing: a look under the hood of miRISC. *Nat Struct Mol Biol* 19(6):586-593.

47. Humphreys DT, Westman BJ, Martin DI, Preiss T. (2005) MicroRNAs control translation initiation by inhibiting eukaryotic initiation factor 4E/cap and poly(A) tail function. *Proc Natl Acad Sci U S A* 102(47):16961-16966.

48. Mathonnet G, Fabian MR, Svitkin YV, Parsyan A, Huck L, Murata T, Biffo S, Merrick WC, Darzynkiewicz E, Pillai RS, Filipowicz W, Duchaine TF, Sonenberg N. (2007) MicroRNA inhibition of translation initiation in vitro by targeting the cap-binding complex eIF4F. *Science* 317(5845):1764-1767.

49. Farazi TA, Hoell JI, Morozov P, Tuschl T. (2013) MicroRNAs in human cancer. *Adv Exp Med Biol* 774:1-20.

50. Lee YS & Dutta A. (2009) MicroRNAs in cancer. *Annu Rev Pathol* 4:199-227.

51. Garofalo M & Croce CM. (2011) microRNAs: Master regulators as potential therapeutics in cancer. *Annu Rev Pharmacol Toxicol* 51:25-43.

52. Lagos-Quintana M, Rauhut R, Yalcin A, Meyer J, Lendeckel W, Tuschl T. (2002) Identification of tissue-specific microRNAs from mouse. *Curr Biol* 12(9):735-739.

53. Bartel DP. (2018) Metazoan MicroRNAs. *Cell* 173(1):20-51.

54. Singh R, Ramasubramanian B, Kanji S, Chakraborty AR, Haque SJ, Chakravarti A. (2016) Circulating microRNAs in cancer: Hope or hype? *Cancer Lett* 381(1):113-121.

55. Calin GA & Croce CM. (2006) MicroRNA signatures in human cancers. *Nat Rev Cancer* 6(11):857-866.

56. Bartels CL & Tsongalis GJ. (2009) MicroRNAs: novel biomarkers for human cancer. *Clin Chem* 55(4):623-631.

57. Concepcion CP, Bonetti C, Ventura A. (2012) The microRNA-17-92 family of microRNA clusters in development and disease. *Cancer J* 18(3):262-267.

58. Kan T, Sato F, Ito T, Matsumura N, David S, Cheng Y, Agarwal R, Paun BC, Jin Z, Olaru AV, Selaru FM, Hamilton JP, Yang J, Abraham JM, Mori Y, Meltzer SJ. (2009) The miR-106b-25 polycistron, activated by genomic amplification, functions as an oncogene by suppressing p21 and Bim. *Gastroenterology* 136(5):1689-1700.

59. Mehlich D, Garbicz F, Włodarski PK. (2018) The emerging roles of the polycistronic miR-106b~25 cluster in cancer – A comprehensive review. *Biomedicine & Pharmacotherapy* 107:1183-1195.

60. Sikand K, Slane SD, Shukla GC. (2009) Intrinsic expression of host genes and intronic miRNAs in prostate carcinoma cells. *Cancer Cell International* 9(1):21.

61. Ramalingam P, Palanichamy JK, Singh A, Das P, Bhagat M, Kassab MA, Sinha S, Chattopadhyay P. (2014) Biogenesis of intronic miRNAs located in clusters by independent transcription and alternative splicing. *RNA* 20(1):76-87.

62. Kim K, Chadalapaka G, Pathi SS, Jin UH, Lee JS, Park YY, Cho SG, Chintharlapalli S, Safe S. (2012) Induction of the transcriptional repressor ZBTB4 in prostate cancer cells by drug-induced targeting of microRNA-17-92/106b-25 clusters. *Mol Cancer Ther* 11(9):1852-1862.

63. Guarnieri AL, Towers CG, Drasin DJ, Oliphant MUJ, Andrysik Z, Hotz TJ, Vartuli RL, Linklater ES, Pandey A, Khanal S, Espinosa JM, Ford HL. (2018) The

miR-106b-25 cluster mediates breast tumor initiation through activation of NOTCH1 via direct repression of NEDD4L. *Oncogene* 37(28):3879-3893.

64. Tsujiura M, Ichikawa D, Komatsu S, Shiozaki A, Takeshita H, Kosuga T, Konishi H, Morimura R, Deguchi K, Fujiwara H, Okamoto K, Otsuji E. (2010) Circulating microRNAs in plasma of patients with gastric cancers. *Br J Cancer* 102(7):1174-1179.

65. Shen G, Jia H, Tai Q, Li Y, Chen D. (2013) miR-106b downregulates adenomatous polyposis coli and promotes cell proliferation in human hepatocellular carcinoma. *Carcinogenesis* 34(1):211-219.

66. Li Y, Chen D, Su Z, Li Y, Liu J, Jin L, Shi M, Jiang Z, Qi Z, Gui Y, Yang S, Mao X, Wu X, Lai Y. (2016) MicroRNA-106b functions as an oncogene in renal cell carcinoma by affecting cell proliferation, migration and apoptosis. *Mol Med Rep* 13(2):1420-1426.

67. Zhang GJ, Li JS, Zhou H, Xiao HX, Li Y, Zhou T. (2015) MicroRNA-106b promotes colorectal cancer cell migration and invasion by directly targeting DLC1. *J Exp Clin Cancer Res* 34:73.

68. Meng F, Henson R, Lang M, Wehbe H, Maheshwari S, Mendell JT, Jiang J, Schmittgen TD, Patel T. (2006) Involvement of human micro-RNA in growth and response to chemotherapy in human cholangiocarcinoma cell lines. *Gastroenterology* 130(7):2113-2129.

69. Kawahigashi Y, Mishima T, Mizuguchi Y, Arima Y, Yokomuro S, Kanda T, Ishibashi O, Yoshida H, Tajiri T, Takizawa T. (2009) MicroRNA profiling of human intrahepatic cholangiocarcinoma cell lines reveals biliary epithelial cell-specific microRNAs. *J Nippon Med Sch* 76(4):188-197.

70. Selaru FM, Olaru AV, Kan T, David S, Cheng Y, Mori Y, Yang J, Paun B, Jin Z, Agarwal R, Hamilton JP, Abraham J, Georgiades C, Alvarez H, Vivekanandan P, Yu W, Maitra A, Torbenson M, Thuluvath PJ, Gores GJ, LaRusso NF, Hruban R, Meltzer SJ. (2009) MicroRNA-21 is overexpressed in human cholangiocarcinoma and regulates programmed cell death 4 and tissue inhibitor of metalloproteinase 3. *Hepatology* 49(5):1595-1601.

71. Razumilava N, Bronk SF, Smoot RL, Fingas CD, Werneburg NW, Roberts LR, Mott JL. (2012) miR-25 targets TNF-related apoptosis inducing ligand (TRAIL) death receptor-4 and promotes apoptosis resistance in cholangiocarcinoma. *Hepatology* 55(2):465-475.

72. Gupta S, Read DE, Deepti A, Cawley K, Gupta A, Oommen D, Verfaillie T, Matus S, Smith MA, Mott JL, Agostinis P, Hetz C, Samali A. (2012) Perk-

dependent repression of miR-106b-25 cluster is required for ER stress-induced apoptosis. *Cell Death Dis* 3:e333.

73. Cai K, Wang Y, Bao X. (2011) MiR-106b promotes cell proliferation via targeting RB in laryngeal carcinoma. *J Exp Clin Cancer Res* 30:73.

74. Li N, Miao Y, Shan Y, Liu B, Li Y, Zhao L, Jia L. (2017) MiR-106b and miR-93 regulate cell progression by suppression of PTEN via PI3K/Akt pathway in breast cancer. *Cell Death Dis* 8(5):e2796.

75. Liu F, Gong J, Huang W, Wang Z, Wang M, Yang J, Wu C, Wu Z, Han B. (2014) MicroRNA-106b-5p boosts glioma tumorigensis by targeting multiple tumor suppressor genes. *Oncogene* 33(40):4813-4822.

76. Dong P, Kaneuchi M, Watari H, Sudo S, Sakuragi N. (2013) MicroRNA-106b modulates epithelial-mesenchymal transition by targeting TWIST1 in invasive endometrial cancer cell lines. *Mol Carcinog*.

77. Wehrkamp CJ, Natarajan SK, Mohr AM, Phillippi MA, Mott JL. (2018) miR-106b-responsive gene landscape identifies regulation of Kruppel-like factor family. *RNA Biol* 15(3):391-403.

78. Natarajan S.K. SMA, Wehrkamp C.J., Mohr A.M., Mott J.L. (2013) MicroRNA function in human diseases. *Medical Epigenetics* 1:106-115.

79. Collins AL, Wojcik S, Liu J, Frankel WL, Alder H, Yu L, Schmittgen TD, Croce CM, Bloomston M. (2014) A differential microRNA profile distinguishes cholangiocarcinoma from pancreatic adenocarcinoma. *Ann Surg Oncol* 21(1):133-138.

80. Chen L, Yan HX, Yang W, Hu L, Yu LX, Liu Q, Li L, Huang DD, Ding J, Shen F, Zhou WP, Wu MC, Wang HY. (2009) The role of microRNA expression pattern in human intrahepatic cholangiocarcinoma. *J Hepatol* 50(2):358-369.

81. Zhu H, Han C, Lu D, Wu T. (2014) miR-17-92 cluster promotes cholangiocarcinoma growth: evidence for PTEN as downstream target and IL-6/Stat3 as upstream activator. *Am J Pathol* 184(10):2828-2839.

82. Liu CZ, Liu W, Zheng Y, Su JM, Li JJ, Yu L, He XD, Chen SS. (2012) PTEN and PDCD4 are bona fide targets of microRNA-21 in human cholangiocarcinoma. *Chin Med Sci J* 27(2):65-72.

83. Li B, Han Q, Zhu Y, Yu Y, Wang J, Jiang X. (2012) Down-regulation of miR-214 contributes to intrahepatic cholangiocarcinoma metastasis by targeting Twist. *FEBS J* 279(13):2393-2398.

84. Yamanaka S, Campbell NR, An F, Kuo SC, Potter JJ, Mezey E, Maitra A, Selaru FM. (2012) Coordinated effects of microRNA-494 induce G(2)/M arrest in human cholangiocarcinoma. *Cell Cycle* 11(14):2729-2738.

85. Huang Q, Liu L, Liu CH, You H, Shao F, Xie F, Lin XS, Hu SY, Zhang CH. (2013) MicroRNA-21 Regulates the Invasion and Metastasis in Cholangiocarcinoma and May Be a Potential Biomarker for Cancer Prognosis. *Asian Pac J Cancer Prev* 14(2):829-834.

86. Karakatsanis A, Papaconstantinou I, Gazouli M, Lyberopoulou A, Polymeneas G, Voros D. (2013) Expression of microRNAs, miR-21, miR-31, miR-122, miR-145, miR-146a, miR-200c, miR-221, miR-222, and miR-223 in patients with hepatocellular carcinoma or intrahepatic cholangiocarcinoma and its prognostic significance. *Mol Carcinog* 52(4):297-303.

87. Lu L, Byrnes K, Han C, Wang Y, Wu T. (2014) miR-21 targets 15-PGDH and promotes cholangiocarcinoma growth. *Mol Cancer Res* 12(6):890-900.

88. Zhang J, Jiao J, Cermelli S, Muir K, Jung KH, Zou R, Rashid A, Gagea M, Zabludoff S, Kalluri R, Beretta L. (2015) miR-21 Inhibition Reduces Liver Fibrosis and Prevents Tumor Development by Inducing Apoptosis of CD24+ Progenitor Cells. *Cancer Res* 75(9):1859-1867.

89. Wang LJ, He CC, Sui X, Cai MJ, Zhou CY, Ma JL, Wu L, Wang H, Han SX, Zhu Q. (2015) MiR-21 promotes intrahepatic cholangiocarcinoma proliferation and growth in vitro and in vivo by targeting PTPN14 and PTEN. *Oncotarget* 6(8):5932-5946.

90. Lin KY, Ye H, Han BW, Wang WT, Wei PP, He B, Li XJ, Chen YQ. (2016) Genome-wide screen identified let-7c/miR-99a/miR-125b regulating tumor progression and stem-like properties in cholangiocarcinoma. *Oncogene* 35(26):3376-3386.

91. Lampis A, Carotenuto P, Vlachogiannis G, Cascione L, Hedayat S, Burke R, Clarke P, Bosma E, Simbolo M, Scarpa A, Yu S, Cole R, Smyth E, Mateos JF, Begum R, Hezelova B, Eltahir Z, Wotherspoon A, Fotiadis N, Bali MA, Nepal C, Khan K, Stubbs M, Hahne JC, Gasparini P, *et al.* (2018) MIR21 Drives Resistance to Heat Shock Protein 90 Inhibition in Cholangiocarcinoma. *Gastroenterology* 154(4):1066-1079.e1065.

92. Ehrlich L, Hall C, Venter J, Dostal D, Bernuzzi F, Invernizzi P, Meng F, Trzeciakowski JP, Zhou T, Standeford H, Alpini G, Lairmore TC, Glaser S. (2017) miR-24 Inhibition Increases Menin Expression and Decreases Cholangiocarcinoma Proliferation. *Am J Pathol* 187(3):570-580.

93. Yao L, Han C, Song K, Zhang J, Lim K, Wu T. (2015) Omega-3 Polyunsaturated Fatty Acids Upregulate 15-PGDH Expression in Cholangiocarcinoma Cells by Inhibiting miR-26a/b Expression. *Cancer Res* 75(7):1388-1398.

94. Zhang J, Han C, Wu T. (2012) MicroRNA-26a promotes cholangiocarcinoma growth by activating beta-catenin. *Gastroenterology* 143(1):246-256 e248.

95. Deng Y & Chen Y. (2017) Increased Expression of miR-29a and Its Prognostic Significance in Patients with Cholangiocarcinoma. *Oncol Res Treat* 40(3):128-132.

96. Hu C, Huang F, Deng G, Nie W, Huang W, Zeng X. (2013) miR-31 promotes oncogenesis in intrahepatic cholangiocarcinoma cells via the direct suppression of RASA1. *Exp Ther Med* 6(5):1265-1270.

97. Han Y, Meng F, Venter J, Wu N, Wan Y, Standeford H, Francis H, Meininger C, Greene J, Jr., Trzeciakowski JP, Ehrlich L, Glaser S, Alpini G. (2016) miR-34a-dependent overexpression of Per1 decreases cholangiocarcinoma growth. *J Hepatol* 64(6):1295-1304.

98. Asukai K, Kawamoto K, Eguchi H, Konno M, Asai A, Iwagami Y, Yamada D, Asaoka T, Noda T, Wada H, Gotoh K, Nishida N, Satoh T, Doki Y, Mori M, Ishii H. (2017) Micro-RNA-130a-3p Regulates Gemcitabine Resistance via PPARG in Cholangiocarcinoma. *Ann Surg Oncol* 24(8):2344-2352.

99. Chu CH, Chou W, Wang F, Yeh CN, Chen TC, Yeh TS. (2016) Expression profile of microRNA-200 family in cholangiocarcinoma arising from choledochal cyst. *J Gastroenterol Hepatol* 31(5):1052-1059.

100. Wang S, Yin J, Li T, Yuan L, Wang D, He J, Du X, Lu J. (2015) Upregulated circulating miR-150 is associated with the risk of intrahepatic cholangiocarcinoma. *Oncol Rep* 33(2):819-825.

101. Jiang X, Ma N, Wang D, Li F, He R, Li D, Zhao R, Zhou Q, Wang Y, Zhang F, Wan M, Kang P, Gao X, Cui Y. (2015) Metformin inhibits tumor growth by regulating multiple miRNAs in human cholangiocarcinoma. *Oncotarget* 6(5):3178-3194.

102. Wang J, Xie C, Pan S, Liang Y, Han J, Lan Y, Sun J, Li K, Sun B, Yang G, Shi H, Li Y, Song R, Liu X, Zhu M, Yin D, Wang H, Song X, Lu Z, Jiang H, Zheng T, Liu L. (2016) N-myc downstream-regulated gene 2 inhibits human cholangiocarcinoma progression and is regulated by leukemia inhibitory factor/MicroRNA-181c negative feedback pathway. *Hepatology* 64(5):1606-1622.

103. Kang PC, Leng KM, Liu YP, Liu Y, Xu Y, Qin W, Gao JJ, Wang ZD, Tai S, Zhong XY, Cui YF. (2018) miR-191 Inhibition Induces Apoptosis Through Reactivating

Secreted Frizzled-Related Protein-1 in Cholangiocarcinoma. *Cell Physiol Biochem* 49(5):1933-1942.

104. Li H, Zhou ZQ, Yang ZR, Tong DN, Guan J, Shi BJ, Nie J, Ding XT, Li B, Zhou GW, Zhang ZY. (2017) MicroRNA-191 acts as a tumor promoter by modulating the TET1-p53 pathway in intrahepatic cholangiocarcinoma. *Hepatology* 66(1):136-151.

105. Silakit R, Loilome W, Yongvanit P, Chusorn P, Techasen A, Boonmars T, Khuntikeo N, Chamadol N, Pairojkul C, Namwat N. (2014) Circulating miR-192 in liver fluke-associated cholangiocarcinoma patients: a prospective prognostic indicator. *J Hepatobiliary Pancreat Sci* 21(12):864-872.

106. Han YL, Yin JJ, Cong JJ. (2018) Downregulation of microRNA-193-3p inhibits the progression of intrahepatic cholangiocarcinoma cells by upregulating TGFBR3. *Exp Ther Med* 15(5):4508-4514.

107. Silakit R, Kitirat Y, Thongchot S, Loilome W, Techasen A, Ungarreevittaya P, Khuntikeo N, Yongvanit P, Yang JH, Kim NH, Yook JI, Namwat N. (2018) Potential role of HIF-1-responsive microRNA210/HIF3 axis on gemcitabine resistance in cholangiocarcinoma cells. *PLoS One* 13(6):e0199827.

108. Xie Y, Wang Y, Li J, Hang Y, Jaramillo L, Wehrkamp CJ, Phillippi MA, Mohr AM, Chen Y, Talmon GA, Mott JL, Oupicky D. (2018) Cholangiocarcinoma therapy with nanoparticles that combine downregulation of MicroRNA-210 with inhibition of cancer cell invasiveness. *Theranostics* 8(16):4305-4320.

109. Li J, Yao L, Li G, Ma D, Sun C, Gao S, Zhang P, Gao F. (2015) miR-221 Promotes Epithelial-Mesenchymal Transition through Targeting PTEN and Forms a Positive Feedback Loop with beta-catenin/c-Jun Signaling Pathway in Extra-Hepatic Cholangiocarcinoma. *PLoS One* 10(10):e0141168.

110. An F, Olaru AV, Mezey E, Xie Q, Li L, Piontek KB, Selaru FM. (2015) MicroRNA-224 Induces G1/S Checkpoint Release in Liver Cancer. *J Clin Med* 4(9):1713-1728.

111. Wan P, Chi X, Du Q, Luo J, Cui X, Dong K, Bing Y, Heres C, Geller DA. (2018) miR-383 promotes cholangiocarcinoma cell proliferation, migration, and invasion through targeting IRF1. *J Cell Biochem*.

112. Goeppert B, Ernst C, Baer C, Roessler S, Renner M, Mehrabi A, Hafezi M, Pathil A, Warth A, Stenzinger A, Weichert W, Bahr M, Will R, Schirmacher P, Plass C, Weichenhan D. (2016) Cadherin-6 is a putative tumor suppressor and target of epigenetically dysregulated miR-429 in cholangiocarcinoma. *Epigenetics* 11(11):780-790.

113. Zhang MY, Li SH, Huang GL, Lin GH, Shuang ZY, Lao XM, Xu L, Lin XJ, Wang HY, Li SP. (2015) Identification of a novel microRNA signature associated with intrahepatic cholangiocarcinoma (ICC) patient prognosis. *BMC Cancer* 15:64.

114. Meng F, Henson R, Wehbe-Janek H, Smith H, Ueno Y, Patel T. (2007) The MicroRNA let-7a modulates interleukin-6-dependent STAT-3 survival signaling in malignant human cholangiocytes. *J Biol Chem* 282(11):8256-8264.

115. Xie Y, Zhang H, Guo XJ, Feng YC, He RZ, Li X, Yu S, Zhao Y, Shen M, Zhu F, Wang X, Wang M, Balakrishnan A, Ott M, Peng F, Qin RY. (2018) Let-7c inhibits cholangiocarcinoma growth but promotes tumor cell invasion and growth at extrahepatic sites. *Cell Death Dis* 9(2):249.

116. Utaijaratrasmi P, Vaeteewoottacharn K, Tsunematsu T, Jamjantra P, Wongkham S, Pairojkul C, Khuntikeo N, Ishimaru N, Sirivatanauksorn Y, Pongpaibul A, Thuwajit P, Thuwajit C, Kudo Y. (2018) The microRNA-15a-PAI-2 axis in cholangiocarcinoma-associated fibroblasts promotes migration of cancer cells. *Mol Cancer* 17(1):10.

117. Han S, Wang D, Tang G, Yang X, Jiao C, Yang R, Zhang Y, Huo L, Shao Z, Lu Z, Zhang J, Li X. (2017) Suppression of miR-16 promotes tumor growth and metastasis through reversely regulating YAP1 in human cholangiocarcinoma. *Oncotarget* 8(34):56635-56650.

118. Mansini AP, Lorenzo Pisarello MJ, Thelen KM, Cruz-Reyes M, Peixoto E, Jin S, Howard BN, Trussoni CE, Gajdos GB, LaRusso NF, Perugorria MJ, Banales JM, Gradilone SA. (2018) MicroRNA (miR)-433 and miR-22 dysregulations induce histone-deacetylase-6 overexpression and ciliary loss in cholangiocarcinoma. *Hepatology* 68(2):561-573.

119. Wang P & Lv L. (2016) miR-26a induced the suppression of tumor growth of cholangiocarcinoma via KRT19 approach. *Oncotarget* 7(49):81367-81376.

120. Fan F, Lu J, Yu W, Zhang Y, Xu S, Pang L, Zhu B. (2018) MicroRNA-26b-5p regulates cell proliferation, invasion and metastasis in human intrahepatic cholangiocarcinoma by targeting S100A7. *Oncol Lett* 15(1):386-392.

121. Wang H, Li C, Jian Z, Ou Y, Ou J. (2015) TGF-beta1 Reduces miR-29a Expression to Promote Tumorigenicity and Metastasis of Cholangiocarcinoma by Targeting HDAC4. *PLoS One* 10(10):e0136703.

122. Mott JL, Kobayashi S, Bronk SF, Gores GJ. (2007) mir-29 regulates Mcl-1 protein expression and apoptosis. *Oncogene* 26(42):6133-6140.

123. Ota Y, Takahashi K, Otake S, Tamaki Y, Okada M, Aso K, Makino Y, Fujii S, Ota T, Haneda M. (2018) Extracellular vesicle-encapsulated miR-30e suppresses cholangiocarcinoma cell invasion and migration via inhibiting epithelial-mesenchymal transition. *Oncotarget* 9(23):16400-16417.

124. Qiao P, Li G, Bi W, Yang L, Yao L, Wu D. (2015) microRNA-34a inhibits epithelial mesenchymal transition in human cholangiocarcinoma by targeting Smad4 through transforming growth factor-beta/Smad pathway. *BMC Cancer* 15:469.

125. Kwon H, Song K, Han C, Zhang J, Lu L, Chen W, Wu T. (2017) Epigenetic Silencing of miRNA-34a in Human Cholangiocarcinoma via EZH2 and DNA Methylation: Impact on Regulation of Notch Pathway. *Am J Pathol* 187(10):2288-2299.

126. Jiao D, Yan Y, Shui S, Wu G, Ren J, Wang Y, Han X. (2017) miR-106b regulates the 5-fluorouracil resistance by targeting Zbtb7a in cholangiocarcinoma. *Oncotarget* 8(32):52913-52922.

127. Deng G, Teng Y, Huang F, Nie W, Zhu L, Huang W, Xu H. (2015) MicroRNA-101 inhibits the migration and invasion of intrahepatic cholangiocarcinoma cells via direct suppression of vascular endothelial growth factor-C. *Mol Med Rep* 12(5):7079-7085.

128. Liu N, Jiang F, He TL, Zhang JK, Zhao J, Wang C, Jiang GX, Cao LP, Kang PC, Zhong XY, Lin TY, Cui YF. (2015) The Roles of MicroRNA-122 Overexpression in Inhibiting Proliferation and Invasion and Stimulating Apoptosis of Human Cholangiocarcinoma Cells. *Sci Rep* 5:16566.

129. Xu Z, Liu G, Zhang M, Zhang Z, Jia Y, Peng L, Zhu Y, Hu J, Huang R, Sun X. (2018) miR-122-5p Inhibits the Proliferation, Invasion and Growth of Bile Duct Carcinoma Cells by Targeting ALDOA. *Cell Physiol Biochem* 48(6):2596-2606.

130. Tian F, Chen J, Zheng S, Li D, Zhao X, Jiang P, Li J, Wang S. (2017) miR-124 targets GATA6 to suppress cholangiocarcinoma cell invasion and metastasis. *BMC Cancer* 17(1):175.

131. Ma J, Weng L, Wang Z, Jia Y, Liu B, Wu S, Cao Y, Sun X, Yin X, Shang M, Mao A. (2018) MiR-124 induces autophagy-related cell death in cholangiocarcinoma cells through direct targeting of the EZH2-STAT3 signaling axis. *Exp Cell Res* 366(2):103-113.

132. Zeng B, Li Z, Chen R, Guo N, Zhou J, Zhou Q, Lin Q, Cheng D, Liao Q, Zheng L, Gong Y. (2012) Epigenetic regulation of miR-124 by hepatitis C virus core protein promotes migration and invasion of intrahepatic cholangiocarcinoma cells by targeting SMYD3. *FEBS Lett* 586(19):3271-3278.

133. Li W, Sun Z, Chen C, Wang L, Geng Z, Tao J. (2018) Sirtuin7 has an oncogenic potential via promoting the growth of cholangiocarcinoma cells. *Biomed Pharmacother* 100:257-266.

134. Wang Q, Tang H, Yin S, Dong C. (2013) Downregulation of microRNA-138 enhances the proliferation, migration and invasion of cholangiocarcinoma cells through the upregulation of RhoC/p-ERK/MMP-2/MMP-9. *Oncol Rep* 29(5):2046-2052.

135. Yu J, Zhang W, Tang H, Qian H, Yang J, Zhu Z, Ren P, Lu B. (2016) Septin 2 accelerates the progression of biliary tract cancer and is negatively regulated by mir-140-5p. *Gene* 589(1):20-26.

136. Yang R, Chen Y, Tang C, Li H, Wang B, Yan Q, Hu J, Zou S. (2014) MicroRNA-144 suppresses cholangiocarcinoma cell proliferation and invasion through targeting platelet activating factor acetylhydrolase isoform 1b. *BMC Cancer* 14:917.

137. Xiong X, Sun D, Chai H, Shan W, Yu Y, Pu L, Cheng F. (2015) MiR-145 functions as a tumor suppressor targeting NUAK1 in human intrahepatic cholangiocarcinoma. *Biochem Biophys Res Commun* 465(2):262-269.

138. Braconi C, Huang N, Patel T. (2010) MicroRNA-dependent regulation of DNA methyltransferase-1 and tumor suppressor gene expression by interleukin-6 in human malignant cholangiocytes. *Hepatology* 51(3):881-890.

139. Wu X, Xia M, Chen D, Wu F, Lv Z, Zhan Q, Jiao Y, Wang W, Chen G, An F. (2016) Profiling of downregulated blood-circulating miR-150-5p as a novel tumor marker for cholangiocarcinoma. *Tumour Biol* 37(11):15019-15029.

140. Zhang S, Xiao J, Chai Y, Du YY, Liu Z, Huang K, Zhou X, Zhou W. (2017) LncRNA-CCAT1 Promotes Migration, Invasion, and EMT in Intrahepatic Cholangiocarcinoma Through Suppressing miR-152. *Dig Dis Sci* 62(11):3050-3058.

141. Li Q, Xia X, Ji J, Ma J, Tao L, Mo L, Chen W. (2017) MiR-199a-3p enhances cisplatin sensitivity of cholangiocarcinoma cells by inhibiting mTOR signaling pathway and expression of MDR1. *Oncotarget* 8(20):33621-33630.

142. Peng F, Jiang J, Yu Y, Tian R, Guo X, Li X, Shen M, Xu M, Zhu F, Shi C, Hu J, Wang M, Qin R. (2013) Direct targeting of SUZ12/ROCK2 by miR-200b/c inhibits cholangiocarcinoma tumourigenesis and metastasis. *Br J Cancer* 109(12):3092-3104.

143. Xie Y, Wehrkamp CJ, Li J, Wang Y, Wang Y, Mott JL, Oupicky D. (2016) Delivery of miR-200c Mimic with Poly(amido amine) CXCR4 Antagonists for Combined Inhibition of Cholangiocarcinoma Cell Invasiveness. *Mol Pharm*.

144. Oishi N, Kumar MR, Roessler S, Ji J, Forgues M, Budhu A, Zhao X, Andersen JB, Ye QH, Jia HL, Qin LX, Yamashita T, Woo HG, Kim YJ, Kaneko S, Tang ZY, Thorgeirsson SS, Wang XW. (2012) Transcriptomic profiling reveals hepatic stem-like gene signatures and interplay of miR-200c and epithelial-mesenchymal transition in intrahepatic cholangiocarcinoma. *Hepatology* 56(5):1792-1803.

145. Canu V, Sacconi A, Lorenzon L, Biagioni F, Lo Sardo F, Diodoro MG, Muti P, Garofalo A, Strano S, D'Errico A, Grazi GL, Cioce M, Blandino G. (2017) MiR-204 down-regulation elicited perturbation of a gene target signature common to human cholangiocarcinoma and gastric cancer. *Oncotarget* 8(18):29540-29557.

146. Meng F, Wehbe-Janek H, Henson R, Smith H, Patel T. (2008) Epigenetic regulation of microRNA-370 by interleukin-6 in malignant human cholangiocytes. *Oncogene* 27(3):378-386.

147. Iwaki J, Kikuchi K, Mizuguchi Y, Kawahigashi Y, Yoshida H, Uchida E, Takizawa T. (2013) MiR-376c down-regulation accelerates EGF-dependent migration by targeting GRB2 in the HuCCT1 human intrahepatic cholangiocarcinoma cell line. *PLoS One* 8(7):e69496.

148. Liu B, Hu Y, Qin L, Peng XB, Huang YX. (2018) MicroRNA-494-dependent WDHDI inhibition suppresses epithelial-mesenchymal transition, tumor growth and metastasis in cholangiocarcinoma. *Dig Liver Dis*.

149. Li J, Tian F, Li D, Chen J, Jiang P, Zheng S, Li X, Wang S. (2014) MiR-605 represses PSMD10/Gankyrin and inhibits intrahepatic cholangiocarcinoma cell progression. *FEBS Lett* 588(18):3491-3500.

150. Zhang D, Li H, Xie J, Jiang D, Cao L, Yang X, Xue P, Jiang X. (2018) Long noncoding RNA LINC01296 promotes tumor growth and progression by sponging miR-5095 in human cholangiocarcinoma. *Int J Oncol* 52(6):1777-1786.

151. Kuo CT, Veselits ML, Leiden JM. (1997) LKLF: A transcriptional regulator of single-positive T cell quiescence and survival. *Science* 277(5334):1986-1990.

152. Buckley AF, Kuo CT, Leiden JM. (2001) Transcription factor LKLF is sufficient to program T cell quiescence via a c-Myc-dependent pathway. *Nat Immunol* 2(8):698-704.

153. Hart GT, Wang X, Hogquist KA, Jameson SC. (2011) Kruppel-like factor 2 (KLF2) regulates B-cell reactivity, subset differentiation, and trafficking molecule expression. *Proc Natl Acad Sci U S A* 108(2):716-721.

154. Jha P & Das H. (2017) KLF2 in Regulation of NF-κB-Mediated Immune Cell Function and Inflammation. *Int J Mol Sci* 18(11):2383.

155. McConnell BB & Yang VW. (2010) Mammalian Kruppel-like factors in health and diseases. *Physiol Rev* 90(4):1337-1381.

156. Yusuf I & Fruman DA. (2003) Regulation of quiescence in lymphocytes. *Trends Immunol* 24(7):380-386.

157. Schuh R, Aicher W, Gaul U, Cote S, Preiss A, Maier D, Seifert E, Nauber U, Schroder C, Kemler R, et al. (1986) A conserved family of nuclear proteins containing structural elements of the finger protein encoded by Kruppel, a Drosophila segmentation gene. *Cell* 47(6):1025-1032.

158. Wieschaus E, Nusslein-Volhard C, Kluding H. (1984) Krüppel, a gene whose activity is required early in the zygotic genome for normal embryonic segmentation. *Dev Biol* 104(1):172-186.

159. Ivanova N, Dobrin R, Lu R, Kotenko I, Levorse J, DeCoste C, Schafer X, Lun Y, Lemischka IR. (2006) Dissecting self-renewal in stem cells with RNA interference. *Nature* 442(7102):533-538.

160. Jiang J, Chan YS, Loh YH, Cai J, Tong GQ, Lim CA, Robson P, Zhong S, Ng HH. (2008) A core Klf circuitry regulates self-renewal of embryonic stem cells. *Nat Cell Biol* 10(3):353-360.

161. Yamane M, Ohtsuka S, Matsuura K, Nakamura A, Niwa H. (2018) Overlapping functions of Kruppel-like factor family members: targeting multiple transcription factors to maintain the naive pluripotency of mouse embryonic stem cells. *Development* 145(10).

162. Kuo CT, Veselits ML, Barton KP, Lu MM, Clendenin C, Leiden JM. (1997) The LKLF transcription factor is required for normal tunica media formation and blood vessel stabilization during murine embryogenesis. *Genes Dev* 11(22):2996-3006.

163. Segre JA, Bauer C, Fuchs E. (1999) Klf4 is a transcription factor required for establishing the barrier function of the skin. *Nat Genet* 22(4):356-360.

164. Shindo T, Manabe I, Fukushima Y, Tobe K, Aizawa K, Miyamoto S, Kawai-Kowase K, Moriyama N, Imai Y, Kawakami H, Nishimatsu H, Ishikawa T,

Suzuki T, Morita H, Maemura K, Sata M, Hirata Y, Komukai M, Kagechika H, Kadowaki T, Kurabayashi M, Nagai R. (2002) Kruppel-like zinc-finger transcription factor KLF5/BTEB2 is a target for angiotensin II signaling and an essential regulator of cardiovascular remodeling. *Nat Med* 8(8):856-863.

165. Moseti D, Regassa A, Kim WK. (2016) Molecular Regulation of Adipogenesis and Potential Anti-Adipogenic Bioactive Molecules. *Int J Mol Sci* 17(1).

166. Banerjee SS, Feinberg MW, Watanabe M, Gray S, Haspel RL, Denkinger DJ, Kawahara R, Hauner H, Jain MK. (2003) The Kruppel-like factor KLF2 inhibits peroxisome proliferator-activated receptor-gamma expression and adipogenesis. *J Biol Chem* 278(4):2581-2584.

167. Anderson KP, Kern CB, Crable SC, Lingrel JB. (1995) Isolation of a gene encoding a functional zinc finger protein homologous to erythroid Kruppel-like factor: identification of a new multigene family. *Mol Cell Biol* 15(11):5957-5965.

168. Schrick JJ, Hughes MJ, Anderson KP, Croyle ML, Lingrel JB. (1999) Characterization of the lung Kruppel-like transcription factor gene and upstream regulatory elements. *Gene* 236(1):185-195.

169. Shields JM & Yang VW. (1997) Two potent nuclear localization signals in the gut-enriched Kruppel-like factor define a subfamily of closely related Kruppel proteins. *J Biol Chem* 272(29):18504-18507.

170. Kaczynski J, Cook T, Urrutia R. (2003) Sp1- and Kruppel-like transcription factors. *Genome Biol* 4(2):206.

171. Dang DT, Pevsner J, Yang VW. (2000) The biology of the mammalian Kruppel-like family of transcription factors. *Int J Biochem Cell Biol* 32(11-12):1103-1121.

172. Camacho-Vanegas O, Till J, Miranda-Lorenzo I, Ozturk B, Camacho SC, Martignetti JA. (2013) Shaking the family tree: identification of novel and biologically active alternatively spliced isoforms across the KLF family of transcription factors. *FASEB J* 27(2):432-436.

173. Wani MA, Conkright MD, Jeffries S, Hughes MJ, Lingrel JB. (1999) cDNA isolation, genomic structure, regulation, and chromosomal localization of human lung Kruppel-like factor. *Genomics* 60(1):78-86.

174. Kozyrev SV, Hansen LL, Poltaraus AB, Domninsky DA, Kisselev LL. (1999) Structure of the human CpG-island-containing lung Kruppel-like factor (LKLF) gene and its location in chromosome 19p13.11-13 locus. *FEBS Lett* 448(1):149-152.

175. Conkright MD, Wani MA, Lingrel JB. (2001) Lung Kruppel-like factor contains an autoinhibitory domain that regulates its transcriptional activation by binding WWP1, an E3 ubiquitin ligase. *J Biol Chem* 276(31):29299-29306.

176. Zhang X, Srinivasan SV, Lingrel JB. (2004) WWP1-dependent ubiquitination and degradation of the lung Kruppel-like factor, KLF2. *Biochem Biophys Res Commun* 316(1):139-148.

177. Lomberk G & Urrutia R. (2005) The family feud: turning off Sp1 by Sp1-like KLF proteins. *Biochem J* 392(Pt 1):1-11.

178. Conkright MD, Wani MA, Anderson KP, Lingrel JB. (1999) A gene encoding an intestinal-enriched member of the Kruppel-like factor family expressed in intestinal epithelial cells. *Nucleic Acids Res* 27(5):1263-1270.

179. Kim Y, Ratziu V, Choi SG, Lalazar A, Theiss G, Dang Q, Kim SJ, Friedman SL. (1998) Transcriptional activation of transforming growth factor beta1 and its receptors by the Kruppel-like factor Zf9/core promoter-binding protein and Sp1. Potential mechanisms for autocrine fibrogenesis in response to injury. *J Biol Chem* 273(50):33750-33758.

180. Matsumoto N, Laub F, Aldabe R, Zhang W, Ramirez F, Yoshida T, Terada M. (1998) Cloning the cDNA for a new human zinc finger protein defines a group of closely related Kruppel-like transcription factors. *J Biol Chem* 273(43):28229-28237.

181. Fisher AB, Chien S, Barakat AI, Nerem RM. (2001) Endothelial cellular response to altered shear stress. *Am J Physiol Lung Cell Mol Physiol* 281(3):L529-533.

182. Chen KD, Li YS, Kim M, Li S, Yuan S, Chien S, Shyy JY. (1999) Mechanotransduction in response to shear stress. Roles of receptor tyrosine kinases, integrins, and Shc. *J Biol Chem* 274(26):18393-18400.

183. Jalali S, del Pozo MA, Chen K, Miao H, Li Y, Schwartz MA, Shyy JY, Chien S. (2001) Integrin-mediated mechanotransduction requires its dynamic interaction with specific extracellular matrix (ECM) ligands. *Proc Natl Acad Sci U S A* 98(3):1042-1046.

184. Dekker RJ, van Soest S, Fontijn RD, Salamanca S, de Groot PG, VanBavel E, Pannekoek H, Horrevoets AJ. (2002) Prolonged fluid shear stress induces a distinct set of endothelial cell genes, most specifically lung Kruppel-like factor (KLF2). *Blood* 100(5):1689-1698.

185. Wang N, Miao H, Li YS, Zhang P, Haga JH, Hu Y, Young A, Yuan S, Nguyen P, Wu CC, Chien S. (2006) Shear stress regulation of Kruppel-like factor 2 expression is flow pattern-specific. *Biochem Biophys Res Commun* 341(4):1244-1251.

186. Davies PF. (1995) Flow-mediated endothelial mechanotransduction. *Physiol Rev* 75(3):519-560.

187. Parmar KM, Larman HB, Dai G, Zhang Y, Wang ET, Moorthy SN, Kratz JR, Lin Z, Jain MK, Gimbrone MA, Jr., Garcia-Cardena G. (2006) Integration of flow-dependent endothelial phenotypes by Kruppel-like factor 2. *J Clin Invest* 116(1):49-58.

188. Huddleson JP, Srinivasan S, Ahmad N, Lingrel JB. (2004) Fluid shear stress induces endothelial KLF2 gene expression through a defined promoter region. *Biol Chem* 385(8):723-729.

189. Yan C, Takahashi M, Okuda M, Lee JD, Berk BC. (1999) Fluid shear stress stimulates big mitogen-activated protein kinase 1 (BMK1) activity in endothelial cells. Dependence on tyrosine kinases and intracellular calcium. *J Biol Chem* 274(1):143-150.

190. Kato Y, Kravchenko VV, Tapping RI, Han J, Ulevitch RJ, Lee JD. (1997) BMK1/ERK5 regulates serum-induced early gene expression through transcription factor MEF2C. *EMBO J* 16(23):7054-7066.

191. Sohn SJ, Li D, Lee LK, Winoto A. (2005) Transcriptional regulation of tissue-specific genes by the ERK5 mitogen-activated protein kinase. *Mol Cell Biol* 25(19):8553-8566.

192. Srivastava M & Pollard HB. (1999) Molecular dissection of nucleolin's role in growth and cell proliferation: new insights. *FASEB J* 13(14):1911-1922.

193. Huddleson JP, Ahmad N, Lingrel JB. (2006) Up-regulation of the KLF2 transcription factor by fluid shear stress requires nucleolin. *J Biol Chem* 281(22):15121-15128.

194. Wang W, Ha CH, Jhun BS, Wong C, Jain MK, Jin ZG. (2010) Fluid shear stress stimulates phosphorylation-dependent nuclear export of HDAC5 and mediates expression of KLF2 and eNOS. *Blood* 115(14):2971-2979.

195. Kwon IS, Wang W, Xu S, Jin ZG. (2014) Histone deacetylase 5 interacts with Kruppel-like factor 2 and inhibits its transcriptional activity in endothelium. *Cardiovasc Res* 104(1):127-137.

196. van Thienen JV, Fledderus JO, Dekker RJ, Rohlena J, van Ijzendoorn GA, Kootstra NA, Pannekoek H, Horrevoets AJ. (2006) Shear stress sustains atheroprotective endothelial KLF2 expression more potently than statins through mRNA stabilization. *Cardiovasc Res* 72(2):231-240.

197. Fledderus JO, van Thienen JV, Boon RA, Dekker RJ, Rohlena J, Volger OL, Bijnens AP, Daemen MJ, Kuiper J, van Berkel TJ, Pannekoek H, Horrevoets AJ. (2007) Prolonged shear stress and KLF2 suppress constitutive proinflammatory transcription through inhibition of ATF2. *Blood* 109(10):4249-4257.

198. Davies PF, Civelek M, Fang Y, Fleming I. (2013) The atherosusceptible endothelium: endothelial phenotypes in complex haemodynamic shear stress regions in vivo. *Cardiovasc Res* 99(2):315-327.

199. Frangos SG, Gahtan V, Sumpio B. (1999) Localization of atherosclerosis: role of hemodynamics. *Arch Surg* 134(10):1142-1149.

200. Sweet DT, Jimenez JM, Chang J, Hess PR, Mericko-Ishizuka P, Fu J, Xia L, Davies PF, Kahn ML. (2015) Lymph flow regulates collecting lymphatic vessel maturation in vivo. *J Clin Invest* 125(8):2995-3007.

201. Oesterle A, Laufs U, Liao JK. (2017) Pleiotropic Effects of Statins on the Cardiovascular System. *Circ Res* 120(1):229-243.

202. Parmar KM, Nambudiri V, Dai G, Larman HB, Gimbrone MA, Jr., Garcia-Cardena G. (2005) Statins exert endothelial atheroprotective effects via the KLF2 transcription factor. *J Biol Chem* 280(29):26714-26719.

203. Sen-Banerjee S, Mir S, Lin Z, Hamik A, Atkins GB, Das H, Banerjee P, Kumar A, Jain MK. (2005) Kruppel-like factor 2 as a novel mediator of statin effects in endothelial cells. *Circulation* 112(5):720-726.

204. Holstein SA & Hohl RJ. (2004) Isoprenoids: remarkable diversity of form and function. *Lipids* 39(4):293-309.

205. Tousoulis D, Psarros C, Demosthenous M, Patel R, Antoniades C, Stefanadis C. (2014) Innate and adaptive inflammation as a therapeutic target in vascular disease: the emerging role of statins. *J Am Coll Cardiol* 63(23):2491-2502.

206. Bu DX, Tarrio M, Grabie N, Zhang Y, Yamazaki H, Stavrakis G, Maganto-Garcia E, Pepper-Cunningham Z, Jarolim P, Aikawa M, Garcia-Cardena G, Lichtman AH. (2010) Statin-induced Kruppel-like factor 2 expression in human and mouse T cells reduces inflammatory and pathogenic responses. *J Clin Invest* 120(6):1961-1970.

207. Marrone G, Maeso-Diaz R, Garcia-Cardena G, Abraldes JG, Garcia-Pagan JC, Bosch J, Gracia-Sancho J. (2015) KLF2 exerts antifibrotic and vasoprotective effects in cirrhotic rat livers: behind the molecular mechanisms of statins. *Gut* 64(9):1434-1443.

208. Wu W, Xiao H, Laguna-Fernandez A, Villarreal G, Jr., Wang KC, Geary GG, Zhang Y, Wang WC, Huang HD, Zhou J, Li YS, Chien S, Garcia-Cardena G, Shyy JY. (2011) Flow-Dependent Regulation of Kruppel-Like Factor 2 Is Mediated by MicroRNA-92a. *Circulation* 124(5):633-641.

209. Loyer X, Potteaux S, Vion AC, Guerin CL, Boulkroun S, Rautou PE, Ramkhelawon B, Esposito B, Dalloz M, Paul JL, Julia P, Maccario J, Boulanger CM, Mallat Z, Tedgui A. (2014) Inhibition of microRNA-92a prevents endothelial dysfunction and atherosclerosis in mice. *Circ Res* 114(3):434-443.

210. Fang Y & Davies PF. (2012) Site-specific microRNA-92a regulation of Kruppel-like factors 4 and 2 in atherosusceptible endothelium. *Arterioscler Thromb Vasc Biol* 32(4):979-987.

211. Doddaballapur A, Michalik KM, Manavski Y, Lucas T, Houtkooper RH, You X, Chen W, Zeiher AM, Potente M, Dimmeler S, Boon RA. (2015) Laminar shear stress inhibits endothelial cell metabolism via KLF2-mediated repression of PFKFB3. *Arterioscler Thromb Vasc Biol* 35(1):137-145.

212. Kuosmanen SM, Kansanen E, Kaikkonen MU, Sihvola V, Pulkkinen K, Jyrkkanen HK, Tuoresmaki P, Hartikainen J, Hippelainen M, Kokki H, Tavi P, Heikkinen S, Levonen AL. (2018) NRF2 regulates endothelial glycolysis and proliferation with miR-93 and mediates the effects of oxidized phospholipids on endothelial activation. *Nucleic Acids Res* 46(3):1124-1138.

213. Yang X, Zhang Q, Gao Z, Yu C, Zhang L. (2018) Down-Regulation of MiR-150 Alleviates Inflammatory Injury Induced by Interleukin 1 via Targeting Kruppel-Like Factor 2 in Human Chondrogenic Cells. *Cellular Physiology and Biochemistry* 47(6):2579-2588.

214. Manoharan P, Basford JE, Pilcher-Roberts R, Neumann J, Hui DY, Lingrel JB. (2014) Reduced levels of microRNAs miR-124a and miR-150 are associated with increased proinflammatory mediator expression in Kruppel-like factor 2 (KLF2)-deficient macrophages. *J Biol Chem* 289(45):31638-31646.

215. Tetreault MP, Yang Y, Katz JP. (2013) Kruppel-like factors in cancer. *Nat Rev Cancer* 13(10):701-713.

216. Piva R, Deaglio S, Fama R, Buonincontri R, Scarfo I, Bruscaggin A, Mereu E, Serra S, Spina V, Brusa D, Garaffo G, Monti S, Dal Bo M, Marasca R, Arcaini L, Neri A, Gattei V, Paulli M, Tiacci E, Bertoni F, Pileri SA, Foa R, Inghirami G, Gaidano G, Rossi D. (2015) The Kruppel-like factor 2 transcription factor gene is recurrently mutated in splenic marginal zone lymphoma. *Leukemia* 29(2):503-507.

217. Wang F, Zhu Y, Huang Y, McAvoy S, Johnson WB, Cheung TH, Chung TK, Lo KW, Yim SF, Yu MM, Ngan HY, Wong YF, Smith DI. (2005) Transcriptional repression of WEE1 by Kruppel-like factor 2 is involved in DNA damage-induced apoptosis. *Oncogene* 24(24):3875-3885.

218. Kawamata H, Nakashiro K, Uchida D, Hino S, Omotehara F, Yoshida H, Sato M. (1998) Induction of TSC-22 by treatment with a new anti-cancer drug, vesnarinone, in a human salivary gland cancer cell. *Br J Cancer* 77(1):71-78.

219. Uchida D, Onoue T, Begum NM, Kuribayashi N, Tomizuka Y, Tamatani T, Nagai H, Miyamoto Y. (2009) Vesnarinone downregulates CXCR4 expression via upregulation of Kruppel-like factor 2 in oral cancer cells. *Mol Cancer* 8:62.

220. Wu J & Lingrel JB. (2004) KLF2 inhibits Jurkat T leukemia cell growth via upregulation of cyclin-dependent kinase inhibitor p21WAF1/CIP1. *Oncogene* 23(49):8088-8096.

221. Zhang D, Dai Y, Cai Y, Suo T, Liu H, Wang Y, Cheng Z, Liu H. (2016) KLF2 is downregulated in pancreatic ductal adenocarcinoma and inhibits the growth and migration of cancer cells. *Tumour Biol* 37(3):3425-3431.

222. Zhang W, Levi L, Banerjee P, Jain M, Noy N. (2015) Kruppel-like factor 2 suppresses mammary carcinoma growth by regulating retinoic acid signaling. *Oncotarget* 6(34):35830-35842.

223. Xie P, Tang Y, Shen S, Wang Y, Xing G, Yin Y, He F, Zhang L. (2011) Smurf1 ubiquitin ligase targets Kruppel-like factor KLF2 for ubiquitination and degradation in human lung cancer H1299 cells. *Biochem Biophys Res Commun* 407(1):254-259.

224. Wang R, Wang Y, Liu N, Ren C, Jiang C, Zhang K, Yu S, Chen Y, Tang H, Deng Q, Fu C, Wang Y, Li R, Liu M, Pan W, Wang P. (2013) FBW7 regulates endothelial functions by targeting KLF2 for ubiquitination and degradation. *Cell Res* 23(6):803-819.

225. Zhao Y & Sun Y. (2013) The FBW7-KLF2 axis regulates endothelial functions. *Cell Res* 23(6):741-743.

226. Saurin AJ, Shao Z, Erdjument-Bromage H, Tempst P, Kingston RE. (2001) A Drosophila Polycomb group complex includes Zeste and dTAFII proteins. *Nature* 412(6847):655-660.

227. Kim KH, Kim W, Howard TP, Vazquez F, Tsherniak A, Wu JN, Wang W, Haswell JR, Walensky LD, Hahn WC, Orkin SH, Roberts CW. (2015) SWI/SNF-

mutant cancers depend on catalytic and non-catalytic activity of EZH2. *Nat Med* 21(12):1491-1496.

228. Taniguchi H, Jacinto FV, Villanueva A, Fernandez AF, Yamamoto H, Carmona FJ, Puertas S, Marquez VE, Shinomura Y, Imai K, Esteller M. (2012) Silencing of Kruppel-like factor 2 by the histone methyltransferase EZH2 in human cancer. *Oncogene* 31(15):1988-1994.

229. Xia R, Jin FY, Lu K, Wan L, Xie M, Xu TP, De W, Wang ZX. (2015) SUZ12 promotes gastric cancer cell proliferation and metastasis by regulating KLF2 and E-cadherin. *Tumour Biol* 36(7):5341-5351.

230. Fang R, Xu J, Lin H, Xu X, Tian F. (2017) The histone demethylase lysine-specific demethylase-1-mediated epigenetic silence of KLF2 contributes to gastric cancer cell proliferation, migration, and invasion. *Tumour Biol* 39(4):1010428317698356.

231. Jiang W, Xu X, Deng S, Luo J, Xu H, Wang C, Sun T, Lei G, Zhang F, Yang C, Zhou L, Wang F, Chen M. (2017) Methylation of kruppel-like factor 2 (KLF2) associates with its expression and non-small cell lung cancer progression. *Am J Transl Res* 9(4):2024-2037.

232. Zang C, Nie FQ, Wang Q, Sun M, Li W, He J, Zhang M, Lu KH. (2016) Long non-coding RNA LINC01133 represses KLF2, P21 and E-cadherin transcription through binding with EZH2, LSD1 in non small cell lung cancer. *Oncotarget* 7(10):11696-11707.

233. Li W, Sun M, Zang C, Ma P, He J, Zhang M, Huang Z, Ding Y, Shu Y. (2016) Upregulated long non-coding RNA AGAP2-AS1 represses LATS2 and KLF2 expression through interacting with EZH2 and LSD1 in non-small-cell lung cancer cells. *Cell Death Dis* 7:e2225.

234. Nie F, Yu X, Huang M, Wang Y, Xie M, Ma H, Wang Z, De W, Sun M. (2017) Long noncoding RNA ZFAS1 promotes gastric cancer cells proliferation by epigenetically repressing KLF2 and NKD2 expression. *Oncotarget* 8(24):38227-38238.

235. Fang J, Sun CC, Gong C. (2016) Long noncoding RNA XIST acts as an oncogene in non-small cell lung cancer by epigenetically repressing KLF2 expression. *Biochem Biophys Res Commun* 478(2):811-817.

236. Lian Y, Wang J, Feng J, Ding J, Ma Z, Li J, Peng P, De W, Wang K. (2016) Long non-coding RNA IRAIN suppresses apoptosis and promotes proliferation by binding to LSD1 and EZH2 in pancreatic cancer. *Tumour Biol* 37(11):14929-14937.

237. Sun M, Nie F, Wang Y, Zhang Z, Hou J, He D, Xie M, Xu L, De W, Wang Z, Wang J. (2016) LncRNA HOXA11-AS Promotes Proliferation and Invasion of Gastric Cancer by Scaffolding the Chromatin Modification Factors PRC2, LSD1, and DNMT1. *Cancer Res* 76(21):6299-6310.

238. Ding J, Xie M, Lian Y, Zhu Y, Peng P, Wang J, Wang L, Wang K. (2017) Long noncoding RNA HOXA-AS2 represses P21 and KLF2 expression transcription by binding with EZH2, LSD1 in colorectal cancer. *Oncogenesis* 6(1):e288.

239. Huang M, Hou J, Wang Y, Xie M, Wei C, Nie F, Wang Z, Sun M. (2017) Long Noncoding RNA LINC00673 Is Activated by SP1 and Exerts Oncogenic Properties by Interacting with LSD1 and EZH2 in Gastric Cancer. *Mol Ther* 25(4):1014-1026.

240. Lian Y, Yan C, Ding J, Xia R, Ma Z, Hui B, Ji H, Zhou J, Wang K. (2017) A novel lncRNA, LL22NC03-N64E9.1, represses KLF2 transcription through binding with EZH2 in colorectal cancer. *Oncotarget* 8(35):59435-59445.

241. Ma Z, Huang H, Wang J, Zhou Y, Pu F, Zhao Q, Peng P, Hui B, Ji H, Wang K. (2017) Long non-coding RNA SNHG15 inhibits P15 and KLF2 expression to promote pancreatic cancer proliferation through EZH2-mediated H3K27me3. *Oncotarget* 8(48):84153-84167.

242. Ma Z, Peng P, Zhou J, Hui B, Ji H, Wang J, Wang K. (2018) Long Non-Coding RNA SH3PXD2A-AS1 Promotes Cell Progression Partly Through Epigenetic Silencing P57 and KLF2 in Colorectal Cancer. *Cell Physiol Biochem* 46(6):2197-2214.

243. Lian Y, Yan C, Xu H, Yang J, Yu Y, Zhou J, Shi Y, Ren J, Ji G, Wang K. (2018) A Novel lncRNA, LINC00460, Affects Cell Proliferation and Apoptosis by Regulating KLF2 and CUL4A Expression in Colorectal Cancer. *Mol Ther Nucleic Acids* 12:684-697.

244. Xu M, Chen X, Lin K, Zeng K, Liu X, Pan B, Xu X, Xu T, Hu X, Sun L, He B, Pan Y, Sun H, Wang S. (2018) The long noncoding RNA SNHG1 regulates colorectal cancer cell growth through interactions with EZH2 and miR-154-5p. *Mol Cancer* 17(1):141.

245. Ohguchi H, Hideshima T, Bhasin MK, Gorgun GT, Santo L, Cea M, Samur MK, Mimura N, Suzuki R, Tai YT, Carrasco RD, Raje N, Richardson PG, Munshi NC, Harigae H, Sanda T, Sakai J, Anderson KC. (2016) The KDM3A-KLF2-IRF4 axis maintains myeloma cell survival. *Nat Commun* 7:10258.

246. Miyoshi K, Kasahara K, Miyazaki I, Asanuma M. (2011) Factors that influence primary cilium length. *Acta Med Okayama* 65(5):279-285.

247. Porter ME & Sale WS. (2000) The 9 + 2 axoneme anchors multiple inner arm dyneins and a network of kinases and phosphatases that control motility. *J Cell Biol* 151(5):F37-42.

248. Beisson J & Wright M. (2003) Basal body/centriole assembly and continuity. *Curr Opin Cell Biol* 15(1):96-104.

249. Wheway G, Nazlamova L, Hancock JT. (2018) Signaling through the Primary Cilium. *Front Cell Dev Biol* 6:8.

250. Falkenburger BH, Jensen JB, Dickson EJ, Suh BC, Hille B. (2010) Phosphoinositides: lipid regulators of membrane proteins. *J Physiol* 588(Pt 17):3179-3185.

251. Phua SC, Nihongaki Y, Inoue T. (2018) Autonomy declared by primary cilia through compartmentalization of membrane phosphoinositides. *Curr Opin Cell Biol* 50:72-78.

252. Boldt K, van Reeuwijk J, Lu Q, Koutroumpas K, Nguyen T-MT, Texier Y, van Beersum SEC, Horn N, Willer JR, Mans DA, Dougherty G, Lamers IJC, Coene KLM, Arts HH, Betts MJ, Beyer T, Bolat E, Gloeckner CJ, Haidari K, Hetterschijt L, Iaconis D, Jenkins D, Klose F, Knapp B, Latour B, *et al.* (2016) An organelle-specific protein landscape identifies novel diseases and molecular mechanisms. *Nat Commun* 7:11491.

253. Elliott KH & Brugmann SA. (2018) Sending mixed signals: Cilia-dependent signaling during development and disease. *Dev Biol*.

254. Spasic M & Jacobs CR. (2017) Primary cilia: Cell and molecular mechanosensors directing whole tissue function. *Seminars in Cell & Developmental Biology* 71:42-52.

255. Singla V & Reiter JF. (2006) The primary cilium as the cell's antenna: signaling at a sensory organelle. *Science* 313(5787):629-633.

256. Ishikawa H & Marshall WF. (2011) Ciliogenesis: building the cell's antenna. *Nat Rev Mol Cell Biol* 12(4):222-234.

257. Hao L & Scholey JM. (2009) Intraflagellar transport at a glance. *J Cell Sci* 122(Pt 7):889-892.

258. Marshall WF & Rosenbaum JL. (2001) Intraflagellar transport balances continuous turnover of outer doublet microtubules: implications for flagellar length control. *J Cell Biol* 155(3):405-414.

259. Grisham JW. (1963) CILIATED EPITHELIAL CELLS IN NORMAL MURINE INTRAHEPATIC BILE DUCTS. *Proc Soc Exp Biol Med* 114:318-320.

260. Ishii M, Vroman B, LaRusso NF. (1989) Isolation and morphologic characterization of bile duct epithelial cells from normal rat liver. *Gastroenterology* 97(5):1236-1247.

261. Larusso NF & Masyuk TV. (2011) The role of cilia in the regulation of bile flow. *Dig Dis* 29(1):6-12.

262. Masyuk TV, Huang BQ, Ward CJ, Masyuk AI, Yuan D, Splinter PL, Punyashthiti R, Ritman EL, Torres VE, Harris PC, LaRusso NF. (2003) Defects in cholangiocyte fibrocystin expression and ciliary structure in the PCK rat. *Gastroenterology* 125(5):1303-1310.

263. Ong AC & Wheatley DN. (2003) Polycystic kidney disease--the ciliary connection. *Lancet* 361(9359):774-776.

264. Halvorson CR, Bremmer MS, Jacobs SC. (2010) Polycystic kidney disease: inheritance, pathophysiology, prognosis, and treatment. *Int J Nephrol Renovasc Dis* 3:69-83.

265. Sanzen T, Harada K, Yasoshima M, Kawamura Y, Ishibashi M, Nakanuma Y. (2001) Polycystic kidney rat is a novel animal model of Caroli's disease associated with congenital hepatic fibrosis. *Am J Pathol* 158(5):1605-1612.

266. Patel V, Chowdhury R, Igarashi P. (2009) Advances in the pathogenesis and treatment of polycystic kidney disease. *Curr Opin Nephrol Hypertens* 18(2):99-106.

267. Nagao S, Kugita M, Yoshihara D, Yamaguchi T. (2012) Animal models for human polycystic kidney disease. *Exp Anim* 61(5):477-488.

268. Davenport JR & Yoder BK. (2005) An incredible decade for the primary cilium: a look at a once-forgotten organelle. *Am J Physiol Renal Physiol* 289(6):F1159-1169.

269. Katsuyama M, Masuyama T, Komura I, Hibino T, Takahashi H. (2000) Characterization of a novel polycystic kidney rat model with accompanying polycystic liver. *Exp Anim* 49(1):51-55.

270. Lager DJ, Qian Q, Bengal RJ, Ishibashi M, Torres VE. (2001) The pck rat: a new model that resembles human autosomal dominant polycystic kidney and liver disease. *Kidney Int* 59(1):126-136.

271. Masyuk TV, Huang BQ, Masyuk AI, Ritman EL, Torres VE, Wang X, Harris PC, Larusso NF. (2004) Biliary dysgenesis in the PCK rat, an orthologous model of autosomal recessive polycystic kidney disease. *Am J Pathol* 165(5):1719-1730.

272. Masyuk AI, Masyuk TV, Splinter PL, Huang BQ, Stroope AJ, LaRusso NF. (2006) Cholangiocyte cilia detect changes in luminal fluid flow and transmit them into intracellular Ca2+ and cAMP signaling. *Gastroenterology* 131(3):911-920.

273. Torrice A, Cardinale V, Gatto M, Semeraro R, Napoli C, Onori P, Alpini G, Gaudio E, Alvaro D. (2010) Polycystins play a key role in the modulation of cholangiocyte proliferation. *Dig Liver Dis* 42(5):377-385.

274. Strotmann R, Harteneck C, Nunnenmacher K, Schultz G, Plant TD. (2000) OTRPC4, a nonselective cation channel that confers sensitivity to extracellular osmolarity. *Nat Cell Biol* 2(10):695-702.

275. Gradilone SA, Masyuk AI, Splinter PL, Banales JM, Huang BQ, Tietz PS, Masyuk TV, Larusso NF. (2007) Cholangiocyte cilia express TRPV4 and detect changes in luminal tonicity inducing bicarbonate secretion. *Proc Natl Acad Sci U S A* 104(48):19138-19143.

276. Chari RS, Schutz SM, Haebig JE, Shimokura GH, Cotton PB, Fitz JG, Meyers WC. (1996) Adenosine nucleotides in bile. *Am J Physiol* 270(2 Pt 1):G246-252.

277. Masyuk AI, Gradilone SA, Banales JM, Huang BQ, Masyuk TV, Lee SO, Splinter PL, Stroope AJ, Larusso NF. (2008) Cholangiocyte primary cilia are chemosensory organelles that detect biliary nucleotides via P2Y12 purinergic receptors. *Am J Physiol Gastrointest Liver Physiol* 295(4):G725-734.

278. Mancinelli R, Onori P, Gaudio E, DeMorrow S, Franchitto A, Francis H, Glaser S, Carpino G, Venter J, Alvaro D, Kopriva S, White M, Kossie A, Savage J, Alpini G. (2009) Follicle-stimulating hormone increases cholangiocyte proliferation by an autocrine mechanism via cAMP-dependent phosphorylation of ERK1/2 and Elk-1. *Am J Physiol Gastrointest Liver Physiol* 297(1):G11-26.

279. Masyuk AI, Huang BQ, Ward CJ, Gradilone SA, Banales JM, Masyuk TV, Radtke B, Splinter PL, LaRusso NF. (2010) Biliary exosomes influence cholangiocyte regulatory mechanisms and proliferation through interaction with primary cilia. *Am J Physiol Gastrointest Liver Physiol* 299(4):G990-999.

280. Keitel V & Haussinger D. (2011) TGR5 in the biliary tree. *Dig Dis* 29(1):45-47.

281. Masyuk AI, Huang BQ, Radtke BN, Gajdos GB, Splinter PL, Masyuk TV, Gradilone SA, LaRusso NF. (2013) Ciliary subcellular localization of TGR5

determines the cholangiocyte functional response to bile acid signaling. *Am J Physiol Gastrointest Liver Physiol* 304(11):G1013-1024.

282. Mansini AP, Peixoto E, Thelen KM, Gaspari C, Jin S, Gradilone SA. (2018) The cholangiocyte primary cilium in health and disease. *Biochimica et Biophysica Acta (BBA) - Molecular Basis of Disease* 1864(4, Part B):1245-1253.

283. Gradilone SA, Radtke BN, Bogert PS, Huang BQ, Gajdos GB, LaRusso NF. (2013) HDAC6 inhibition restores ciliary expression and decreases tumor growth. *Cancer Res* 73(7):2259-2270.

284. Razumilava N, Gradilone SA, Smoot RL, Mertens JC, Bronk SF, Sirica AE, Gores GJ. (2014) Non-canonical Hedgehog signaling contributes to chemotaxis in cholangiocarcinoma. *J Hepatol* 60(3):599-605.

285. McMillan R & Matsui W. (2012) Molecular pathways: the hedgehog signaling pathway in cancer. *Clin Cancer Res* 18(18):4883-4888.

286. El Khatib M, Kalnytska A, Palagani V, Kossatz U, Manns MP, Malek NP, Wilkens L, Plentz RR. (2013) Inhibition of hedgehog signaling attenuates carcinogenesis in vitro and increases necrosis of cholangiocellular carcinoma. *Hepatology* 57(3):1035-1045.

287. Corbit KC, Aanstad P, Singla V, Norman AR, Stainier DY, Reiter JF. (2005) Vertebrate Smoothened functions at the primary cilium. *Nature* 437(7061):1018-1021.

288. Mansini AP, Peixoto E, Jin S, Richard S, Gradilone SA. (2018) The chemosensory function of primary cilia regulates cholangiocyte migration, invasion and tumor growth. *Hepatology*.

289. Knuth A, Gabbert H, Dippold W, Klein O, Sachsse W, Bitter-Suermann D, Prellwitz W, Meyer zum Buschenfelde KH. (1985) Biliary adenocarcinoma. Characterisation of three new human tumor cell lines. *J Hepatol* 1(6):579-596.

290. Murakami T, Yano H, Maruiwa M, Sugihara S, Kojiro M. (1987) Establishment and characterization of a human combined hepatocholangiocarcinoma cell line and its heterologous transplantation in nude mice. *Hepatology* 7(3):551-556.

291. Miyagiwa M, Ichida T, Tokiwa T, Sato J, Sasaki H. (1989) A new human cholangiocellular carcinoma cell line (HuCC-T1) producing carbohydrate antigen 19/9 in serum-free medium. *In Vitro Cell Dev Biol* 25(6):503-510.

292. Homma S, Nagamori S, Fujise K, Yamazaki K, Hasumura S, Sujino H, Matsuura T, Shimizu K, Kameda H, Takaki K. (1987) Human bile duct carcinoma cell line producing abundant mucin in vitro. *Gastroenterol Jpn* 22(4):474-479.

293. Scherdin G, Garbrecht M, Klouche M, Hossfeld DK, Holzel F. (1987) *In vitro* interaction of a-difluoromethyl-ornithine (DFMO) and human recombinant interferon-gamma (rIFN-gamma) on human cancer cell lines. *Immunobiology* 175:1-143.

294. Saha SK, Gordan JD, Kleinstiver BP, Vu P, Najem MS, Yeo JC, Shi L, Kato Y, Levin RS, Webber JT, Damon LJ, Egan RK, Greninger P, McDermott U, Garnett MJ, Jenkins RL, Rieger-Christ KM, Sullivan TB, Hezel AF, Liss AS, Mizukami Y, Goyal L, Ferrone CR, Zhu AX, Joung JK, *et al.* (2016) Isocitrate Dehydrogenase Mutations Confer Dasatinib Hypersensitivity and SRC Dependence in Intrahepatic Cholangiocarcinoma. *Cancer Discov* 6(7):727-739.

295. Lai GH, Zhang Z, Shen XN, Ward DJ, Dewitt JL, Holt SE, Rozich RA, Hixson DC, Sirica AE. (2005) erbB-2/neu transformed rat cholangiocytes recapitulate key cellular and molecular features of human bile duct cancer. *Gastroenterology* 129(6):2047-2057.

296. Grubman SA, Perrone RD, Lee DW, Murray SL, Rogers LC, Wolkoff LI, Mulberg AE, Cherington V, Jefferson DM. (1994) Regulation of intracellular pH by immortalized human intrahepatic biliary epithelial cell lines. *Am J Physiol* 266(6 Pt 1):G1060-1070.

297. Banales JM, Saez E, Uriz M, Sarvide S, Urribarri AD, Splinter P, Tietz Bogert PS, Bujanda L, Prieto J, Medina JF, LaRusso NF. (2012) Up-regulation of microRNA 506 leads to decreased Cl-/HCO3- anion exchanger 2 expression in biliary epithelium of patients with primary biliary cirrhosis. *Hepatology* 56(2):687-697.

298. Graham FL, Smiley J, Russell WC, Nairn R. (1977) Characteristics of a human cell line transformed by DNA from human adenovirus type 5. *J Gen Virol* 36(1):59-74.

299. Trapnell C, Roberts A, Goff L, Pertea G, Kim D, Kelley DR, Pimentel H, Salzberg SL, Rinn JL, Pachter L. (2012) Differential gene and transcript expression analysis of RNA-seq experiments with TopHat and Cufflinks. *Nat Protoc* 7(3):562-578.

300. Bartonicek N & Enright AJ. (2010) SylArray: a web server for automated detection of miRNA effects from expression data. *Bioinformatics* 26(22):2900-2901.

301. Rehmsmeier M, Steffen P, Hochsmann M, Giegerich R. (2004) Fast and effective prediction of microRNA/target duplexes. *RNA* 10(10):1507-1517.

302. Bailey TL, Boden M, Buske FA, Frith M, Grant CE, Clementi L, Ren J, Li WW, Noble WS. (2009) MEME SUITE: tools for motif discovery and searching. *Nucleic Acids Res* 37(Web Server issue):W202-208.

303. Lal A, Thomas MP, Altschuler G, Navarro F, O'Day E, Li XL, Concepcion C, Han YC, Thiery J, Rajani DK, Deutsch A, Hofmann O, Ventura A, Hide W, Lieberman J. (2011) Capture of microRNA-bound mRNAs identifies the tumor suppressor miR-34a as a regulator of growth factor signaling. *PLoS Genet* 7(11):e1002363.

304. Martinez Molina D, Jafari R, Ignatushchenko M, Seki T, Larsson EA, Dan C, Sreekumar L, Cao Y, Nordlund P. (2013) Monitoring drug target engagement in cells and tissues using the cellular thermal shift assay. *Science* 341(6141):84-87.

305. Shiraishi J, Tatsumi T, Keira N, Akashi K, Mano A, Yamanaka S, Matoba S, Asayama J, Yaoi T, Fushiki S, Fliss H, Nakagawa M. (2001) Important role of energy-dependent mitochondrial pathways in cultured rat cardiac myocyte apoptosis. *Am J Physiol Heart Circ Physiol* 281(4):H1637-1647.

306. Telford WG, King LE, Fraker PJ. (1991) Evaluation of glucocorticoid-induced DNA fragmentation in mouse thymocytes by flow cytometry. *Cell Prolif* 24(5):447-459.

307. Dardik A, Chen L, Frattini J, Asada H, Aziz F, Kudo FA, Sumpio BE. (2005) Differential effects of orbital and laminar shear stress on endothelial cells. *J Vasc Surg* 41(5):869-880.

308. Kim H, Yang KH, Cho H, Gwak G, Park SC, Kim JI, Yun SS, Moon IS. (2015) Different Effects of Orbital Shear Stress on Vascular Endothelial Cells: Comparison with the Results of In Vivo Study with Rats. *Vasc Specialist Int* 31(2):33-40.

309. Hinderliter PM, Minard KR, Orr G, Chrisler WB, Thrall BD, Pounds JG, Teeguarden JG. (2010) ISDD: A computational model of particle sedimentation, diffusion and target cell dosimetry for in vitro toxicity studies. *Part Fibre Toxicol* 7(1):36.

310. Deveraux QL, Roy N, Stennicke HR, Van Arsdale T, Zhou Q, Srinivasula SM, Alnemri ES, Salvesen GS, Reed JC. (1998) IAPs block apoptotic events induced by caspase-8 and cytochrome c by direct inhibition of distinct caspases. *EMBO J* 17(8):2215-2223.

311. Deveraux QL, Takahashi R, Salvesen GS, Reed JC. (1997) X-linked IAP is a direct inhibitor of cell-death proteases. *Nature* 388(6639):300-304.

312. Liston P, Roy N, Tamai K, Lefebvre C, Baird S, Cherton-Horvat G, Farahani R, McLean M, Ikeda JE, MacKenzie A, Korneluk RG. (1996) Suppression of apoptosis in mammalian cells by NAIP and a related family of IAP genes. *Nature* 379(6563):349-353.

313. Kurita S, Mott JL, Cazanave SC, Fingas CD, Guicciardi ME, Bronk SF, Roberts LR, Fernandez-Zapico ME, Gores GJ. (2011) Hedgehog inhibition promotes a switch from Type II to Type I cell death receptor signaling in cancer cells. *PLoS One* 6(3):e18330.

314. Clawson KA, Borja-Cacho D, Antonoff MB, Saluja AK, Vickers SM. (2010) Triptolide and TRAIL combination enhances apoptosis in cholangiocarcinoma. *J Surg Res* 163(2):244-249.

315. Du C, Fang M, Li Y, Li L, Wang X. (2000) Smac, a mitochondrial protein that promotes cytochrome c-dependent caspase activation by eliminating IAP inhibition. *Cell* 102(1):33-42.

316. Liu Z, Sun C, Olejniczak ET, Meadows RP, Betz SF, Oost T, Herrmann J, Wu JC, Fesik SW. (2000) Structural basis for binding of Smac/DIABLO to the XIAP BIR3 domain. *Nature* 408(6815):1004-1008.

317. Wu G, Chai J, Suber TL, Wu JW, Du C, Wang X, Shi Y. (2000) Structural basis of IAP recognition by Smac/DIABLO. *Nature* 408(6815):1008-1012.

318. Nikolovska-Coleska Z, Xu L, Hu Z, Tomita Y, Li P, Roller PP, Wang R, Fang X, Guo R, Zhang M, Lippman ME, Yang D, Wang S. (2004) Discovery of embelin as a cell-permeable, small-molecular weight inhibitor of XIAP through structure-based computational screening of a traditional herbal medicine three-dimensional structure database. *J Med Chem* 47(10):2430-2440.

319. Hu R, Zhu K, Li Y, Yao K, Zhang R, Wang H, Yang W, Liu Z. (2011) Embelin induces apoptosis through down-regulation of XIAP in human leukemia cells. *Med Oncol* 28(4):1584-1588.

320. Ahn KS, Sethi G, Aggarwal BB. (2007) Embelin, an inhibitor of X chromosome-linked inhibitor-of-apoptosis protein, blocks nuclear factor-kappaB (NF-kappaB) signaling pathway leading to suppression of NF-kappaB-regulated antiapoptotic and metastatic gene products. *Mol Pharmacol* 71(1):209-219.

321. Kim SW, Kim SM, Bae H, Nam D, Lee JH, Lee SG, Shim BS, Kim SH, Ahn KS, Choi SH, Sethi G. (2013) Embelin inhibits growth and induces apoptosis through the suppression of Akt/mTOR/S6K1 signaling cascades. *Prostate* 73(3):296-305.

322. Brandts JF & Lin LN. (1990) Study of strong to ultratight protein interactions using differential scanning calorimetry. *Biochemistry* 29(29):6927-6940.

323. Fukada H, Sturtevant JM, Quiocho FA. (1983) Thermodynamics of the binding of L-arabinose and of D-galactose to the L-arabinose-binding protein of Escherichia coli. *J Biol Chem* 258(21):13193-13198.

324. Shrake A & Ross PD. (1990) Ligand-induced biphasic protein denaturation. *J Biol Chem* 265(9):5055-5059.

325. Shrake A & Ross PD. (1992) Origins and consequences of ligand-induced multiphasic thermal protein denaturation. *Biopolymers* 32(8):925-940.

326. Che Y, Ye F, Xu R, Qing H, Wang X, Yin F, Cui M, Burstein D, Jiang B, Zhang DY. (2012) Co-expression of XIAP and cyclin D1 complex correlates with a poor prognosis in patients with hepatocellular carcinoma. *Am J Pathol* 180(5):1798-1807.

327. Dai Y, Desano J, Qu Y, Tang W, Meng Y, Lawrence TS, Xu L. (2011) Natural IAP inhibitor Embelin enhances therapeutic efficacy of ionizing radiation in prostate cancer. *Am J Cancer Res* 1(2):128-143.

328. Heo JY, Kim HJ, Kim SM, Park KR, Park SY, Kim SW, Nam D, Jang HJ, Lee SG, Ahn KS, Kim SH, Shim BS, Choi SH. (2011) Embelin suppresses STAT3 signaling, proliferation, and survival of multiple myeloma via the protein tyrosine phosphatase PTEN. *Cancer Lett* 308(1):71-80.

329. Munshi SR & Rao SS. (1972) Antifertility activity of an indigenous plant preparation (ROC-101). I. Effect on reproduction. *Indian J Med Res* 60(7):1054-1060.

330. Gupta OP, Ali MM, Ray Ghatak BJ, Atal CK. (1977) Some pharmacological investigations of embelin and its semisynthetic derivatives. *Indian J Physiol Pharmacol* 21(1):31-39.

331. Mori T, Doi R, Kida A, Nagai K, Kami K, Ito D, Toyoda E, Kawaguchi Y, Uemoto S. (2007) Effect of the XIAP inhibitor Embelin on TRAIL-induced apoptosis of pancreatic cancer cells. *J Surg Res* 142(2):281-286.

332. Siegelin MD, Gaiser T, Siegelin Y. (2009) The XIAP inhibitor Embelin enhances TRAIL-mediated apoptosis in malignant glioma cells by down-regulation of the short isoform of FLIP. *Neurochem Int* 55(6):423-430.

333. Li Y, Li D, Yuan S, Wang Z, Tang F, Nie R, Weng J, Ma L, Tang B. (2013) Embelin-induced MCF-7 breast cancer cell apoptosis and blockade of MCF-7 cells in the G2/M phase via the mitochondrial pathway. *Oncol Lett* 5(3):1005-1009.

334. Taghiyev A, Sun D, Gao ZM, Liang R, Wang L. (2012) Embelin-induced apoptosis of HepG2 human hepatocellular carcinoma cells and blockade of HepG2 cells in the G2/M phase via the mitochondrial pathway. *Exp Ther Med* 4(4):649-654.

335. Aird KM, Ding X, Baras A, Wei J, Morse MA, Clay T, Lyerly HK, Devi GR. (2008) Trastuzumab signaling in ErbB2-overexpressing inflammatory breast cancer correlates with X-linked inhibitor of apoptosis protein expression. *Mol Cancer Ther* 7(1):38-47.

336. Kubista M, Akerman B, Norden B. (1987) Characterization of interaction between DNA and 4',6-diamidino-2-phenylindole by optical spectroscopy. *Biochemistry* 26(14):4545-4553.

337. Yasujima T, Ohta K, Inoue K, Yuasa H. (2011) Characterization of human OCT1-mediated transport of DAPI as a fluorescent probe substrate. *J Pharm Sci* 100(9):4006-4012.

338. Yasujima T, Ohta KY, Inoue K, Ishimaru M, Yuasa H. (2010) Evaluation of 4',6-diamidino-2-phenylindole as a fluorescent probe substrate for rapid assays of the functionality of human multidrug and toxin extrusion proteins. *Drug Metab Dispos* 38(4):715-721.

339. Francis R, Barton MK, Kimble J, Schedl T. (1995) gld-1, a tumor suppressor gene required for oocyte development in Caenorhabditis elegans. *Genetics* 139(2):579-606.

340. Maciejowski J, Ugel N, Mishra B, Isopi M, Hubbard EJ. (2006) Quantitative analysis of germline mitosis in adult C. elegans. *Dev Biol* 292(1):142-151.

341. Cliby WA, Lewis KA, Lilly KK, Kaufmann SH. (2002) S phase and G2 arrests induced by topoisomerase I poisons are dependent on ATR kinase function. *J Biol Chem* 277(2):1599-1606.

342. Petrocca F, Visone R, Onelli MR, Shah MH, Nicoloso MS, de Martino I, Iliopoulos D, Pilozzi E, Liu CG, Negrini M, Cavazzini L, Volinia S, Alder H, Ruco LP, Baldassarre G, Croce CM, Vecchione A. (2008) E2F1-regulated microRNAs impair TGFbeta-dependent cell-cycle arrest and apoptosis in gastric cancer. *Cancer Cell* 13(3):272-286.

343. Yang TS, Yang XH, Chen X, Wang XD, Hua J, Zhou DL, Zhou B, Song ZS. (2014) MicroRNA-106b in cancer-associated fibroblasts from gastric cancer promotes cell migration and invasion by targeting PTEN. *FEBS Lett* 588(13):2162-2169.

344. Vinther J, Hedegaard MM, Gardner PP, Andersen JS, Arctander P. (2006) Identification of miRNA targets with stable isotope labeling by amino acids in cell culture. *Nucleic Acids Res* 34(16):e107.

345. Baek D, Villen J, Shin C, Camargo FD, Gygi SP, Bartel DP. (2008) The impact of microRNAs on protein output. *Nature* 455(7209):64-71.

346. Selbach M, Schwanhausser B, Thierfelder N, Fang Z, Khanin R, Rajewsky N. (2008) Widespread changes in protein synthesis induced by microRNAs. *Nature* 455(7209):58-63.

347. Lim LP, Lau NC, Garrett-Engele P, Grimson A, Schelter JM, Castle J, Bartel DP, Linsley PS, Johnson JM. (2005) Microarray analysis shows that some microRNAs downregulate large numbers of target mRNAs. *Nature* 433(7027):769-773.

348. Shin C, Nam JW, Farh KK, Chiang HR, Shkumatava A, Bartel DP. (2010) Expanding the microRNA targeting code: functional sites with centered pairing. *Mol Cell* 38(6):789-802.

349. Helwak A, Kudla G, Dudnakova T, Tollervey D. (2013) Mapping the human miRNA interactome by CLASH reveals frequent noncanonical binding. *Cell* 153(3):654-665.

350. Chuang TD, Luo X, Panda H, Chegini N. (2012) miR-93/106b and their host gene, MCM7, are differentially expressed in leiomyomas and functionally target F3 and IL-8. *Mol Endocrinol* 26(6):1028-1042.

351. Lewis BP, Shih IH, Jones-Rhoades MW, Bartel DP, Burge CB. (2003) Prediction of mammalian microRNA targets. *Cell* 115(7):787-798.

352. Reczko M, Maragkakis M, Alexiou P, Grosse I, Hatzigeorgiou AG. (2012) Functional microRNA targets in protein coding sequences. *Bioinformatics* 28(6):771-776.

353. Kremer-Tal S, Reeves HL, Narla G, Thung SN, Schwartz M, Difeo A, Katz A, Bruix J, Bioulac-Sage P, Martignetti JA, Friedman SL. (2004) Frequent inactivation of the tumor suppressor Kruppel-like factor 6 (KLF6) in hepatocellular carcinoma. *Hepatology* 40(5):1047-1052.

354. D'Astolfo DS, Gehrau RC, Bocco JL, Koritschoner NP. (2008) Silencing of the transcription factor KLF6 by siRNA leads to cell cycle arrest and sensitizes cells to apoptosis induced by DNA damage. *Cell Death Differ* 15(3):613-616.

355. Jin W, Di G, Li J, Chen Y, Li W, Wu J, Cheng T, Yao M, Shao Z. (2007) TIEG1 induces apoptosis through mitochondrial apoptotic pathway and promotes apoptosis induced by homoharringtonine and velcade. *FEBS Lett* 581(20):3826-3832.

356. Grimson A, Farh KK, Johnston WK, Garrett-Engele P, Lim LP, Bartel DP. (2007) MicroRNA targeting specificity in mammals: determinants beyond seed pairing. *Mol Cell* 27(1):91-105.

357. Knitt DS, Narlikar GJ, Herschlag D. (1994) Dissection of the role of the conserved G.U pair in group I RNA self-splicing. *Biochemistry* 33(46):13864-13879.

358. Yu T, Chen X, Zhang W, Liu J, Avdiushko R, Napier DL, Liu AX, Neltner JM, Wang C, Cohen D, Liu C. (2016) KLF4 regulates adult lung tumor-initiating cells and represses K-Ras-mediated lung cancer. *Cell Death Differ* 23(2):207-215.

359. Jianwei Z, Enzhong B, Fan L, Jian L, Ning A. (2013) Effects of Kruppel-like factor 6 on osteosarcoma cell biological behavior. *Tumour Biol* 34(2):1097-1105.

360. Chiam K, Ryan NK, Ricciardelli C, Day TK, Buchanan G, Ochnik AM, Murti K, Selth LA, BioResource APC, Butler LM, Tilley WD, Bianco-Miotto T. (2013) Characterization of the prostate cancer susceptibility gene KLF6 in human and mouse prostate cancers. *Prostate* 73(2):182-193.

361. Narla G, Kremer-Tal S, Matsumoto N, Zhao X, Yao S, Kelley K, Tarocchi M, Friedman SL. (2007) In vivo regulation of p21 by the Kruppel-like factor 6 tumor-suppressor gene in mouse liver and human hepatocellular carcinoma. *Oncogene* 26(30):4428-4434.

362. Song KD, Kim DJ, Lee JE, Yun CH, Lee WK. (2012) KLF10, transforming growth factor-beta-inducible early gene 1, acts as a tumor suppressor. *Biochem Biophys Res Commun* 419(2):388-394.

363. Yin P, Lin Z, Reierstad S, Wu J, Ishikawa H, Marsh EE, Innes J, Cheng Y, Pearson K, Coon JS, 5th., Kim JJ, Chakravarti D, Bulun SE. (2010) Transcription factor KLF11 integrates progesterone receptor signaling and proliferation in uterine leiomyoma cells. *Cancer Res* 70(4):1722-1730.

364. Jing D, Bhadri VA, Beck D, Thoms JA, Yakob NA, Wong JW, Knezevic K, Pimanda JE, Lock RB. (2015) Opposing regulation of BIM and BCL2 controls

glucocorticoid-induced apoptosis of pediatric acute lymphoblastic leukemia cells. *Blood* 125(2):273-283.

365. Huang MD, Chen WM, Qi FZ, Sun M, Xu TP, Ma P, Shu YQ. (2015) Long non-coding RNA TUG1 is up-regulated in hepatocellular carcinoma and promotes cell growth and apoptosis by epigenetically silencing of KLF2. *Mol Cancer* 14:165.

366. Huang X, Li X, Guo B. (2008) KLF6 induces apoptosis in prostate cancer cells through up-regulation of ATF3. *J Biol Chem* 283(44):29795-29801.

367. Chen H, Chen L, Sun L, Zhen H, Li X, Zhang Q. (2011) A small interfering RNA targeting the KLF6 splice variant, KLF6-SV1, as gene therapy for gastric cancer. *Gastric Cancer* 14(4):339-352.

368. Jarnagin WR, Fong Y, DeMatteo RP, Gonen M, Burke EC, Bodniewicz BJ, Youssef BM, Klimstra D, Blumgart LH. (2001) Staging, resectability, and outcome in 225 patients with hilar cholangiocarcinoma. *Ann Surg* 234(4):507-517; discussion 517-509.

369. Marin JJG, Lozano E, Briz O, Al-Abdulla R, Serrano MA, Macias RIR. (2017) Molecular Bases of Chemoresistance in Cholangiocarcinoma. *Curr Drug Targets* 18(8):889-900.

370. Khan SA, Davidson BR, Goldin RD, Heaton N, Karani J, Pereira SP, Rosenberg WM, Tait P, Taylor-Robinson SD, Thillainayagam AV, Thomas HC, Wasan H. (2012) Guidelines for the diagnosis and treatment of cholangiocarcinoma: an update. *Gut* 61(12):1657-1669.

371. Banales JM, Cardinale V, Carpino G, Marzioni M, Andersen JB, Invernizzi P, Lind GE, Folseraas T, Forbes SJ, Fouassier L, Geier A, Calvisi DF, Mertens JC, Trauner M, Benedetti A, Maroni L, Vaquero J, Macias RIR, Raggi C, Perugorria MJ, Gaudio E, Boberg KM, Marin JJG, Alvaro D. (2016) Cholangiocarcinoma: current knowledge and future perspectives consensus statement from the European Network for the Study of Cholangiocarcinoma (ENS-CCA). *Nature Reviews Gastroenterology &Amp; Hepatology* 13:261.

372. de Groen PC, Gores GJ, LaRusso NF, Gunderson LL, Nagorney DM. (1999) Biliary tract cancers. *N Engl J Med* 341(18):1368-1378.

373. Chapman MH, Webster GJ, Bannoo S, Johnson GJ, Wittmann J, Pereira SP. (2012) Cholangiocarcinoma and dominant strictures in patients with primary sclerosing cholangitis: a 25-year single-centre experience. *Eur J Gastroenterol Hepatol* 24(9):1051-1058.

374. Qian M-B, Utzinger J, Keiser J, Zhou X-N. (2016) Clonorchiasis. *The Lancet* 387(10020):800-810.

375. Welzel TM, Mellemkjaer L, Gloria G, Sakoda LC, Hsing AW, Ghormli LE, Olsen JH, McGlynn KA. (2006) Risk factors for intrahepatic cholangiocarcinoma in a low-risk population: A nationwide case-control study. *International Journal of Cancer* 120(3):638-641.

376. Shaib YH, El-Serag HB, Davila JA, Morgan R, McGlynn KA. (2005) Risk factors of intrahepatic cholangiocarcinoma in the United States: A case-control study. *Gastroenterology* 128(3):620-626.

377. Loeuillard E, Fischbach SR, Gores GJ, Rizvi S. (2018) Animal models of cholangiocarcinoma. *Biochim Biophys Acta Mol Basis Dis*.

378. Thamavit W, Pairojkul C, Tiwawech D, Itoh M, Shirai T, Ito N. (1993) Promotion of cholangiocarcinogenesis in the hamster liver by bile duct ligation after dimethylnitrosamine initiation. *Carcinogenesis* 14(11):2415-2417.

379. Yang H, Li TW, Peng J, Tang X, Ko KS, Xia M, Aller MA. (2011) A mouse model of cholestasis-associated cholangiocarcinoma and transcription factors involved in progression. *Gastroenterology* 141(1):378-388, 388 e371-374.

380. Sirica AE, Zhang Z, Lai GH, Asano T, Shen XN, Ward DJ, Mahatme A, Dewitt JL. (2008) A novel "patient-like" model of cholangiocarcinoma progression based on bile duct inoculation of tumorigenic rat cholangiocyte cell lines. *Hepatology* 47(4):1178-1190.

381. Yamada D, Rizvi S, Razumilava N, Bronk SF, Davila JI, Champion MD, Borad MJ, Bezerra JA, Chen X, Gores GJ. (2015) IL-33 facilitates oncogene-induced cholangiocarcinoma in mice by an interleukin-6-sensitive mechanism. *Hepatology* 61(5):1627-1642.

382. Macutkiewicz C, Plastow R, Chrispijn M, Filobbos R, Ammori BA, Sherlock DJ, Drenth JP, O'Reilly DA. (2012) Complications arising in simple and polycystic liver cysts. *World journal of hepatology* 4(12):406-411.

383. Yuan K, Frolova N, Xie Y, Wang D, Cook L, Kwon Y-J, Steg AD, Serra R, Frost AR. (2010) Primary Cilia Are Decreased in Breast Cancer: Analysis of a Collection of Human Breast Cancer Cell Lines and Tissues. *Journal of Histochemistry & Cytochemistry* 58(10):857-870.

384. Seeley ES, Carriere C, Goetze T, Longnecker DS, Korc M. (2009) Pancreatic cancer and precursor pancreatic intraepithelial neoplasia lesions are devoid of primary cilia. *Cancer Res* 69(2):422-430.

385. Moser JJ, Fritzler MJ, Rattner JB. (2009) Primary ciliogenesis defects are associated with human astrocytoma/glioblastoma cells. *BMC Cancer* 9(1):448.

386. Gradilone SA, Pisarello MJL, LaRusso NF. (2017) Primary Cilia in Tumor Biology: The Primary Cilium as a Therapeutic Target in Cholangiocarcinoma. *Curr Drug Targets* 18(8):958-963.

387. Basten SG, Willekers S, Vermaat JS, Slaats GG, Voest EE, van Diest PJ, Giles RH. (2013) Reduced cilia frequencies in human renal cell carcinomas versus neighboring parenchymal tissue. *Cilia* 2(1):2.

388. Nauli SM, Jin X, AbouAlaiwi WA, El-Jouni W, Su X, Zhou J. (2013) Non-motile primary cilia as fluid shear stress mechanosensors. *Methods Enzymol* 525:1-20.

389. Yoshimura S, Egerer J, Fuchs E, Haas AK, Barr FA. (2007) Functional dissection of Rab GTPases involved in primary cilium formation. *J Cell Biol* 178(3):363-369.

390. Pazour GJ, Dickert BL, Vucica Y, Seeley ES, Rosenbaum JL, Witman GB, Cole DG. (2000) Chlamydomonas IFT88 and Its Mouse Homologue, Polycystic Kidney Disease Gene Tg737, Are Required for Assembly of Cilia and Flagella. *J Cell Biol* 151(3):709.

391. Tucker RW, Pardee AB, Fujiwara K. (1979) Centriole ciliation is related to quiescence and DNA synthesis in 3T3 cells. *Cell* 17(3):527-535.

392. Izawa I, Goto H, Kasahara K, Inagaki M. (2015) Current topics of functional links between primary cilia and cell cycle. *Cilia* 4:12.

393. Kim S & Tsiokas L. (2011) Cilia and cell cycle re-entry: more than a coincidence. *Cell Cycle* 10(16):2683-2690.

394. Yan X & Zhu X. (2013) Branched F-actin as a negative regulator of cilia formation. *Exp Cell Res* 319(2):147-151.

395. Mirvis M, Stearns T, James Nelson W. (2018) Cilium structure, assembly, and disassembly regulated by the cytoskeleton. *Biochem J* 475(14):2329-2353.

396. Mammoto A, Mammoto T, Ingber DE. (2012) Mechanosensitive mechanisms in transcriptional regulation. *J Cell Sci* 125(Pt 13):3061-3073.

397. Álvarez-Satta M & Matheu A. (2018) Primary cilium and glioblastoma. *Therapeutic Advances in Medical Oncology* 10:1758835918801169.

398. Deng YZ, Cai Z, Shi S, Jiang H, Shang YR, Ma N, Wang JJ, Guan DX, Chen TW, Rong YF, Qian ZY, Zhang EB, Feng D, Zhou QL, Du YN, Liu DP, Huang XX, Liu

LM, Chin E, Li DS, Wang XF, Zhang XL, Xie D. (2018) Cilia loss sensitizes cells to transformation by activating the mevalonate pathway. *J Exp Med* 215(1):177-195.

399. Hassounah NB, Nunez M, Fordyce C, Roe D, Nagle R, Bunch T, McDermott KM. (2017) Inhibition of Ciliogenesis Promotes Hedgehog Signaling, Tumorigenesis, and Metastasis in Breast Cancer. *Molecular Cancer Research* 15(10):1421.

400. Dekker RJ, Boon RA, Rondaij MG, Kragt A, Volger OL, Elderkamp YW, Meijers JC, Voorberg J, Pannekoek H, Horrevoets AJ. (2006) KLF2 provokes a gene expression pattern that establishes functional quiescent differentiation of the endothelium. *Blood* 107(11):4354-4363.

401. Nauli SM, Alenghat FJ, Luo Y, Williams E, Vassilev P, Li X, Elia AE, Lu W, Brown EM, Quinn SJ, Ingber DE, Zhou J. (2003) Polycystins 1 and 2 mediate mechanosensation in the primary cilium of kidney cells. *Nat Genet* 33(2):129-137.

402. Sathanoori R, Rosi F, Gu BJ, Wiley JS, Muller CE, Olde B, Erlinge D. (2015) Shear stress modulates endothelial KLF2 through activation of P2X4. *Purinergic Signal* 11(1):139-153.

403. Strayer DS, Hoek JB, Thomas AP, White MK. (1999) Cellular activation by Ca2+ release from stores in the endoplasmic reticulum but not by increased free Ca2+ in the cytosol. *Biochem J* 344 Pt 1:39-46.

404. Kaur G, Ly-Huynh JD, Jans DA. (2014) Intracellular calcium levels can regulate Importin-dependent nuclear import. *Biochem Biophys Res Commun* 450(1):812-817.

405. Soliman EM, Rodrigues MA, Gomes DA, Sheung N, Yu J, Amaya MJ, Nathanson MH, Dranoff JA. (2009) Intracellular calcium signals regulate growth of hepatic stellate cells via specific effects on cell cycle progression. *Cell Calcium* 45(3):284-292.

406. Kim J, Jo H, Hong H, Kim MH, Kim JM, Lee J-K, Heo WD, Kim J. (2015) Actin remodelling factors control ciliogenesis by regulating YAP/TAZ activity and vesicle trafficking. *Nat Commun* 6:6781.

407. Drummond ML, Li M, Tarapore E, Nguyen TTL, Barouni BJ, Cruz S, Tan KC, Oro AE, Atwood SX. (2018) Actin polymerization controls cilia-mediated signaling. *J Cell Biol* 217(9):3255-3266.

408. Hanahan D & Weinberg RA. (2000) The Hallmarks of Cancer. *Cell* 100(1):57-70.

409. Hanahan D & Weinberg Robert A. (2011) Hallmarks of Cancer: The Next Generation. *Cell* 144(5):646-674.

410. Ebert MS & Sharp PA. (2012) Roles for microRNAs in conferring robustness to biological processes. *Cell* 149(3):515-524.

411. Garzon R, Marcucci G, Croce CM. (2010) Targeting microRNAs in cancer: rationale, strategies and challenges. *Nat Rev Drug Discov* 9(10):775-789.

412. Hosseinahli N, Aghapour M, Duijf PHG, Baradaran B. (2018) Treating cancer with microRNA replacement therapy: A literature review. *Journal of Cellular Physiology* 233(8):5574-5588.

413. Chakraborty C, Sharma AR, Sharma G, Doss CGP, Lee SS. (2017) Therapeutic miRNA and siRNA: Moving from Bench to Clinic as Next Generation Medicine. *Mol Ther Nucleic Acids* 8:132-143.

414. Mullard A. (2018) FDA approves landmark RNAi drug. *Nature Reviews Drug Discovery* 17:613.

415. Wang Y, Li J, Chen Y, Oupický D. (2015) Balancing polymer hydrophobicity for ligand presentation and siRNA delivery in dual function CXCR4 inhibiting polyplexes. *Biomaterials science* 3(7):1114-1123.

416. Conlan RS, Pisano S, Oliveira MI, Ferrari M, Mendes Pinto I. (2017) Exosomes as Reconfigurable Therapeutic Systems. *Trends Mol Med* 23(7):636-650.

417. Olaizola P, Lee-Law PY, Arbelaiz A, Lapitz A, Perugorria MJ, Bujanda L, Banales JM. (2018) MicroRNAs and extracellular vesicles in cholangiopathies. *Biochim Biophys Acta Mol Basis Dis* 1864(4 Pt B):1293-1307.

418. Arbelaiz A, Azkargorta M, Santos-Laso Á, Perugorria MJ, Erice O, Gonzalez E, Lapitz A, Izquierdo L, Olaizola P, Lee PY, Arregi A, Jimenez-Aguero R, Lacasta A, Ibarra C, Sánchez-Campos A, Jimeno JP, Krawczyk M, Lammert F, Marzioni M, Macias R, Marín JJ, Patel T, Gores G, Martinez I, Elortza F, *et al.* (2017) THU-074 - Serum extracellular vesicles contain protein biomarkers for primary sclerosing cholangitis and cholangiocarcinoma. *J Hepatol* 66(1, Supplement):S207-S208.

419. Koshkin AA, Singh SK, Nielsen P, Rajwanshi VK, Kumar R, Meldgaard M, Olsen CE, Wengel J. (1998) LNA (Locked Nucleic Acids): Synthesis of the adenine, cytosine, guanine, 5-methylcytosine, thymine and uracil bicyclonucleoside monomers, oligomerisation, and unprecedented nucleic acid recognition. *Tetrahedron* 54(14):3607-3630.

420. Kaur H, Arora A, Wengel J, Maiti S. (2006) Thermodynamic, Counterion, and Hydration Effects for the Incorporation of Locked Nucleic Acid Nucleotides into DNA Duplexes. *Biochemistry* 45(23):7347-7355.